

การแยกประเภทของนิเวศโอไรต์โดยใช้เซ็นเซอร์เชิงจุพราโมเลกุลในสารละลายน้ำ

นางสาวจิราภรณ์ ไชยแจ่ม

วิทยานิพนธ์นี้เป็นส่วนหนึ่งของการศึกษาตามหลักสูตรปริญญาวิทยาศาสตรมหาบัณฑิต

สาขาวิชาเคมี ภาควิชาเคมี

คณะวิทยาศาสตร์ จุฬาลงกรณ์มหาวิทยาลัย

ปีการศึกษา 2554

ลิขสิทธิ์ของจุฬาลงกรณ์มหาวิทยาลัย

บทคัดย่อและแฟ้มข้อมูลฉบับเต็มของวิทยานิพนธ์ตั้งแต่ปีการศึกษา 2554 ที่ให้บริการในคลังปัญญาจุฬาฯ (CUIR)

เป็นแฟ้มข้อมูลของนิสิตเจ้าของวิทยานิพนธ์ที่ส่งผ่านทางบัณฑิตวิทยาลัย

The abstract and full text of theses from the academic year 2011 in Chulalongkorn University Intellectual Repository (CUIR) are the thesis authors' files submitted through the Graduate School.

DISCRIMINATION OF NUCLEOTIDES BY SUPRAMOLECULAR SENSORS
IN AQUEOUS SOLUTION

Miss Chiraporn Chaicham

A Thesis Submitted in Partial Fulfillment of the Requirements
for the Degree of Master of Science Program in Chemistry

Department of Chemistry

Faculty of Science

Chulalongkorn University

Academic Year 2011

Copyright of Chulalongkorn University

Thesis Title DISCRIMINATION OF NUCLEOTIDES BY SUPRAMOLECULAR
 SENSORS IN AQUEOUS SOLUTION
By Miss Chiraporn Chaicham
Field of Study Chemistry
Thesis Advisor Assistant Professor Boosayarat Tomapatanaget, Ph.D.

Accepted by the Faculty of Science, Chulalongkorn University in Partial
Fulfillment of the Requirements for the Master's Degree

..... Dean of the Faculty of Science
(Professor Supot Hannongbua, Dr.rer.nat.)

THESIS COMMITTEE

..... Chairman
(Associate Professor Tirayut Vilaivan, Ph.D.)

..... Thesis Advisor
(Assistant Professor Boosayarat Tomapatanaget, Ph.D.)

..... Examiner
(Associate Professor Nongnuj Muangsin, Ph.D.)

..... External Examiner
(Nantanit Wanichacheva, Ph.D.)

จิราภรณ์ ไชยแจ่ม : การแยกประเภทของนิวคลีโอไทด์โดยใช้เซ็นเซอร์เชิงซูพราโมเลกุล
ในสารละลายน้ำ. (DISCRIMINATION OF NUCLEOTIDES BY
SUPRAMOLECULAR SENSORS IN AQUEOUS SOLUTION) อ. ที่ปรึกษา
วิทยานิพนธ์หลัก : ผศ. ดร. บุญรัตน์ ธรรมพัฒน์กิจ , 140 หน้า.

ในงานวิจัยนี้มีจุดมุ่งหมายเพื่อ การ ออกแบบและสังเคราะห์โมเลกุลเซ็นเซอร์สำหรับ
ตรวจวัดนิวคลีโอไทด์ด้วยเทคนิคฟลูออเรสเซนซ์ สำหรับอนุภาคทองคำระดับนาโนที่ถูกนำมาใช้ในการ
การตรวจวัดนิวคลีโอไทด์จะแบ่งออกเป็น 2 ประเภท ได้แก่ การเกิดสารประกอบเชิงซ้อน ระหว่างนิ
วคลีโอไทด์กับอนุภาคทองคำระดับนาโนและฟลูออโรฟอร์ และการแทนที่ของฟลูออโรฟอร์ด้วยนิ
วคลีโอไทด์บนอนุภาคทองคำระดับนาโน โดยอาศัยกระบวนการถ่ายโอนพลังงานระหว่างหมู่ฟลูออ
โรฟอร์และอนุภาคทองคำระดับนาโน ผลจากการทดลองของทั้งสองระบบไม่สามารใช้ในการ
ตรวจวัดนิวคลีโอไทด์ได้

สำหรับการแยกแยะประเภทของนิวคลีโอไทด์โดยใช้การวิเคราะห์ห่อหุ้มประกอบหลัก
โมเลกุลเซ็นเซอร์ที่ใช้ในการศึกษานี้จะประกอบด้วยอนุพันธ์ของไพรีนและควมาริน (**Pydpa** และ
Es) สำหรับใช้ในการแยกประเภทของนิวคลีโอไทด์ ในขั้นต้นได้เตรียมสารประกอบเชิงซ้อนของ
เซ็นเซอร์โมเลกุล **Pydpa-Zn**, **Pydpa-Cu**, **Es-Zn** และ **Es-Cu** เพื่อใช้จับกับ นิวคลีโอไทด์ ซึ่ง
หมู่ฟอสเฟตของนิวคลีโอไทด์ สามารถเกิดอันตรกิริยาทางไฟฟ้าสถิตกับสารประกอบเชิงซ้อนของ
เซ็นเซอร์โมเลกุลได้ จากนั้นได้ศึกษาความสามารถในการเกิดสารประกอบเชิงซ้อน โดยใช้เทคนิค
ฟลูออเรสเซนซ์สเปกโทรโฟโตเมตริ พบว่า **Pydpa-Zn**, **Es-Zn** และ **Es-Cu** มีความจำเพาะต่อ
PPi สูง ได้ค่าคงที่การจับ ($\log K$) ของ **Pydpa-Zn**, **Es-Zn** และ **Es-Cu** กับ PPI เท่ากับ 8.83,
5.23 และ 4.64 ตามลำดับ นอกจากนี้ผู้วิจัยได้นำการวิเคราะห์ห่อหุ้มประกอบหลัก มาใช้แยกประเภท
ของนิวคลีโอไทด์โดยการสร้างเป็นเซ็นเซอร์อาร์เรย์ (การรวมกันของข้อมูลแต่ละเซ็นเซอร์) และ
สร้างเป็นเซ็นเซอร์ใหม่ (การรวมกันของเซ็นเซอร์ โมเลกุล) ซึ่งเป็นที่น่าสนใจว่าข้อมูลที่ศึกษาได้
จากการ รวมกันของ เซ็นเซอร์ **Pydpa-Zn+Es-Cu** จะแสดงการจำแนกกลุ่มของนิวคลีโอไทด์
PPi, ATP, UTP, ADP, UDP และ GDP ได้อย่างชัดเจน และเปอร์เซ็นต์ความถูกต้องของการ
ทำนายเชิงกลุ่มเป็น 92%

ภาควิชาเคมี..... ลายมือชื่อนิสิต

สาขาวิชาเคมี..... ลายมือชื่อ อ.ที่ปรึกษาวิทยานิพนธ์หลัก.....

ปีการศึกษา2554.....

5272255123 : MAJOR CHEMISTRY

KEYWORDS : PRICIPAL COMPONENT ANALYSIS (PCA) / NUCLEOTIDES /
SENSOR

CHIRAPORN CHAICHAM: DISCRIMINATION OF NUCLEOTIDES BY
SUPRAMOLECULAR SENSORS IN AQUEOUS SOLUTION. ADVISOR:
ASST. PROF. BOOSAYARAT TOMAPATANAGET, Ph.D., 140 pp.

This research aims to design and synthesize the molecular sensors for nucleotides sensing. In the case of the energy transfer, gold nanoparticles were used to study on the complexation related two processes including i) the complexation of nucleotides with the modified gold nanoparticles and fluorophore and ii) the fluorophore replacement on the gold nanoparticles by nucleotides. Unfortunately, the detection of nucleotides using the concepts of the fluorescence quenching by gold nanoparticles under both processes has not been achieved.

For nucleotides discrimination using Principal Component Analysis (PCA), the molecular sensors containing pyrene and coumarin derivatives (**Pydpa** and **Es**) were used for discrimination of various nucleotides in aqueous solution. Initially, the complexation of **Pydpa-Zn**, **Pydpa-Cu**, **Es-Zn**, and **Es-Cu** were prepared as the sensory molecules to recognize the phosphate anion based nucleotides undergone the electrostatic interaction. The complexation studies of these sensors were carried out by fluorescence spectrophotometry. It was found that **Pydpa-Zn**, **Es-Zn**, and **Es-Cu** showed a high selectivity to PPI with the log *K* values of 8.83, 5.23 and 4.64, respectively. In addition, the PCA method was applied to classify the types of nucleotides by creation of the sensor arrays (the combinatorial data) and the mixed sensors (the combinatorial sensors). Interestingly, the combinatorial sensors of **Pydpa-Zn+Es-Cu** showed a highly potential discrimination of PPI, ATP, UTP, ADP, UDP and GDP with 92% classification accuracy.

Department :Chemistry..... Student's Signature

Field of Study :Chemistry..... Advisor's Signature

Academic Year :2011.....

ACKNOWLEDGEMENTS

I wish to express deepest appreciation to my thesis advisor, Assist. Prof. Dr. Boosayarat Tomapatanaget for kindness, constant encouragement, suggestions and assistance, involving supports throughout my master degree career. In addition, I would like to thank Assoc. Prof. Dr. Tirayut Vilaivan, Assoc. Prof. Dr. Nongnuj Muangsin and Dr. Nantanit Wanichacheva for their interest, value suggestions, comments as committee members and thesis examiners.

This thesis would not be successful without kindness, encouragement, and helps of the members of the Supramolecular Chemistry Research Unit. Particularly, Mr. Anusak Chaicham provides for consultation and assistance about my research. Moreover, I would like to thanks Dr. Kanet Wongravee for their assistance for using MATLAB program and provides guidance on the Principal Component Analysis (PCA).

I would like to thanks the Human Resource Development in Science Project (Science Achievement Scholarship of Thailand, SAST) to support covering full tuition and stipend in academic program. Moreover, I wish to thanks many supporting for the Center for Petroleum, Petrochemicals, and Advanced Materials. Finally, I would like to express my deepest gratitude to my family for their love, care, kindness, encouragement and other assistance throughout my life.

CONTENTS

	Page
Abstract in Thai.....	iv
Abstract in English.....	v
Acknowledgements.....	vi
Contents.....	vii
List of Tables	xiii
List of Figures.....	xvi
List of Schemes.....	xxiv
List of Abbreviations	xxv
CHAPTER I INTRODUCTION.....	1
1.1 Concept of supramolecular chemistry.....	1
1.2 Molecular recognition	1
1.3 Absorption of UV-visible light	2
1.4 Phenomena of fluorescence	4
1.5 Cation-Anion sensors.....	5
1.6 Determination of the stoichiometry of a complex by the method of continuous variations (Job's method)	7
1.7 Selectivity of receptors	8
1.8 Principal Component Analysis (PCA)	9
CHAPTER II LITERATURE REVIEWS.....	13
2.1 Literature reviews.....	13

2.1.1 Nucleotides.....	13
2.1.2 Receptor of metal-sensing.....	14
2.1.3 Nucleotides sensing.....	16
2.1.4 Application of gold nanoparticles.....	20
2.1.5 Nucleotides sensing by using Principal Component Analysis (PCA)...	23
2.2 Objective and scope of this research.....	24
CHAPTER III EXPERIMENTAL.....	26
3.1. Materials and Physical measurements.....	26
3.2. Synthesis of gold nanoparticles.....	26
3.2.1. Synthesis of Gold nanoparticles in H ₂ O.....	27
3.2.2. Synthesis of Gold nanoparticles in toluene	27
3.3. Modification of gold nanoparticles	27
3.3.1 Modification of gold nanoparticles in H ₂ O using citrate as a stabilizer.	27
3.3.1.1 Modification of gold nanoparticles by Monodpa	27
3.3.1.2 Modification of gold nanoparticles by Didpa	28
3.3.1.3 Modification of gold nanoparticles by Didpa_1	28
3.3.1.4 Modification of gold nanoparticles by Didpa_1-Zn	28
3.3.2 Modification of gold nanoparticles in toluene using tetraalkyl- ammonium bromides (TOABr) as a stabilizer.....	28

3.3.2.1 Modification of gold nanoparticles by Didpa_1-Zn in 10% toluene in DMSO.....	28
3.4. Metal sensing	29
3.5. Complexation studies for nucleotides detection	29
3.5.1 Using gold nanoparticles for using the nucleotides detection.....	29
3.5.1.1 Complexation studies between fluorophore and modified gold nanoparticles by fluorescence spectroscopy.....	30
3.5.1.1.1 Modification of gold nanoparticles parts.....	30
3.5.1.1.2 Fluorophore as a boronic acid parts.....	39
3.5.1.1.3 Complexation studies of AuNPs-Didpa\subsetZn²⁺ and PBI-(B(OH)₂)₂ for nucleotides detection.....	40
3.5.1.1.4 Complexation studies of Didpa_1-Zn and PBI-(B(OH)₂)₂ for nucleotides detection.....	41
3.5.1.1.5 Complexation studied of PBI-(B(OH)₂)₂ with nucleotides anions.....	41
3.5.1.2 Complexation studies by using replacement procedure	42
3.5.1.2.1 Synthesis pathway of Rhodpa	42
3.5.1.2.2 Fluorophore replacement studies by fluorescence spectroscopy.....	44
3.5.2 Complexation studies by using Pricipal Component Analysis (PCA) for discrimination of nucleotides.....	45
3.5.2.1 Synthesis pathway of pyrene derivative.....	45

3.5.2.2	Complexation studies of Esculetin with metal ions (Zn^{2+} and Cu^{2+}) by UV-visible spectroscopy.....	47
3.5.2.2.1	Titration studies of Esculetin with $Zn(ClO_4)_2$ using UV-visible spectroscopy	47
3.5.2.2.2	Titration studies of Esculetin with $Cu(NO_3)_2$ using UV-visible spectroscopy	49
3.6.	Complexation studies of Pydpa-Zn , Pydpa-Cu , Es-Zn and Es-Cu with various nucleotides by fluorescence spectroscopy.....	50
3.6.1	Complexation studies of Pydpa-Zn with various nucleotides.....	50
3.6.2	Titration studies of Pydpa-Zn with PPI using fluorescence spectroscopy.....	50
3.6.3	Complexation studies of Pydpa-Zn and Es-Zn with various nucleotides by fluorescence spectroscopy.....	52
3.7.	Job's plot study.....	52
3.7.1	Job's plot study of Esculetin with Zn^{2+} ion.....	52
3.7.2	Job's plot study of Pydpa-Zn with PPI.....	53
	CHAPTER IV RESULTS AND DISCUSSION.....	55
4.1.	Optical properties of gold nanoparticles.....	55
4.4.1	Gold nanoparticles in H_2O	56
4.4.2	Gold nanoparticles in toluene.....	56
4.2.	Modification of gold nanoparticles.....	57

4.2.1 Modification of gold nanoparticles in H ₂ O with Monodpa , Didpa , Didpa_1 and Didpa_1-Zn	57
4.3. Study on the metal sensing by using modified gold nanoparticles with Monodpa and Didpa_1	59
4.4. Nucleotides detection.....	61
4.4.1 Application of gold nanoparticles for nucleotides detection.....	61
4.4.1.1 Complexation between fluorophore and gold nanoparticles for nucleotides sensing.....	61
4.4.1.1.1 Modification of gold nanoparticles part of Monodpa , Didpa and Didpa_1	62
4.4.1.1.2 Synthesis of boronic acid based fluorophore part.....	73
4.4.1.1.3 Complexation studies of nucleotides detection by using AuNPs-Didpa ⊂ Zn²⁺ with PBI-(B(OH)₂)₂	74
4.4.1.1.4 Complexation studies between AuNPs-Didpa_1-Zn and PBI-(B(OH)₂)₂ for nucleotides detection.....	77
4.4.1.2 Fluorophore replacement with nucleotides using gold nanoparticles and Rhodpa-Cu	79
4.4.1.2.1 Synthesis and characterization of Rhodpa	80
4.4.1.3 Complexation studies of fluorophore replacement with nucleotides	84
4.4.2 Nucleotides sensing by using Principal Component Analysis (PCA).....	86
4.4.2.1 Synthesis and characterization of Pydpa	87

4.4.2.2 Synthesis and characterization of Pydpa-Zn	88
4.4.2.3 Synthesis and characterization of Pydpa-Cu	90
4.4.2.4 Complexation studies of Pydpa-Zn , Pydpa-Cu , Es-Zn and Es-Cu with nucleotides by using fluorescesnce spectroscopy.....	93
4.5.Sensor Arrays	107
4.5.1 Study on the clustering discrimination of all sensors with nucleotides including PPI	107
4.5.2 Study on the clustering discrimination of all sensors with nucleotides the excluded PPI	111
CHAPTER V CONCLUSION.....	120
References.....	122
Appendix.....	130
Vita.....	140

LIST OF TABLES

Table		Page
1.1	Time scale of each transition	5
3.1	The amounts of metal ions were used in UV-visible studies	29
3.2	The amounts of nucleotides were used in fluorescence studies.....	40
3.3	The concentration of Zn^{2+} ion was used in complexation studies of Esculetin	48
3.4	The concentration of Cu^{2+} ion was used in complexation studies of Esculetin	49
3.5	The concentration of PPi anion was used in complexation studies of Pydpa-Zn	50
3.6	Amounts of Esculetin and Zn^{2+} cation and HEPES buffer pH 7.4 were used in Job's plot experiment.....	53
3.7	Amounts of Pydpa-Zn and PPi anion and HEPES buffer pH 7.4 were used in Job's plot experiment.....	54
4.1	% accuracy of both sensor arrays for 10 nucleotides by cross-validation LDA.....	115

LIST OF FIGURES

Figure	Page
1.1 Possible electronic transitions in organic molecules	3
1.2 Jablonski diagram	4
1.3 Chemosensors based on the binding site-signaling unit	6
1.4 Job's plots for a 1:1 complex	8
1.5 Principal Component Analysis	11
1.6 PCA as a form of variable reduction	12
1.7 Graphical representation of samples in the original space (Left) and the position of samples in PC spaces (Right)	12
2.1 Composition of nucleotides	13
2.2 Molecular structure of DPA derivative of sensor 1	14
2.3 (A) Absorption and emission spectra of 1 upon addition of Zn^{2+} in MeOH and (B) molecular structure of $1 \cdot Zn^{2+}$ ion	15
2.4 Molecular structure of sensor 2	15
2.5 (A) Fluorescence response of sensor 2 with metal ions and (B) Fluorescent emission spectra of sensor 2 in the presence of different concentration of Cu^{2+} in EtOH:H ₂ O (40:60 v/v, 50mM HEPES buffer, pH 7.2).....	16
2.6 (A) Molecular sensor and (B) fluorescence changing of sensor 3 in 0.01 M HEPES buffer (pH 7.4) upon addition the anions.....	17
2.7 Explanation of responded mechanism of sensor 3 with PPI	17

2.8	(A) Molecular structure of sensor 4 , (B) absorption spectra of sensor 4 upon addition various nucleotides in HEPES buffer (pH 7.2) and (C) Light microscopy images for before and after added the sensor 4	18
2.9	(A) Fluorescence response of poly(HMAM-co-MDCPDP) in H ₂ O: EtOH (2:5 v/v, pH 7) upon addition of various metal ions and (B) The fluorescence “on-off-on” of sensor 5 upon addition of Cu ²⁺ and PPI, respectively.	19
2.10	A) Modification of gold nanoparticles with derivatives fullerenethiol and (B) fluorescence spectra of fullerenethiol before and after modified gold nanoparticles.....	20
2.11	Plasmon absorption spectra of (A) Dex@AuNPs , (B) ABA@AuNPs , (C) RBITC@AuNPs and (D) in the presence of glucose (0.138 μM)..	21
2.12	(A) Fluorescence spectra of RBITC (left) and RBITC@AuNPs (right) and (B) fluorescence spectra of RBITC@AuNPs upon the increasement of glucose.....	22
2.13	(A) Receptor and indicators used for MIDA assay and (B) possibility of three sensors for analyst.....	23
2.14	(A) Absorption spectra of three sensor and (B) LDA score plot of three sensors for discrimination of six nucleotides.....	24
2.15	Molecular structures were studied in this work.....	25
4.1	Diagram of the conceptually sensing purposes used in this research....	55
4.2	UV-visible spectrum of gold nanoparicles using citrate as stabilizer in H ₂ O.....	56
4.3	UV-visible spectrum of gold nanoparicles was synthesized in toluene..	57

4.4	UV-visible spectra of functionalized gold nanoparticles with Monodpa (A), Didpa (B), Didpa_1 (C) and Didpa_1-Zn (D).....	58
4.5	UV-visible absorption spectra of AuNPs-Monodpa before and after adding various metal ions.....	59
4.6	UV-visible absorption spectra of AuNPs-Didpa_1 before and after adding various metal ions.....	60
4.7	¹ H-NMR spectrum of compound 1.....	63
4.8	¹ H-NMR spectrum of compound 2.....	64
4.9	¹ H-NMR spectrum of Monodpa	65
4.10	¹ H-NMR spectrum of compound 3.....	66
4.11	¹ H-NMR spectrum of compound 4.....	67
4.12	¹ H-NMR spectrum of compound 5.....	68
4.13	¹ H-NMR spectrum of Didpa	69
4.14	¹ H-NMR spectrum of compound 6.....	70
4.15	¹ H-NMR spectrum of Didpa_1	71
4.16	¹ H-NMR spectrum of Didpa_1-Zn	72
4.17	¹ H-NMR spectrum of PBI-(B(OH)₂)₂	73
4.18	(A) Absorption (1x10 ⁻⁴ M) and (B) emission (1x10 ⁻⁵ M) spectrum of PBI-(B(OH)₂)₂ in DMSO.....	74
4.19	Complexation of PBI-(B(OH)₂)₂ and AuNPs-Didpa ⊂Zn ²⁺ upon adding various nucleotides.....	75

4.20	Absorption spectra of Didpa_1 and Didpa_1-Zn in DMSO ($1 \times 10^{-4} \text{M}$).....	76
4.21	UV-visible spectra of Didpa_1-Zn -functionalized gold nanoparticles (red).....	77
4.22	Complexation of PBI-(B(OH)₂)₂ and AuNPs-Didpa_1-Zn upon adding various nucleotides.....	78
4.23	Fluorescence spectra of PBI-(B(OH)₂)₂ before and after adding various nucleotides in aqueous solution of 0.01 M HEPES (pH 7.4)...	78
4.24	¹ H-NMR spectrum of compound 7.....	81
4.25	¹ H-NMR spectrum of compound 8.....	82
4.26	¹ H-NMR spectrum of Rhodpa	83
4.27	Model of Rhodpa bound Cu^{2+} ion.....	83
4.28	(A) Absorption ($1 \times 10^{-5} \text{M}$) and (B) emission ($1 \times 10^{-6} \text{M}$) spectra of Rhodpa and Rhodpa-Cu in DMSO ($1 \times 10^{-4} \text{M}$).....	84
4.29	Fluorescence spectra of Rhodpa-Cu and AuNPs upon adding various nucleotides.....	85
4.30	¹ H-NMR spectrum of Pydpa	88
4.31	¹ H-NMR spectrum of Pydpa-Zn complex.....	89
4.32	(A) Absorption spectra of sensor at $1 \times 10^{-4} \text{M}$ and (B) emission spectra of sensor at $1 \times 10^{-5} \text{M}$ in DMSO.....	90
4.33	(A) Normalized absorption spectra of Pydpa and Pydpa-Cu complex at $1 \times 10^{-4} \text{M}$ and (B) emission spectra of Pydpa and Pydpa-Cu complex at $1 \times 10^{-5} \text{M}$ in DMSO.....	91

4.34	(A) Normalized absorption spectra of $1 \times 10^{-4} \text{M}$ of sensors in DMSO and (B) emission spectra of $1 \times 10^{-5} \text{M}$ of sensors in DMSO.....	92
4.35	Job's plot of Esculetin and Zn^{2+} using fluorescence intensity at 470 nm suggests 2:1 stoichiometry.....	92
4.36	Job's plot of Esculetin and Cu^{2+} using fluorescence intensity at 470 nm suggests 2:1 stoichiometry.....	93
4.37	Fluorescence emission spectra of Pydpa-Zn ($1 \times 10^{-5} \text{M}$) upon the addition of various nucleotide anions (10 equiv) in aqueous solution of HEPES buffer 0.01 M, pH 7.4. ($\lambda_{\text{ex}} = 346 \text{ nm}$).....	94
4.38	Fluorescence titration spectra of Pydpa-Zn ($1 \times 10^{-5} \text{M}$) in aqueous solution (0.01M HEPES buffer, pH 7.4) upon the incremented addition of PPI. ($\lambda_{\text{ex}} = 346 \text{ nm}$).....	95
4.39	Comparing experimental data and calculated data of Pydpa-Zn and PPI using fluorescence titration at 384 nm for calculation of the association constant (K). ($\lambda_{\text{ex}} = 346 \text{ nm}$).....	95
4.40	Job's plot of Pydpa-Zn and PPI using fluorescence intensity at 386 nm under excitation wavelength at 346 nm.....	96
4.41	The proposed structures of Pydpa-Zn ⊂PPI complexes.....	96
4.42	PCA score plot of Pydpa-Zn upon the addition of various nucleotide anions (10 equiv) in aqueous solution of HEPES buffer 0.01 M, pH 7.4. PCA score plot shows clustering for all 11 samples.....	97
4.43	Possibility structure of Pydpa-Cu	97

4.44	Fluorescence emission spectra of Pydpa-Cu (1×10^{-5} M) upon the addition of various nucleotide anions (10 equiv) in aqueous solution of HEPES buffer 0.01 M, pH 7.4. ($\lambda_{\text{ex}} = 346$ nm).....	98
4.45	PCA score plot of Pydpa-Cu upon the addition of various nucleotide anions (10 equiv) in aqueous solution of HEPES buffer 0.01 M, pH 7.4. PCA score plot shows clustering for all 11 samples.....	98
4.46	Fluorescence emission spectra of Es-Zn (1×10^{-5} M) upon the addition of various nucleotide anions (10 equiv) in aqueous solution of HEPES buffer 0.01 M, pH 7.4. ($\lambda_{\text{ex}} = 380$ nm).....	99
4.47	Fluorescence titration spectra of Es-Zn (1×10^{-5} M) in aqueous solution (0.01M HEPES buffer, pH 7.4) upon gradually adding of PPI. ($\lambda_{\text{ex}} = 380$ nm).....	100
4.48	Comparing experiment data and calculated data of Es-Zn and PPI using fluorescence titration at 470 nm for calculation of association constant (K). ($\lambda_{\text{ex}} = 380$ nm).....	101
4.49	Job's plot of Es-Zn and PPI using fluorescence intensity at 470 nm under excitation wavelength 380 nm.....	101
4.50	PCA score plot of Es-Zn upon the addition of various nucleotide anions (10 equiv) in aqueous solution of HEPES buffer 0.01 M, pH 7.4. PCA score plot shows clustering for all 11 samples.....	102
4.51	Fluorescence emission spectra of Es-Cu (1×10^{-5} M) upon the addition of various nucleotide anions (10 equiv) in aqueous solution of HEPES buffer 0.01 M, pH 7.4. ($\lambda_{\text{ex}} = 380$ nm).....	103
4.52	PCA score plot of Es-Cu upon the addition of various nucleotide anions (10 equiv) in aqueous solution of HEPES buffer 0.01 M, pH 7.4. PCA score plot shows clustering for all 11 samples.....	103

4.53	Fluorescence titration spectra of Es-Cu (1×10^{-5} M) in aqueous solution (0.01M HEPES buffer, pH 7.4) upon gradually adding of PPI. ($\lambda_{\text{ex}} = 380$ nm).....	104
4.54	Comparing experiment data and calculated data of Es-Zn and PPI using fluorescence titration at 470 nm for calculation of association constant (K). ($\lambda_{\text{ex}} = 380$ nm).....	105
4.55	Job's plot of Es-Cu and PPI using fluorescence intensity at 470 nm under excitation wavelength at 380 nm.....	105
4.56	The classification of nucleotide by using Principal Component Analysis (PCA).....	106
4.57	PCA score plot of sensor arrays of Pydpa-Zn / Es-Zn / Es-Cu upon addition of various nucleotide anions (10 equiv) in aqueous solution of HEPES buffer 0.01 M, pH 7.4.....	108
4.58	PCA score plots of sensor arrays (A) Pydpa-Zn / Es-Zn , (B) Pydpa-Zn / Es-Cu and (C) Es-Zn / Es-Cu upon the addition of various nucleotide anions (10 equiv) in aqueous solution of HEPES buffer 0.01 M, pH 7.4. Sensor array including the fluorescence data of PPI anion for determining of PCA analysis.....	110
4.59	PCA score plot of sensor arrays Pydpa-Zn / Es-Zn / Es-Cu upon the addition of various nucleotide anions (10 equiv) in aqueous solution of HEPES buffer 0.01 M, pH 7.4. Sensor array excluding fluorescence data of PPI anion for determining of PCA analysis.....	112
4.60	PCA scores plot of sensor arrays of nucleotides sensors upon the addition of various nucleotide anions (10 equiv) in aqueous solution of HEPES buffer 0.01 M, pH 7.4. Sensor array excluded the fluorescence data of PPI anion for determining of PCA analysis.....	114

4.61	Fluorescence emission spectra of Pydpa-Zn+Es-Zn (1×10^{-5} M) upon the addition of various nucleotide anions (10 equiv) in aqueous solution of HEPES buffer 0.01 M, pH 7.4. ($\lambda_{\text{ex}} = 346$ nm).....	117
4.62	PCA score plot of Pydpa-Zn+Es-Zn upon the addition of various nucleotide anions (10 equiv) in aqueous solution of HEPES buffer 0.01 M, pH 7.4. The PCA score plot shows clustering for all 11 samples.....	117
4.63	Fluorescence emission spectra of Pydpa-Zn+Es-Cu (1×10^{-5} M) upon the addition of various nucleotide anions (10 equiv) in aqueous solution of HEPES buffer 0.01 M, pH 7.4. ($\lambda_{\text{ex}} = 346$ nm).....	118
4.64	PCA score plot of Pydpa-Zn+Es-Cu upon the addition of various nucleotide anions (10 equiv) in aqueous solution of HEPES buffer 0.01 M, pH 7.4. PCA score plot shows clustering for all 11 samples...	119
A1	Compared to the NMR spectra between PBI-(B(OH)₂)₂ (a), ATP (b) and PBI-(B(OH)₂)₂+ATP (c).....	131
A2	PCA score plot of Pydpa-Zn / Pydpa-Zn+Es-Zn upon addition of various nucleotide anions (10 equiv) in an aqueous solution of HEPES buffer 0.01 M, pH 7.4.....	131
A3	PCA score plot of Pydpa-Zn / Pydpa-Zn+Es-Cu upon addition of various nucleotide anions (10 equiv) in an aqueous solution of HEPES buffer 0.01 M, pH 7.4.....	132
A4	PCA score plot of Es-Zn / Pydpa-Zn+Es-Zn upon addition of various nucleotide anions (10 equiv) in an aqueous solution of HEPES buffer 0.01 M, pH 7.4.....	132

A5	PCA score plot of Es-Zn / Pydpa-Zn+Es-Cu upon addition of various nucleotide anions (10 equiv) in an aqueous solution of HEPES buffer 0.01 M, pH 7.4.....	133
A6	PCA score plot of Es-Cu / Pydpa-Zn+Es-Zn upon addition of various nucleotide anions (10 equiv) in an aqueous solution of HEPES buffer 0.01 M, pH 7.4.....	133
A7	PCA score plot of Es-Cu / Pydpa-Zn+Es-Cu upon addition of various nucleotide anions (10 equiv) in an aqueous solution of HEPES buffer 0.01 M, pH 7.4.....	134
A8	PCA score plot of Pydpa-Zn+Es-Zn / Pydpa-Zn+Es-Cu upon addition of various nucleotide anions (10 equiv) in an aqueous solution of HEPES buffer 0.01 M, pH 7.4.....	134
A9	PCA score plot of Pydpa-Zn / Es-Zn / Pydpa-Zn+Es-Zn upon addition of various nucleotide anions (10 equiv) in an aqueous solution of HEPES buffer 0.01 M, pH 7.4.....	135
A10	PCA score plot of Pydpa-Zn / Es-Zn / Pydpa-Zn+Es-Cu upon addition of various nucleotide anions (10 equiv) in an aqueous solution of HEPES buffer 0.01 M, pH 7.4.....	135
A11	PCA score plot of Pydpa-Zn / Es-Cu / Pydpa-Zn+Es-Zn upon addition of various nucleotide anions (10 equiv) in an aqueous solution of HEPES buffer 0.01 M, pH 7.4.....	136
A12	PCA score plot of Pydpa-Zn / Es-Cu / Pydpa-Zn+Es-Cu upon addition of various nucleotide anions (10 equiv) in an aqueous solution of HEPES buffer 0.01 M, pH 7.4.....	136

A13	PCA score plot of Pydpa-Zn / Es-Zn / Pydpa-Zn+Es-Zn / Pydpa-Zn+Es-Cu upon addition of various nucleotide anions (10 equiv) in an aqueous solution of HEPES buffer 0.01 M, pH 7.4.....	137
A14	PCA score plot of Pydpa-Zn / Es-Cu / Pydpa-Zn+Es-Zn / Pydpa-Zn+Es-Cu upon addition of various nucleotide anions (10 equiv) in an aqueous solution of HEPES buffer 0.01 M, pH 7.4.....	137
A15	PCA score plot of Es-Zn / Es-Cu / Pydpa-Zn+Es-Zn / Pydpa-Zn+Es-Cu upon addition of various nucleotide anions (10 equiv) in an aqueous solution of HEPES buffer 0.01 M, pH 7.4.....	138
A16	PCA score plot of Pydpa-Zn / Es-Zn / Es-Cu / Pydpa-Zn+Es-Zn upon addition of various nucleotide anions (10 equiv) in an aqueous solution of HEPES buffer 0.01 M, pH 7.4.....	138
A17	PCA score plot of Pydpa-Zn / Es-Zn / Es-Cu / Pydpa-Zn+Es-Cu upon addition of various nucleotide anions (10 equiv) in an aqueous solution of HEPES buffer 0.01 M, pH 7.4.....	139
A18	PCA score plot of Pydpa-Zn / Es-Zn / Es-Cu / Pydpa-Zn+Es-Zn / Pydpa-Zn+Es-Cu upon addition of various nucleotide anions (10 equiv) in an aqueous solution of HEPES buffer 0.01 M, pH 7.4.....	139

LIST OF SCHEMES

Scheme		Page
4.1	Concept of nucleotides sensing by gold nanoparticles via energy transfer process.....	62
4.2	Synthesis pathway of Monodpa	62
4.3	Synthesis pathway of Didpa	65
4.4	Synthesis pathway of Didpa_1	69
4.5	Synthesis pathway of Didpa_1-Zn	71
4.6	Synthesis pathway of PBI-(B(OH)₂)₂	73
4.7	Concept of nucleotides sensing by fluorophore replacement with nucleotides.....	79
4.8	Synthesis pathway of Rhodpa	80
4.9	Concept of nucleotides sensing by Principal Component Analysis (PCA).....	86
4.10	Synthesis pathway of Pydpa	87
4.11	Synthesis pathway of Pydpa-Zn	88
4.12	Synthesis pathway of Pydpa-Cu	90

LIST OF ABBREVIATIONS

°C	Degree Celsius
¹³ C-NMR	Carbon nuclear magnetic resonance
¹ H-NMR	Proton nuclear magnetic resonance
equiv.	Equivalent
g	Gram
Hz	Hertz
J	Coupling constant
mmol	Millimole
mL	Milliliter
nm	Nanometer
M	Molar
M ⁻¹	Per molar
δ	Chemicalshift
ppm	Part per million
s, d, t, m	Splitting patterns of ¹ H-NMR (singlet, doublet, triplet, multiplet)

CHAPTER I

INTRODUCTION

1.1 Concept of supramolecular chemistry

The importance of supramolecular chemistry becomes to be a major role with various disciplines such as organic, inorganic, physic, polymer and computational modeling [1]. The definition of supramolecular chemistry may be expressed in chemistry system of the association of two or more chemical species were formed held together by intermolecular forces such as hydrogen bonding, dipole-dipole, charge transfer, van der waals, or π - π stacking interactions [2]. The significant concepts of supramolecular chemistry have been demonstrated including the molecular self-assembly, folding, molecular recognition, host-guest chemistry, mechanically-interlocked molecular architectures, and dynamic covalent chemistry [3]. The structure of supramolecular systems divided into three types: i) molecular recognition; ii) translocation and iii) transformation [4]. Furthermore, supramolecular is studied more widely than the others and we will describe the major of fundamental concept of supramolecular chemistry by initially starting from molecular recognition.

1.2 Molecular recognition

Molecular recognition is a binding and specific selection with another molecule (a guest) which displays important role in biological system such as the recognition of the ammonium ion by a macrotricyclic cryptand, catalysis, and the self-replication of DNA [5]. The specific interaction of molecular recognition occurs through non-covalent bond. Moreover, molecular recognition implies a pattern-recognition process through a structurally well of intermolecular interactions. Factors influence a high degree of molecular recognition between host and guest as follow:

- a) Steric (shape and size) complementarity;
- b) Interactional complementarity;
- c) Large areas of contact between receptor and substrate;
- d) Multiple interaction sites;
- e) Strong overall binding;
- f) Inclusion and Dynamics;
- g) Medium effects on molecular recognition. [6]

1.3 Absorption of UV-visible light

Organic molecules containing π -electrons or non-bonding electrons (n-electrons) can absorb ultraviolet or visible light. The different molecules absorb the radiation of different wavelengths [7]. The molecular structure shows absorption spectrum corresponding to a number of absorption bands. Many organic molecules possess conjugated system which related the electronic excitations of the energy levels between the highest occupied molecular orbital (HOMO) and the lowest unoccupied molecular orbital (LUMO) corresponding to the molecular orbitals of the systems. When electrons of an atom or molecule receive energy, they are excited from ground state to excited state. In particular, the absorption of radiation of organic molecules can rotate and vibrate with respect to each other. The spectrum of molecule containing conjugated systems has stronger absorptions which considered from electronic transition. A diagram shown the various kinds of electronic excitation that may occur in organic molecules depicted in Figure 1.1.

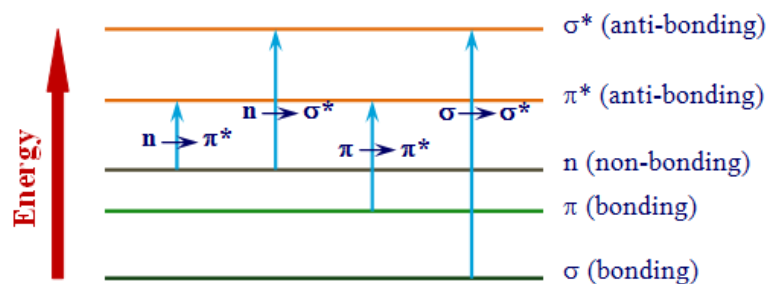


Figure 1.1 Possible electronic transitions in organic molecules

To understand conjugated systems, functionalized-molecule with functional groups of donor or acceptor group will perform charge transfer band (CT). In particular of molecule composed of donor and acceptor group, upon excitation with light, electron charge is transferred from donor to acceptor which influences on the absorption spectrum of chromophore. The phenomenon absorptions of chromophore have four patterns as follow:

- bathochromic (red) shift:** absorption spectrum shifted to longer wavelengths (λ_{\max} up);
- hypsochromic (blue) shift:** absorption spectrum shifted to lower wavelengths (λ_{\max} down);
- hyperchromic shift:** increased absorption light (ϵ_{\max} up);
- hypochromic shift:** decreased absorption light (ϵ_{\max} down).

Many inorganic species show charge-transfer absorption and are called charge-transfer complexes. For a complex to demonstrate charge-transfer behavior, one of its components must have electron donating properties and another component must be able to accept electrons. Absorption of radiation then involves the transfer of an electron from the donor to an orbital associated with the acceptor. The importance of conjugation is designed the chromogenic reagent that the interaction with anions in conjugated system displays resulting color change of molecule.

1.4 Phenomena of fluorescence

Luminescence is the phenomenon of the molecule absorbed and emitted of light at a longer wavelength. It is basically divided into two types; fluorescence and phosphorescence. The difference of both types is depending on the nature of excited state.

Fluorescence phenomenon is the emission of light from singlet-excited states which unchanged the spin multiplicity. From Table 1.1, the fluorescence lifetimes are approximated too short nearly nanoseconds level. Phosphorescence is the emission of light from triplet-excited states which changed the spin multiplicity. The emission rate of phosphorescence is too long estimated lifetimes in milliseconds to seconds level.

Generation of fluorescence or phosphorescence through excitation of a molecule by light is represented by Jablonski diagrams (Figure 1.2). A typical Jablonski diagram is basically an energy diagram that illustrated a singlet ground electronic state (S_0), singlet first (S_1) and second electronic excited state (S_2). After molecule received energy from light, electrons within molecule were excited from singlet ground state (S_0) to a higher vibrational energy level of excited state S_1 or S_2 , after that rapidly relaxing to the lowest energy level and release energy in the form light that call as fluorescence. The molecules in the S_1 state can undergo a spin conversion to the first triplet state (T_1), and the emission light is called phosphorescence light [8].

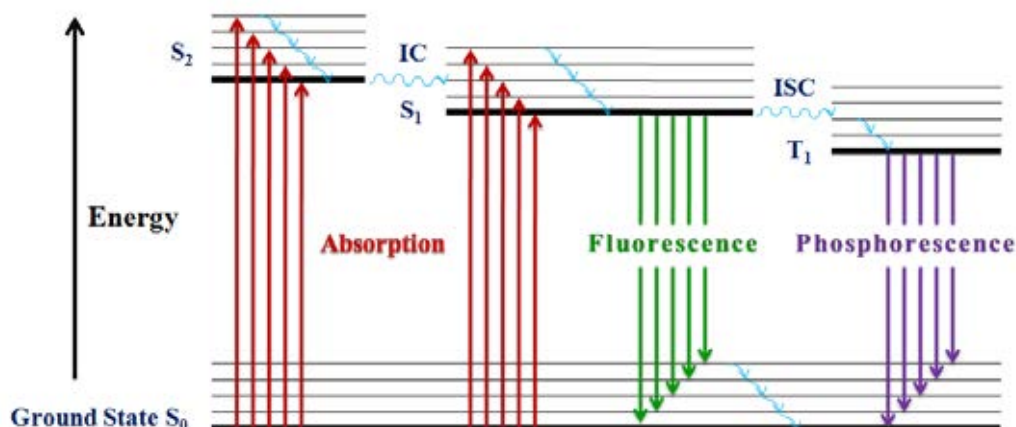


Figure 1.2 Jablonski diagram.

Table 1.1 Time scale of each transition

Transition	Time Scale
Absorption	10^{-15} s
Internal Conversion	10^{-14} - 10^{-11} s
Vibrational Relaxation	10^{-14} - 10^{-11} s
Fluorescence	10^{-9} - 10^{-7} s
Intersystem Crossing	10^{-8} - 10^{-3} s
Phosphorescence	10^{-4} - 10^{-1} s

Furthermore, factors affecting on fluorescence and phosphorescence signal are discussed as follow:

- a) Fluorescence and Structure;
- b) Structural Rigidity;
- c) Solvent Nature;
- d) Temperature;
- e) pH;
- f) Dissolved Oxygen;
- g) Concentration.

1.5 Cation-Anion sensors

Currently, selective recognition and sensing of cations and anions by artificial receptors have been explored in various areas [9-10]. Researchers have focused on designing and developing of molecular sensors used as the artificial receptors for selective toward a specific analyte. The particular cation-anion sensors were designed for sensing specific guests depending on their geometry such as spherical, linear,

tetrahedral and trigonal planar [11-14]. For instance, crown ether can bind with Na^+ , K^+ , and Mg^{2+} cations specifically because the shape of receptor and geometry of guests fit perfectly. Moreover, this receptor can be used as a polymer electrode showing a high responsibility toward selective ion. Furthermore, the important characteristic for good sensors are stability, metal selectivity, metal affinity, signal transduction, fluorescent signaling changing, kinetically rapid sensitization, ease of delivery to target systems, and availability. In the case of designing of sensor, [15] it should be accepted both recognition and signaling moieties. The signaling moiety acts as a signal transducer, into an optical signal expressing as the changes in the photophysical characteristics of the fluorophore. These changes are due to the influence of photoinduced processes such as electron transfer, charge transfer, energy transfer or disappearances, etc [16-19]. Thus, selective recognition and sensing of cations and anions are importance in many fields, ranging from environmental monitoring and industrial purposes to clinical diagnostics. In order to understand the molecular sensor, Figure 1.3 shows the model of chemosensor consisted of the signaling unit and binding site. Generally, the signal of signaling unit has been changed upon forming complex with a specific guest at binding site.

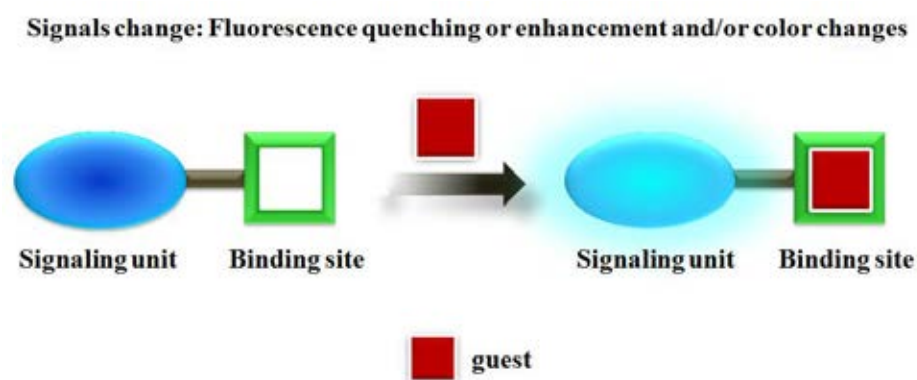


Figure 1.3 Chemosensors based on the binding site-signaling unit.

The important role of anion-cation sensors depends on the appropriation of shape and geometry of guest. Thus, the design and synthesis of molecular sensors are very important in the purpose of improvement for sensing guest species.

1.6 Determination of the stoichiometry of a complex by the method of continuous variations (Job's method) [20]

The determination of the complex formula could be accomplished in a variety of ways. One of the simpler techniques for determining the empirical composition of binary compounds or complexes is known as the method of continuous variation or Job's Method. To determine the stoichiometry of complex M_mL_l formed according to the equilibrium and the formation constant (β) for the metal (M)—ligand (L) reaction is given by



with

$$\beta_{ml} = \frac{[M_m L_l]}{[M]^m [L]^l} \quad 1.2$$

The principle of the method as follow: the fluorescence intensity Y is measured for a series of solutions consisting of the ligand and the metal that if C is the molar concentration of each of the metal and the ligand, thus, the sum of the total concentration of ligand and metal is constant.

$$C_L + C_M = C = \text{constant}$$

The position of the maximum of Y is then related to the ration m/l . The complex product is equal to Y_0 and the value of Y is related to no metal added ($x=0$). When plotting the variations in fluorescence intensity versus x , it is convenient to subtract the fluorescence intensity that would be measured in the absence of metal at every concentration.

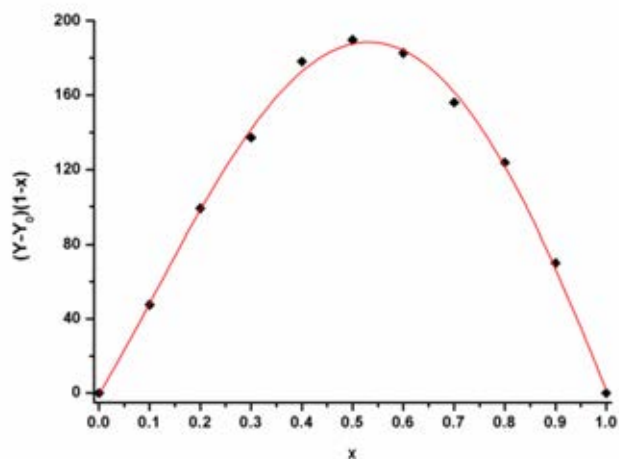
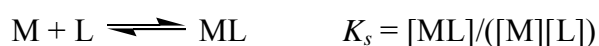


Figure 1.4 Job's plots for a 1:1 complex

1.7 Selectivity of receptors [21]

In general, the selectivity of a receptor toward guest is illustrated in the form of the stability constant (K_s). The chemists and biochemists can use a stability constant to determine the properties of metal-ligand reactions in water and biological systems. There are several methodologies for considering of binding constant such as NMR spectroscopy, UV-visible and fluorescence spectroscopy and electrochemical techniques.

The stability constant [22-23] (K_s) is the equilibrium constant that occurred from the equilibrium between the free ligand L, free metal and the complex ML. In general terms, the stability constant of a metal complex can be calculated as follows:



Where K_s is the stability constant;

M is the amount of metal ion;

L is the amount of a ligand.

It is easy to derive the following relation involving the absorbance A_0 of the free ligand and the absorbance A of the solution at a given wavelength where ε_L and ε_{ML} are the molar extinction coefficients of the ligand and the complex, respectively. The quantity $A_0/(A_0-A)$ is plotted versus $[M]^{-1}$, and the stability constant is then given by the ratio of intercept/slope.

$$\frac{A_0}{A_0 - A} = \frac{\varepsilon_L}{\varepsilon_L - \varepsilon_{ML}} \left(\frac{1}{K_s[M]} + 1 \right)$$

The various methods for determining the stability constants from fluorimetric data were previously discussed [29]. The best of them using the relation with Φ_L and Φ_{ML} are the quantum yields of the ligand and the complex, respectively. The quantity $IF^0/(IF-IF^0)$ is plotted versus $[M]^{-1}$, and the stability constant is then given by the ratio of intercept/slope.

$$\frac{I_F^0}{I_F^0 - I_F} = \frac{\varepsilon_L \Phi_L}{\varepsilon_L \Phi_L - \varepsilon_{ML} \Phi_{ML}} \left(\frac{1}{K_s[M]} + 1 \right)$$

1.8 Principal Component Analysis (PCA) [24]

Principal Component Analysis (PCA) is a statistic procedure that reduces data dimensionality by performing a covariance analysis between factors. Recently, the application of PCA has found in many fields such as face recognition and image compression. In chemistry, PCA is probably the most widespread multivariate chemometric technique, and it is regarded as the technique that most significantly changed the chemist's view of data analysis. Therefore, it will be easier to extract useful information from the reduced data set. One aim of chemometrics is to obtain these predictions after first treating the chromatogram as a multivariate data matrix, and then performing PCA. Each compound in the mixture is a 'chemical' factor with its associated spectra and elution profile, which can be related to principal components (PCs) by a mathematical transformation. Principal Components are a set of variables that define a projection expressing the maximum amount of variance in

the data and are all orthogonal to previous PCs of the same data. In matrix terms, this can be written as:

$$X = T \cdot P + E$$

Where:

X is the original data matrix;

T is the scores matrix;

P is the loadings matrix;

E is the error matrix.

To calculate the scores and loading matrices, if the original data matrix contains I samples and J variables, PCs are calculated until a sufficient amount of variance is described which if the number of PCs is denoted by A , so the maximum number of components is equal to I when $J > I$ or J , in case of $I > J$.

The dimension of T will be $I \times A$;

The dimension of P will be $A \times J$.

The matrices T and P are composed of several such vectors, one for each principal component. The first scores vector and the first loading vector are often called the eigenvectors of the first principal component. Figure 1.5 illustrates graphical representation of PCA.

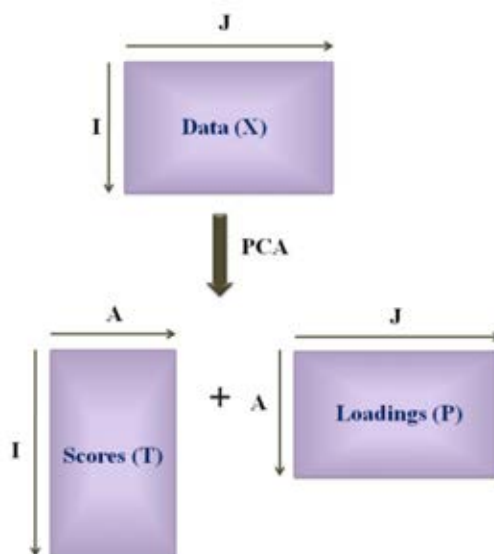


Figure 1.5 Principal Component Analysis

There are a number of important features of scores and loadings. It is important to recognize the aim of PCA involves finding mathematical functions that contain certain properties which can then be related to chemical factors, and in themselves PCs are simply abstract mathematical entities.

All scores and loadings vectors have the following property:

- a) Linearity;
- b) Large variances have important structure;
- c) The principal components are orthogonal.[25]

After PCA, the original variables are reduced to a number of significant principal components. PCA can be used as a form of variable reduction, reducing the large original data set to a much smaller more manageable data set which can be interpreted more easily, as illustrated in Figure 1.6.

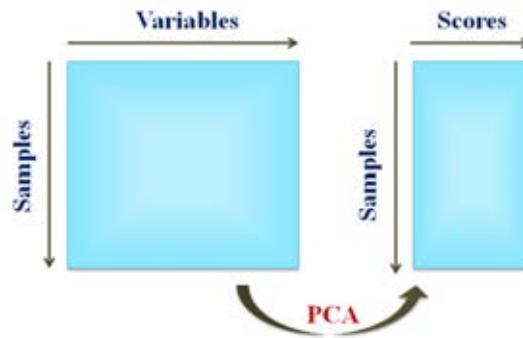


Figure 1.6 PCA as a form of variable reduction

A simple example of principal component of the data is illustrated in Figure below. It can be seen that the main variance is along PC1 and that PC2 is orthogonal to PC1.

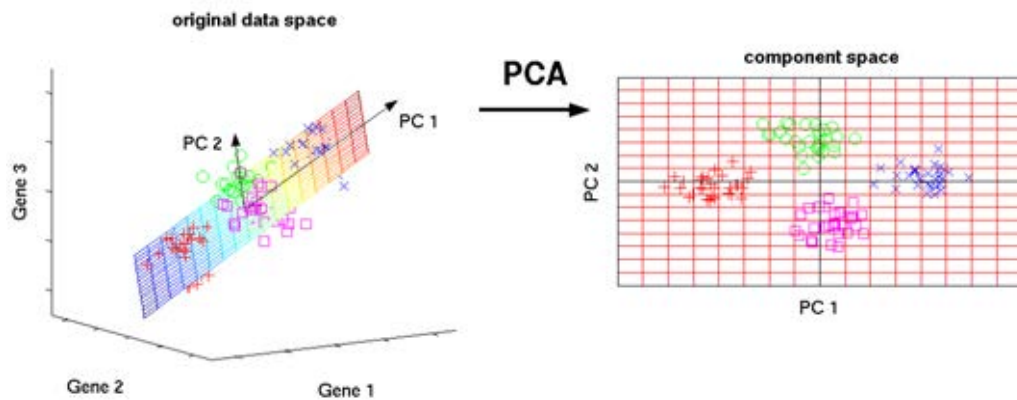


Figure 1.7 Graphical representation of samples in the original space (Left) and the position of samples in PC spaces (Right)

CHEAPTER II

LITERATURE REVIEWS

2.1 Literature reviews

2.1.1 Nucleotides

Nucleotides are the building blocks of all nucleic acids which are essentially biological molecules for life. In the biological system, nucleic acids are divided into two types, deoxyribonucleic acid (DNA) and ribonucleic acid (RNA). In cells, information stored in DNA is used to control cellular activities through the formation of RNA messages [26]. Thus, nucleoside chemistry plays a vital role in the development of the most important drugs used to combat cancer and viral diseases [27]. Typically, nucleotides consisting of a five carbon sugar (ribose in RAN or deoxyribose in DNA), a nitrogenous base and a phosphate group are the basic structure of DNA in living creature (Figure 2.1).

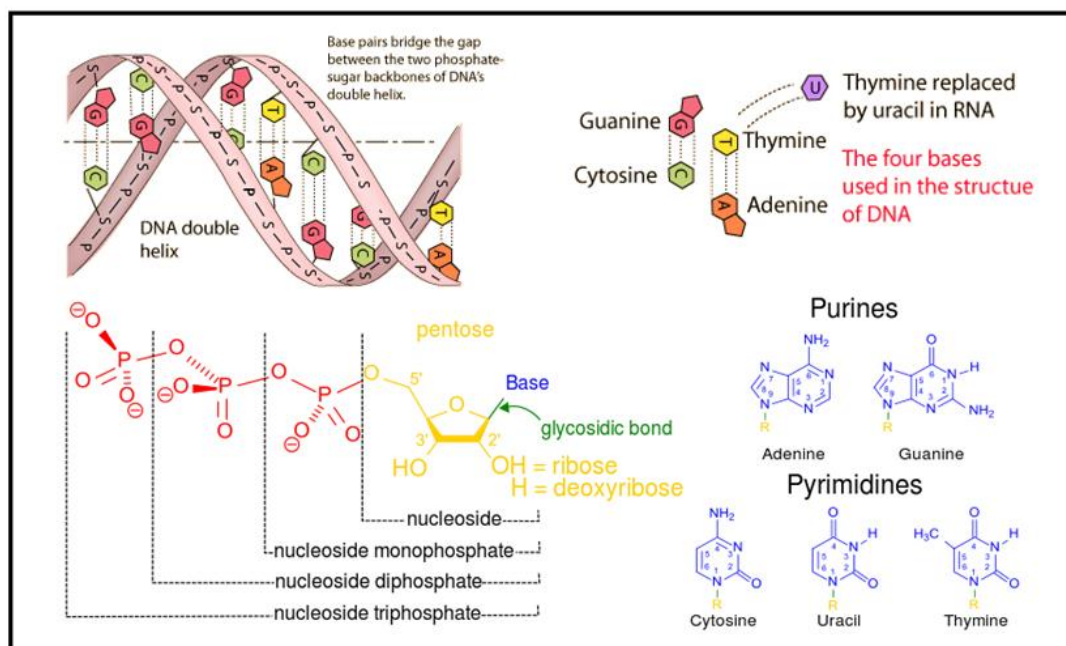


Figure 2.1 Composition of nucleotides.

2.1.2 Receptor of metal-sensing

In recent years, many researches have been focused on the study for metal sensing, especially Zn^{2+} and Cu^{2+} ions because they can apply to bind with the phosphate groups based on nucleotides [28]. Generally, ligands are commonly used to bind with Zn^{2+} ions such as dipicolylamine (DPA) [29-30], porphyrin [31] and organic ligand [32]. Ligand construction was designed in the form of tridentate ligands for tetrahedral zinc model complexes by the groups of Burzlaff [33-34]. DPA is the most popular ligand because it has three positions of nitrogen atom for coordination toward transition metal ions. Lim and coworkers [35] have been successfully designed and synthesized a new molecular sensor for a high selectivity toward Zn^{2+} ions. They used coumarin derivatives which containing dipicolylamine as a binding site as shown in Figure 2.2.

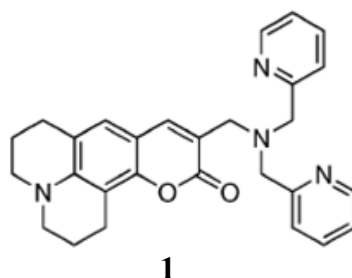


Figure 2.2 Molecular structure of DPA derivative of sensor **1**.

The spectrophotometric titration of sensor **1** with Zn^{2+} ion showed in Figure 2.3A. The bathochromic shift (31 nm) in absorption spectra upon the addition of Zn^{2+} demonstrated the metal ion-induced perturbation of the chromophore electronic structure. Moreover, incremental addition of Zn^{2+} showed a red shift ($\Delta\lambda_{\text{em}} = 21$ nm) of the maximum emission band from 484 to 505 nm. Considering the complexation of $1 \cdot \text{Zn}^{2+}$, the binding mode between sensor molecule **1** and Zn^{2+} displayed for coordinations of Zn^{2+} towards three nitrogen atoms of DPA and one oxygen atom of lactone.

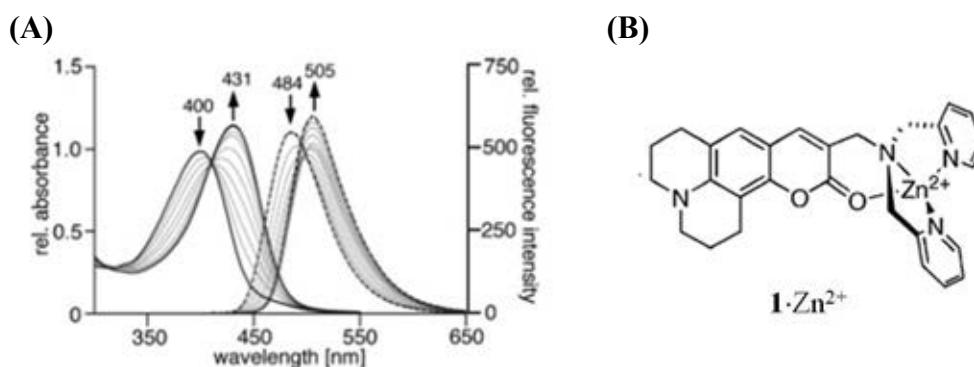


Figure 2.3 (A) Absorption and emission spectra of **1** upon addition of Zn^{2+} in MeOH and (B) molecular structure of $\mathbf{1}\cdot\text{Zn}^{2+}$ ion.

In the case of Cu sensor, many researches reported the fluorescence quenching in the presence of Cu^{2+} ion [36] and a few researches reported the performance of fluorescence enhancement [37]. For example of Cu^{2+} , Xu and coworkers have reported the fluorescence enhancement of sensor molecule upon binding with Cu^{2+} . They designed the fluorogenic sensor containing of 1,8-naphthalimide as a fluorophore and a picolyl group as a binding site for Cu^{2+} ion as shown in Figure 2.5 [38].

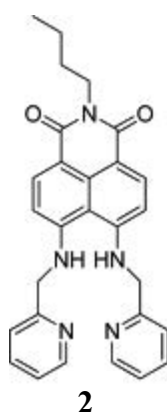


Figure 2.4 Molecular structure of sensor **2**

The sensor **2** showed a 50 nm blue shift of fluorescence emission and provided high selectivity for Cu^{2+} over other heavy and transition metal ions in an ethanol-water solution (40:60, v/v) as shown in Figure 2.5A. This result indicated that Cu^{2+} induced to change of charge-transfer of the emissive species, including fluorescence color changes from green to blue upon the addition of Cu^{2+} ion as shown in Figure 2.5B.

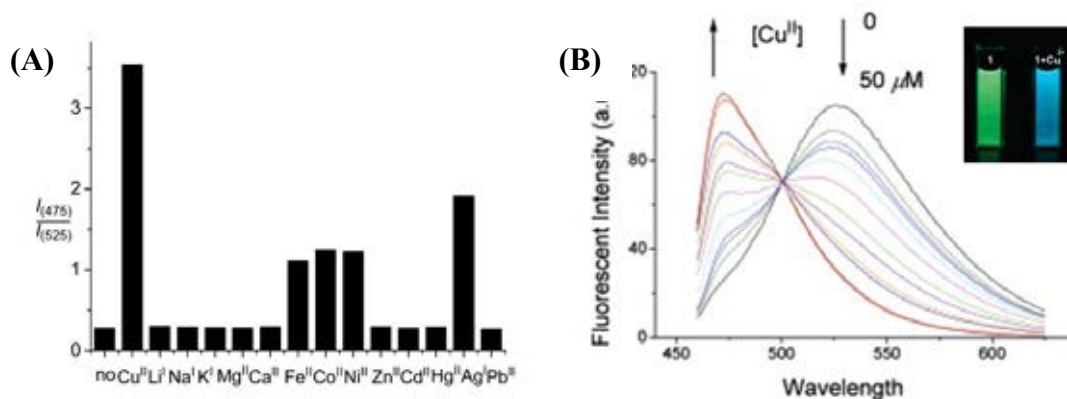


Figure 2.5 (A) Fluorescence response of sensor **2** with metal ions and (B) Fluorescent emission spectra of sensor **2** in the presence of different concentration of Cu^{2+} in in EtOH:H₂O (40:60 v/v, 50mM HEPES buffer, pH 7.2).

2.1.3 Nucleotides sensing

Application of fluorescent sensing of Zn or Cu complex has been developed for nucleotides sensing. Molecular sensor for binuclear Zn complex would be appreciated to design because it can coordinate with the phosphate and nucleobase on nucleotides [39-42]. For examples, Chen and coworker [43] have been reported of Zn-complex for high selectivity toward PPi which is a product of ATP hydrolysis and it is important issue in cancer research [44]. The molecular structure was designed into binuclear Zn(II) complex bound to dipicolylamine as shown in Figure 2.6A.

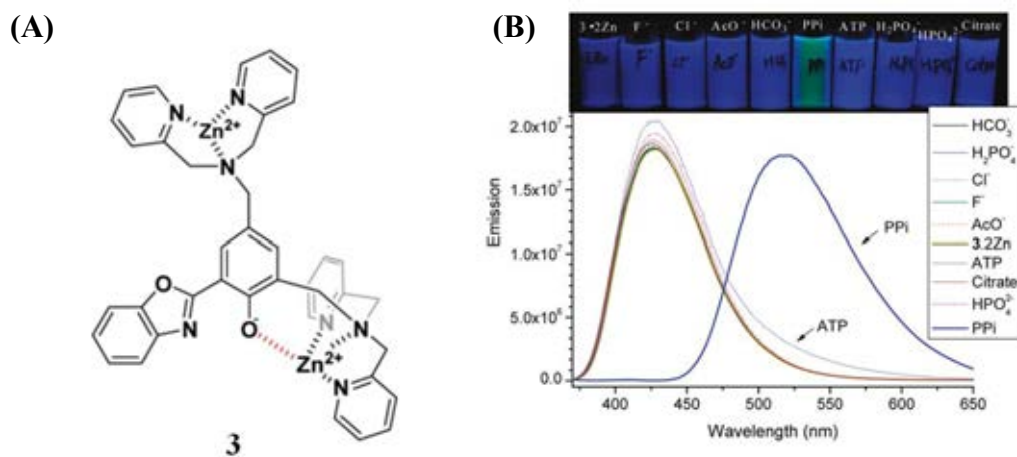


Figure 2.6 (A) Molecular sensor and (B) fluorescence changing of sensor **3** in 0.01 M HEPES buffer (pH 7.4) upon addition the anions.

Fluorescence signal of sensor **3** responded to PPI over other anions. The fluorescence spectrum shifted from 420 nm to 518 nm and the fluorescence color changed from blue to green (Figure 2.6B). A large shift of emission band stemmed from excited state intramolecular proton transfer (ESIPT) which was explained in Figure 2.7.

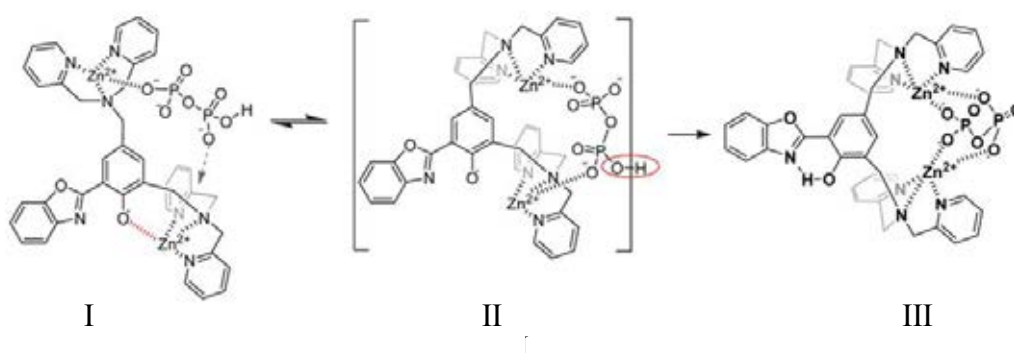


Figure 2.7 Explanation of responded mechanism of sensor **3** with PPI.

In 2007, Jose and coworker [45] have been successfully sensing of ATP by the naked-eyes. The Chemosensor consisted of amino-phenylazo as a signaling unit and the DPA bound with Zn^{2+} as a binding site for coordination with nucleotides (Figure 2.8A). UV-visible spectroscopy was used for complexation studies between sensor **4** and various nucleotides. The results showed the bathochromic shift from 463 to 484 nm upon the addition of ATP into solution of sensor **4**·Zn as shown in Figure 2.8B. The color solution changed from pale yellow to light pink upon the adding of ATP. Furthermore, complex **4**·Zn can be used as a dye in yeast cells which can visualize under normal light of microscopy (Figure 2.8C).

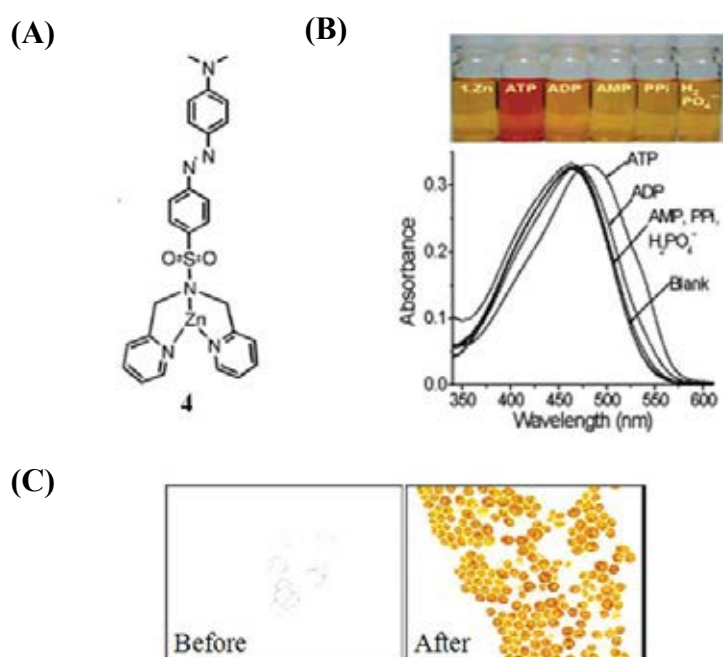


Figure 2.8 (A) Molecular structure of sensor **4**, (B) absorption spectra of sensor **4** upon addition various nucleotides in HEPES buffer (pH 7.2) and (C) Light microscopy images for before and after added the sensor **4**.

Moreover, Cu-complex for nucleotides sensing have also reported by Gou and coworkers [46]. They designed and synthesized sensor **5** which is a hydrophilic film fluorescence sensor based on poly(HEMA-co-DCPDP) for monitoring high throughput bioprocessing in continuous system. The results showed that the binding ability of sensor **5** had a highly selective and sensitive sensing to Cu^{2+} ions over other metal (Figure 2.9A). In the presence of Cu^{2+} , sensor **5** showed a strong fluorescence

quenching due to the capture of Cu^{2+} ion by receptor DPA. The fluorescence quenching may be rationalized by the reduction of the electron donating ability of amino group resulting in a decrease of the ICT efficiency. Interestingly, the strongly fluorescence enhancement was observed upon the addition of PPI (Figure 2.9B). The significant fluorescence enhancement might be attributed to the electrostatic interaction between PPI and Cu^{2+} to reduce the magnitude of the electron withdrawing.

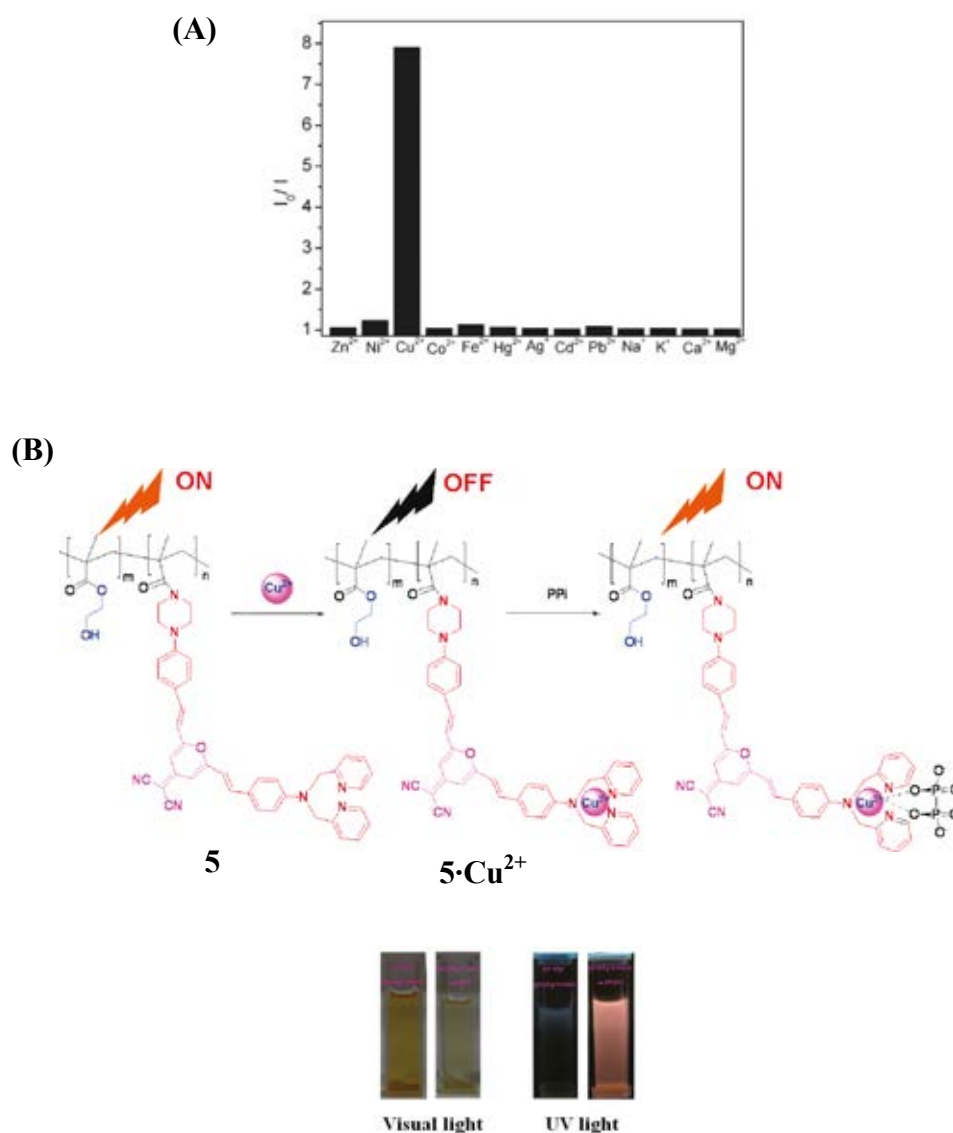


Figure 2.9 (A) Fluorescence response of poly(HMAM-co-MDCPDP) in H_2O : EtOH (2:5 v/v, pH 7) upon addition of various metal ions and (B) The fluorescence “on-off-on” of sensor **5** upon addition of Cu^{2+} and PPI, respectively.

2.1.4 Application of gold nanoparticles

Metallic nanoparticles such as gold and silver are extensively studied which they can detect analytes in the low levels. Particularly, gold nanoparticles demonstrated a large plasmon absorption band in the visible region dependent on size and shape [47]. The property of gold nanoparticles in the optical property is the color change of solution upon changing the size of the gold nanoparticles including fluorescence quenching upon packing on the surface of gold nanoparticles. For example, Sudeep and coworkers [48] improved the surface of the gold nanoparticles with fullerene derivative (Fullerenethiol). From the fluorescence spectra, fullerenethiol were quenched upon coated the gold nanoparticles as showed in the Figure 2.10. This result showed the energy transfer from fullerene to gold nanoparticles.

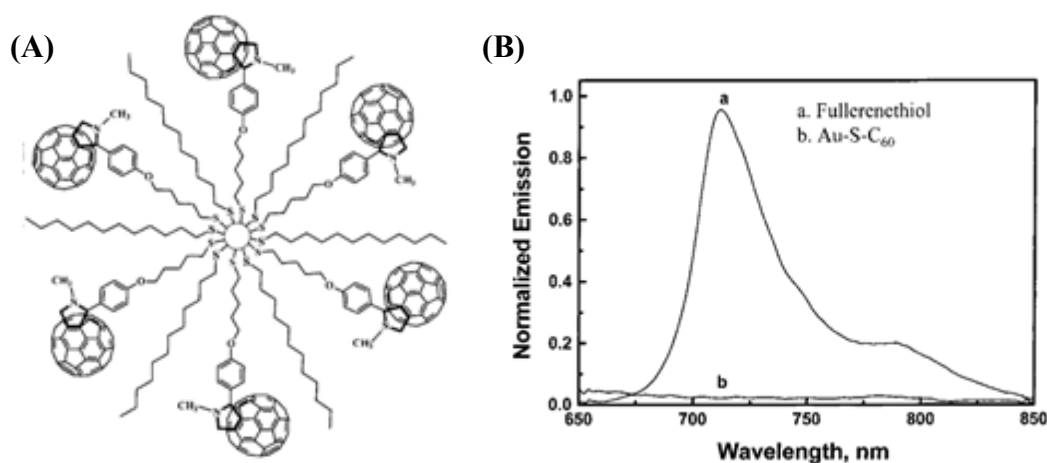


Figure 2.10 (A) Modification of gold nanoparticles with derivatives fullerenethiol and (B) fluorescence spectra of fullerenethiol before and after modified gold nanoparticles.

In 2011, Manju and Sreenivasan [49] have been studied the detection of glucose in tear fluid which glucose concentration in tears related the blood glucose concentration by application the gold nanoparticles in this research. He synthesized gold nanoparticles using dextran as a stabilizer (**Dex@AuNPs**) which showed absorption band at 530 nm. The modified gold nanoparticles with aminophenyl

boronic acid through Schiff's base reaction (**ABA@AuNPs**) as a binding site for glucose and complexed with Rhodamine_B isothiocyanate (**RBITC@AuNPs**) were prepared. From the UV-visible spectroscopy, the surface plasmon band of **ABA@AuNPs** and **RBITC@AuNPs** exhibited at 536 and 544 nm, respectively (Figure 2.11). Upon RBITC coated on the surface of gold nanoparticles, fluorescence spectrum showed hypsochromic shift ($\Delta\lambda = 16$) from 594 to 578 nm stemmed from hydrophobic environment and exhibited fluorescence quenching via fluorescence resonance energy transfer or electron transfer type mechanism (Figure 2.12A). For detection of glucose in tears fluid, fluorescence of **RBITC** was increased upon the increasement of glucose (Figure 2.12B). The indicated that glucose had a strong affinity to boronic acid and the glucose concentration can detect in the range of micromolar.

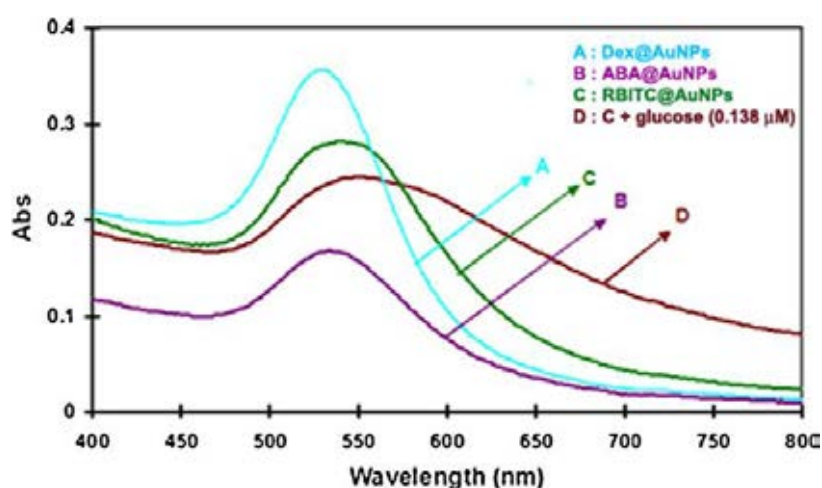


Figure 2.11 Plasmon absorption spectra of (A) **Dex@AuNPs**, (B) **ABA@AuNPs**, (C) **RBITC@AuNPs** and (D) in the presence of glucose (0.138 μM)

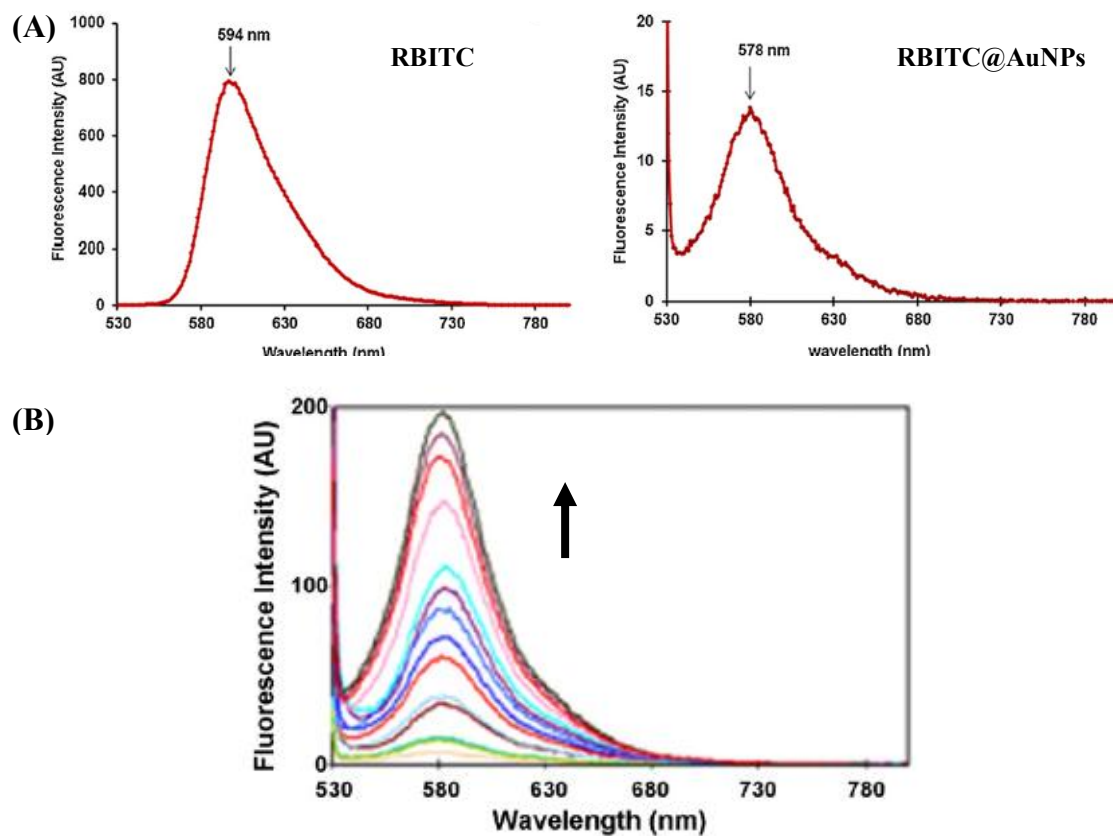


Figure 2.12 (A) Fluorescence spectra of **RBITC** (left) and **RBITC@AuNPs** (right) and (B) fluorescence spectra of **RBITC@AuNPs** upon the increase of glucose.

2.1.5 Nucleotides sensing by using Principal Component Analysis (PCA)

In addition, a few research used the mathematical procedure for classification of nucleotides. The “Principal Component Analysis (PCA)” is a mathematical procedure which is widely used owing to separate a similar material such as metal [50-53], peptide [54-55] and disease [56]. The principle of PCA reduced dimensionality of the large original data set to a much smaller data for easy interpretation. For example of using PCA method for discrimination of nucleotides, Buryak and coworkers [57] have studied the nucleotides detection in aqueous solution using multicomponent indicators displacement assay (MIDA). Recognition pattern applied the Rh complex as a receptor and three different indicators (Mordant Yellow 10, Gallocyanine and Evans Blue) as shown in Figure 2.13A. Indicators for MIDA assay have a different binding ability with Rh complex inducing the absorption change in different regions. Possibility of three sensors responded to the different analyt as show in Figure 2.13B.

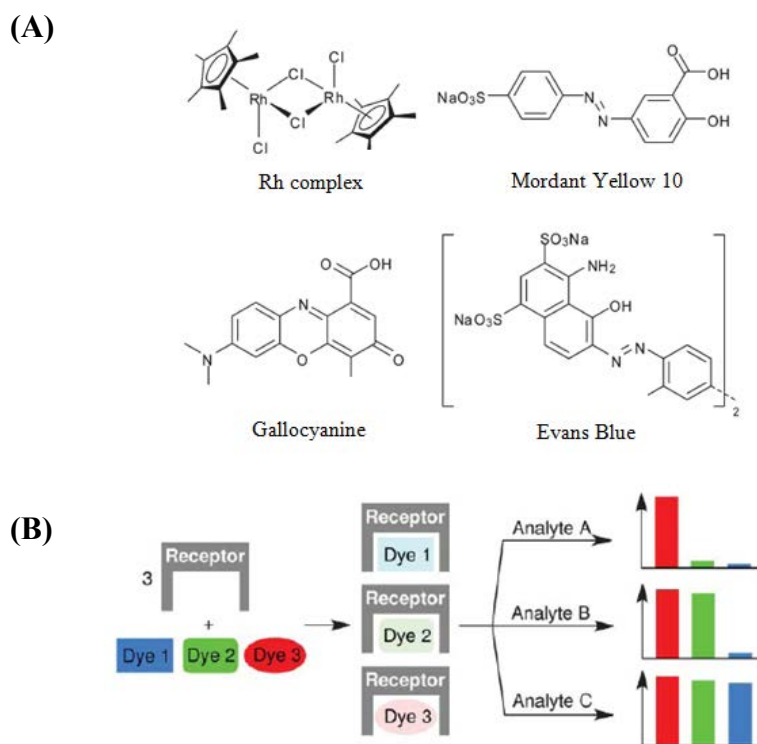


Figure 2.13 (A) Receptor and indicators used for MIDA assay and (B) possibility of three sensors for analyt.

Efficiency coordination of Rh complex with three dyes showed the different association constants of $3.7(\pm 0.3) \times 10^4 \text{ M}^{-1}$ and $2.3(\pm 0.2) \times 10^6 \text{ M}^{-1}$, corresponding to Mordant Yellow 10 and Gallocyanine, respectively, while the binding ability of Evans Blue with Rh complex cannot be calculated. Figure 2.14A represented the absorption spectra of three sensors in phosphate buffer (pH 7.4). The discrimination of six nucleotides including ATP, ADP, AMP, cAMP, PPi and GTP was investigated by Linear Discriminant Analysis (LDA). The results showed a successful classification of nucleotides as shown in Figure 2.14B.

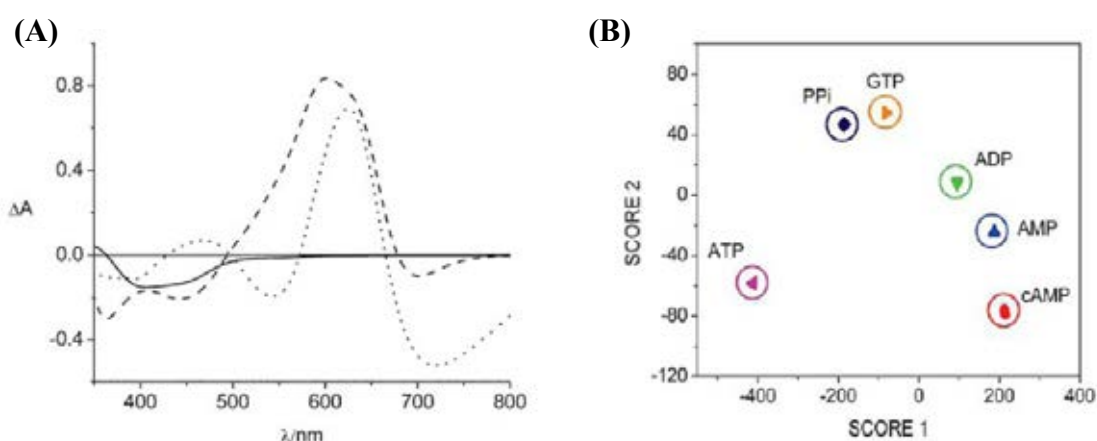
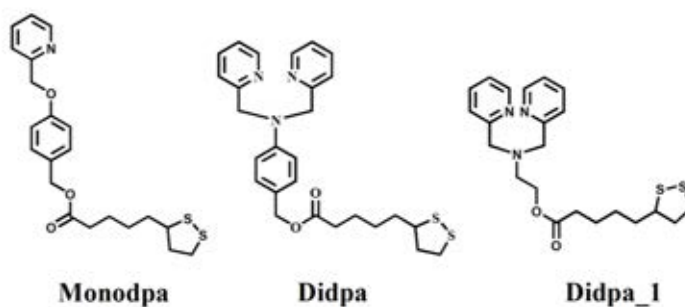


Figure 2.14 (A) Absorption spectra of three sensor and (B) LDA score plot of three sensors for discrimination of six nucleotides.

2.2 Objective and scope of this research

The main goals of this research are to design and synthesize the molecular sensors for nucleotide detection. The concepts of nucleotide sensing in this research have been studied into two approaches: i) the energy transfer from fluorophore to gold nanoparticles; and ii) the discrimination of the similarity of nucleotides by Principal Component Analysis (PCA) method. Both concepts employed UV-visible and fluorescence spectroscopy. Furthermore, the modification of gold nanoparticles with **Monodpa**, **Didpa** or **Didpa_1** was studied for metal sensing upon the aggregation of gold nanoparticles by UV-visible spectroscopy. Molecular structures were used in this research as shown in Figure 2.15.

Receptor for modification of AuNPs



Chromosensor for nucleotides sensing

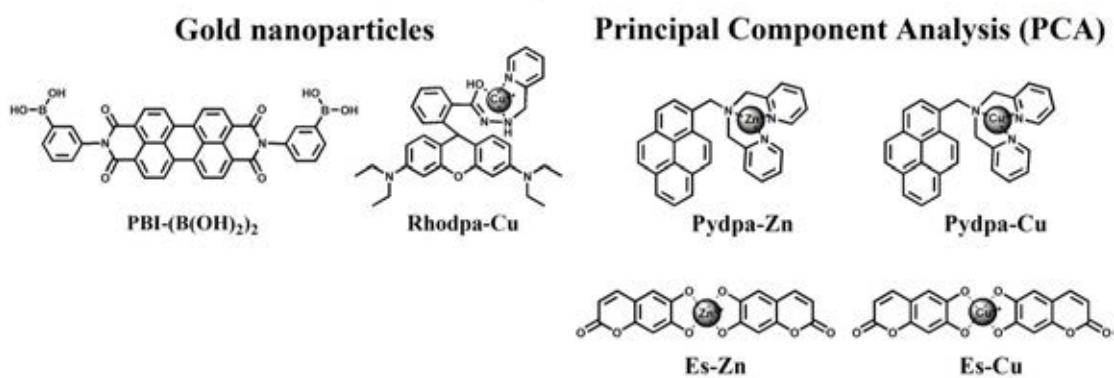


Figure 2.15 Molecular structures were studied in this work.

CHAPTER III

EXPERIMENTAL SECTION

3.1 Materials and Physical measurements

All materials were obtained from Aldrich, Fluka, BDH, Merk, Carlo-reba or Lab scan. The solvents as a commercial grade solvents such as dichloromethane, methanol, toluene, ethyl acetate, acetone and dimethyl formamide were purified by distillation prior to use. The preparation of **Rhodpa-Cu** was according to the published procedure [58]. The solvents used in UV-visible and fluorescence measurement (AR grade, Lab Scan: dimethyl sulfoxide, dichloromethane and toluene) were dried over molecular sieve before used. Nuclear magnetic resonance (^1H and ^{13}C) spectra were measured on Varian 200, 400 and Bruker DRX 400 MHz. The chemical shifts were given in part per million (ppm). ESI-MS was performed on Bruker Daltonic using 2-cyano-4-hydroxy cinnamic acid (CCA) as matrix. Absorption spectra were obtained using on a Varian Cary 50 UV-Vis spectrophotometer. Fluorescence spectra were obtained using on Varian spectrofluorometer. The excitation and emission slit of all emission spectra were collected at 5 nm.

3.2 Synthesis of gold nanoparticles

Gold nanoparticles were synthesized in two systems using the different stabilizers and solvents:

- i) Synthesis of gold nanoparticles in H_2O using citrate as a stabilizer;
- ii) Synthesis of gold nanoparticles in toluene using tetraalkylammonium bromides (TOABr) as a stabilizer

3.2.1 Synthesis of Gold nanoparticles in H₂O

Gold nanoparticles were synthesized according to recently reported procedures [59-61]. Aqueous solution of hydrogen tetrachloroaurate (20 mL, 0.25 mM) and sodium citrate (20 mL, 2.5 mM) were mixed and stirred for 20 min. A portion of aqueous sodium borohydride (0.5 mL, 0.1 M) was added into the mixture. Immediately, the solution was turned to red and kept stirring for 2 h to ensure the complete reaction.

3.2.2 Synthesis of Gold nanoparticles in toluene

Gold nanoparticles in toluene were prepared using as phase-transfer of tetraalkylammonium bromides (TOABr) [62]. An aqueous solution of hydrogen tetrachloroaurate (30 mL, 30 mM) was mixed with tetraoctylammonium bromide in toluene (80 mL, 50 mM). The two-phase was vigorously stirred for 30 min. Tetrachloroaurate was transferred to the organic phase. An aqueous sodium borohydride (25 mL, 0.4 M) was slowly added while the solution was vigorously stirred. The color of solution was turned to ruby red and the mixture was stirred continuously for 15 minute to ensure the complete reaction. The organic phase was extracted and neutralized with 3 M HCl. The solution was washed with milli Q water five times and dried over anhydrous sodium sulfate to afford a ruby-colored gold nanoparticle which should be was stored in dark at room temperature.

3.3 Modification of gold nanoparticles

3.3.1 Modification of gold nanoparticles in H₂O using citrate as a stabilizer

3.3.1.1. Modification of gold nanoparticles by Monodpa

Aqueous solution of gold nanoparticles (0.001 M 10 mL) was added with a portion of **Monodpa** (40.31 mg 0.01 M) in 10 mL dichloromethane and the mixture was stirred vigorously for 2 h. **Monodpa** was transferred to the aqueous phase and the red color of solution did not change.

3.3.1.2. Modification of gold nanoparticles by Didpa

Aqueous solution of gold nanoparticles (0.001 M 10 mL) was added with a portion of **Didpa** (49.32 mg 0.01 M) in 10 mL dichloromethane and the mixture was stirred vigorously for 2 h. **Didpa** was transferred to the aqueous phase. Instantly, the red color of solution was turned to purple.

3.3.1.3. Modification of gold nanoparticles by Didpa_1

Aqueous solution of gold nanoparticles (0.001 M 10 mL) was added with a portion of **Didpa_1** (43.12 mg 0.01 M) in 10 mL dichloromethane and the mixture was stirred vigorously for 2 h. **Didpa_1** was transferred to the aqueous phase. Instantly, the red color of solution was turned to purple.

3.3.1.4. Modification of gold nanoparticles by Didpa_1-Zn

Aqueous solution of gold nanoparticles (0.001 M 10 mL) was added with a portion of **Didpa_1-Zn** (49.51 mg 0.01 M) in 10 mL dichloromethane and the mixture was stirred vigorously for 2 h. **Didpa_1-Zn** was transferred to the aqueous phase. Instantly, the red color of solution was turned to blue.

3.3.2 Modification of gold nanoparticles in toluene using tetraalkyl-ammonium bromides (TOABr) as a stabilizer

3.3.2.1. Modification of gold nanoparticles by Didpa_1-Zn in 10% toluene in DMSO

Gold nanoparticles (0.01 M 1.0 mL) were diluted in 9.0 mL dimethyl sulfoxide and then the portion of **Didpa_1-Zn** (49.51 mg 0.1 M) in 1.0 mL dimethylsulfoxide was added into the solution of gold nanoparticles. The mixture was stirred for 2 h. Consequently, the color of solution was changed from red to red-pink.

3.4 Metal sensing

Typically, 1.0×10^{-4} M of modified gold nanoparticles with **Monodpa** or **Didpa_1** was prepared in milli Q water. The stock solution of metal ions (0.01 M) in H₂O (Cd²⁺, Co²⁺, Cu²⁺ and Zn²⁺) was prepared in 5 mL volumetric flask (showed in Table 3.1).

The 1.0 mL of modified gold nanoparticles with **Monodpa** was putted in cuvette and diluted to 2 mL. After that, the solution of each metal ion (10 μ L) was putted in cuvette and stirred for 1 min. The absorption spectra were recorded from 200-800 nm.

Table 3.1 The amounts of metal ions used in UV-visible studies.

Metal	Mw	weight (mg)
Cd(NO ₃) ₂ ·4H ₂ O	308.47	15.42
Co(NO ₃) ₂ ·6H ₂ O	291.04	14.55
Cu(NO ₃) ₂ ·3H ₂ O	241.60	12.08
Zn(NO ₃) ₂ ·6H ₂ O	297.48	14.87

3.5 Complexation studies for nucleotides detection

In this research, we have studied the nucleotides sensing which are divided into two different processes: i) using the gold nanoparticles and ii) using the Principal Component Analysis (PCA).

3.5.1 Using gold nanoparticles for using the nucleotides detection

Gold nanoparticles used for nucleotides sensing procedure are divided into two systems as following:

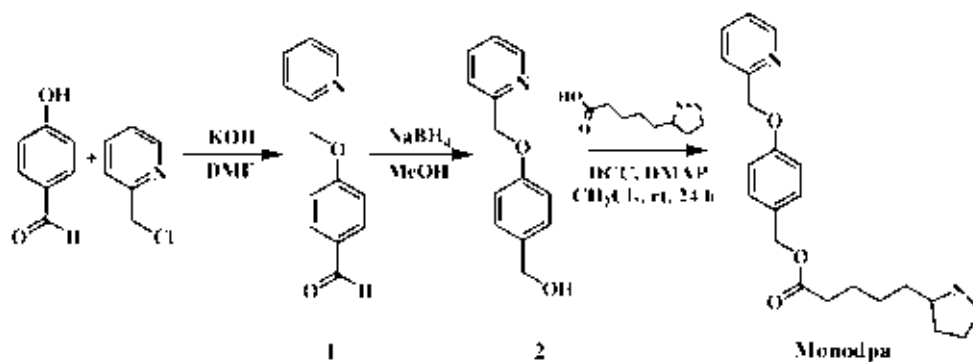
- i) Complexation between fluorophore and gold nanoparticles;
- ii) Fluorophore replacement with nucleotides.

3.5.1.1 Complexation studies between fluorophore and modified gold nanoparticles by fluorescence spectroscopy

3.5.1.1.1 Modification of gold nanoparticles parts

Preparation of 4-(pyridin-2-ylmethoxy)benzyl 5-(1,2-dithiolan-3-yl)pentanoate

(Monodpa)



• Synthesis of 4-(pyridin-2-ylmethoxy)benzaldehyde (1)

4-hydroxybenzaldehyde (1.709 g, 14 mmol) and potassium hydroxide (0.729 g, 13 mmol) was dissolved in anhydrous dimethyl formamide (25 mL) and stirred for 1 h. A portion of 2-(chloromethyl) pyridine hydrochloride (0.980 g, 6.0 mmol) in 5 mL dimethyl formamide was added to the mixture solution and stirred for 24 h at room temperature. The reaction mixture was extracted with ethyl acetate and washed with saturated sodium chloride. The organic phase was dried over anhydrous sodium sulfate and the solvent was removed in vacuum to give the yellow solid of compound **1** (0.647 g, 53%).

Characterization data for compound **1**

¹H-NMR spectrum (400 MHz, CDCl₃) : δ (in ppm) = 9.88 (s, 1H), 8.62 (d, 1H, *J* = 4.8 Hz), 7.84 (d, 2H, *J* = 6.8 Hz), 7.73 (t, 1H, *J* = 7.6), 7.50 (d, 1H, *J* = 6 Hz), 7.28 (d, 1H, *J* = 12 Hz), 7.10 (d, 2H, *J* = 8.4 Hz), 5.29 (s, 2H)

MS(ESI): *m/z* for C₁₃H₁₁NO₂ = 213.190 [M+H]⁺

- **Synthesis of compound (4-(pyridin-2-ylmethoxy)phenyl)methanol (2)**

The solution of compound **1** (0.5 g, 2.35 mmol) in methanol was carefully added to the solution of sodium borohydride (1.778 g, 47 mmol) in methanol which was placed in ice bath. After stirred at room temperature for 2 h, the solution mixture was treated with 3M HCl to adjust pH 7. The solvent was removed under reduced pressure and the residue was extracted with dichloromethane. The organic phase was dried over anhydrous sodium sulfate and evaporated under vacuum to give the yellow solid of compound **2** (0.454 g, 90%).

Characterization data for compound 2

¹H-NMR spectrum (400 MHz, CDCl₃) : δ (in ppm) = 8.59 (d, 1H, *J* = 4 Hz), 7.71 (t, 1H, *J* = 7.6 Hz), 7.51 (d, 1H, *J* = 8 Hz), 7.21-7.30 (m, 3H), 6.96 (d, 2H, *J* = 8.8 Hz), 5.19 (s, 2H), 4.62 (s, 2H)

MS(ESI): *m/z* for C₁₃H₁₃NO₂ = 215.095 [M+H]⁺

- **Synthesis of 4-(pyridin-2-ylmethoxy)benzyl 5-(1,2-dithiolan-3-yl)pentanoate (Monodpa)**

Compound **2** (0.454 g, 2 mmol), dicyclohexyl carbodiimide, DCC (0.435 g, 2 mmol) and 4-dimethylamino pyridine, DMAP (0.129 g, 1.0 mmol) were stirred in 30 mL dichloromethane for 30 min. Into the reaction mixture, (±)-α- lipoic acid (0.435 g, 2 mmol) in 20 mL dichloromethane was added dropwise over 30 min and the reaction mixture was stirred at room temperature for 24 h and then treated with 3M HCl to adjust pH 7.0. The mixture was extracted with dichloromethane. The organic phase was dried over anhydrous sodium sulfate and evaporated by rotary evaporater. The crude product was purified by column chromatography using 40% ethyl acetate in dichloromethane to give the yellow oil of **Monodpa** (0.196 g, 32%).

Characterization data for Monodpa

¹H-NMR spectrum (400 MHz, CDCl₃) : δ (in ppm) = 8.59 (d, 1H, J = 4 Hz), 7.71 (t, 1H, J = 8 Hz), 7.51 (d, 1H, J = 7.6 Hz), 7.21-7.30 (m, 3H), 6.97 (d, 2H, J = 8.8 Hz), 5.21 (s, 2H), 5.04 (s, 2H), 3.52-3.57 (m, 1H), 3.06-3.19 (m, 2H), 2.41-2.47 (m, 1H), 2.34 (t, 2H, J = 7.6 Hz), 1.83-1.95 (m, 1H), 1.63-1.69 (m, 4H), 1.39-1.49 (m, 2H)

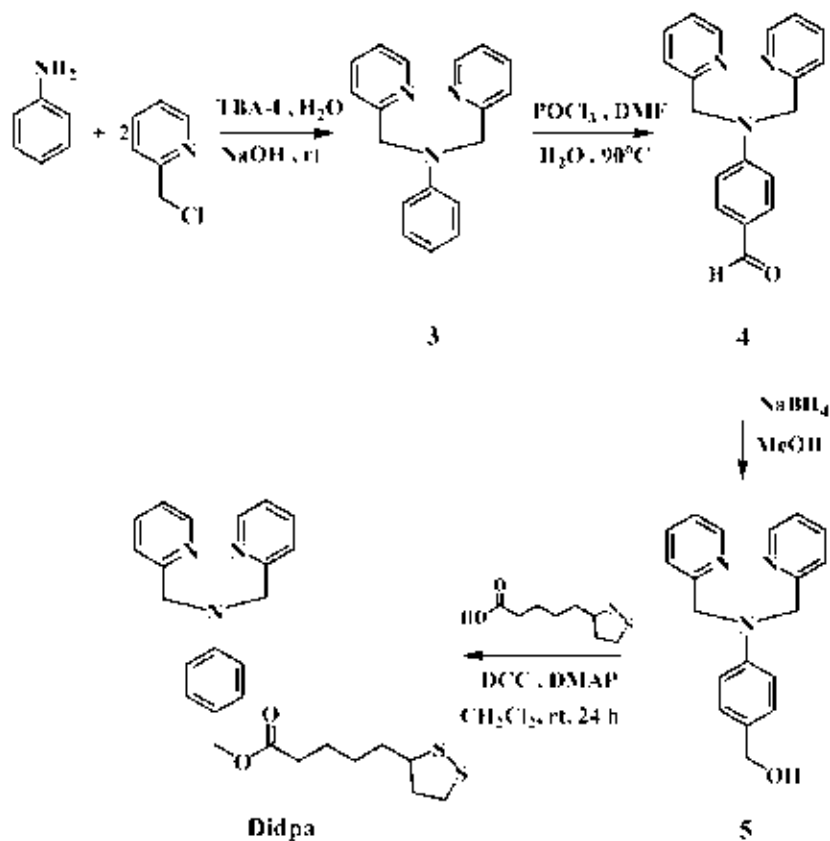
¹³C-NMR spectrum (100 MHz, CDCl₃) : δ (in ppm) = 24.6, 28.8, 34.6, 35.6, 38.4, 40.2, 56.4, 66.4, 70.8, 115.5, 121.9, 123.2, 129.1, 131.5, 136.2, 148.6, 156.7, 158.7, 173.1

ESI-HRMS:

calcd for C₂₁H₂₅NO₃S₂Na m/z = 426.1174 [M+H]⁺

Found = 426.1382 [M+H]⁺

Preparation of 4-(bis(pyridin-2-ylmethyl)amino)benzyl 5-(1,2-dithiolan-3-yl)pentanoate (Didpa)



• **Synthesis of *N,N*-bis(pyridin-2-ylmethyl)benzenamine (3)**

The aqueous mixture of aniline (1 g, 10.737 mmol), sodium hydroxide (1.074 g, 26.843 mmol) and tetrabutylammonium iodide, TBA-I was stirred at room temperature for 1 h. The solution of 2-chloromethylpyridine (4.37 g, 26.843 mmol) in H₂O was added into the mixture and the mixture solution was stirred at room temperature for 24 h. And then, it was extracted with dichloromethane. The organic phase was dried over anhydrous sodium sulfate and evaporated under reduced pressure. The crude product was purified by column chromatography using 20% ethyl acetate in dichloromethane to afford a white solid of compound **3** (0.864 g, 29%).

Characterization data for compound 3

¹H-NMR spectrum (400 MHz, CDCl₃) : δ (in ppm) = 8.59 (d, 2H, J = 4.8 Hz), 7.63 (t, 2H, J = 7.6 Hz), 7.27 (d, 2H, J = 9.6 Hz), 7.14-7.19 (m, 4H), 6.66-6.74 (m, 3H), 4.83 (s, 4H)

MS(ESI): m/z for C₁₈H₁₇N₃ = 275.398 [M+H]⁺

• Synthesis of 4-(bis(pyridin-2-ylmethyl)amino)benzaldehyde (4)

POCl₃ (0.891 mL, 9.736 mmol) was added slowly into fresh dimethyl formamide (1.13 mL, 14.604 mmol) under nitrogen atmosphere. The solution of POCl₃ was stirred in an ice bath for 1 h. After the red solution was observed, the solution of compound 3 (0.335 g, 1.217 mmol) in 1 mL of dimethyl formamide was added into the reaction. The mixture was heated at 90°C for 3 h and then treated with potassium carbonate (7.0 g) to adjust pH 6-8 and extracted with dichloromethane. The organic phase was dried over anhydrous sodium sulfate and the solvent was removed in vacuum to give the yellow oil of compound 4 (0.314 g, 85 %).

Characterization data for compound 4

¹H-NMR spectrum (400 MHz, CDCl₃) : δ (in ppm) = 9.73 (s, 1H), 8.61 (d, 2H, J = 4.0 Hz), 7.64-7.69 (m, 4H), 7.20-7.23 (m, 4H), 6.78 (d, 2H, J = 9.2 Hz), 4.91 (s, 4H)

MS(ESI): m/z for C₁₉H₁₇N₃O = 303.137 [M+H]⁺

• Synthesis of (4-(bis(pyridin-2-ylmethyl)amino)phenyl)methanol (5)

The solution of compound 4 (0.242 g, 0.798 mmol) in methanol was carefully added to the solution of sodium borohydride (0.604 g, 15.96 mmol) in methanol which was placed in ice bath. After stirred at room temperature for 2 h, the solution

mixture was treated with 3M HCl to adjust pH 7. The solvent was removed under reduced pressure and the residue was extracted with dichloromethane. The organic phase was dried over anhydrous sodium sulfate and evaporated under vacuum to give the yellow solid of compound **5** (0.195 g, 80%).

Characterization data for compound **5**

¹H-NMR spectrum (400 MHz, CDCl₃) : δ (in ppm) = 8.58 (d, 2H, J = 4.4 Hz), 7.62 (t, 2H, J = 7.2 Hz), 7.25 (t, 2H, J = 7.6 Hz), 7.17 (t, 4H, J = 7.6 Hz), 6.67 (d, 2H, J = 8.4 Hz), 4.82 (s, 4H), 4.53 (s, 2H)

MS(ESI): m/z for C₁₉H₁₉N₃O = 305.153 [M+H]⁺

• Synthesis of 4-(bis(pyridin-2-ylmethyl)amino)benzyl 5-(1,2-dithiolan-3-yl)pentanoate (**Didpa**)

A mixture of compound **5** (0.327 g, 1.072 mmol), dicyclohexyl carbodiimide, DCC ((0.221 g, 1.072 mmol) and 4-dimethylamino pyridine, DMAP (0.065 g, 0.536 mmol) in 30 mL dichloromethane was stirred at room temperature for 15 min. The (±)- α - lipoic acid (0.221 g, 1.072 mmol) in 20 mL dichloromethane was added dropwise over 30 min into the mixture solution which was, then, stirred at room temperature for 24 h. The solution mixture was extracted with dichloromethane. The combined organic phase was dried over anhydrous sodium sulfate and evaporated under reduced pressure. The crude product was purified by column chromatography using 10% methanol in ethyl acetate to afford the yellow oil of **Didpa** (0.158 g, 30%).

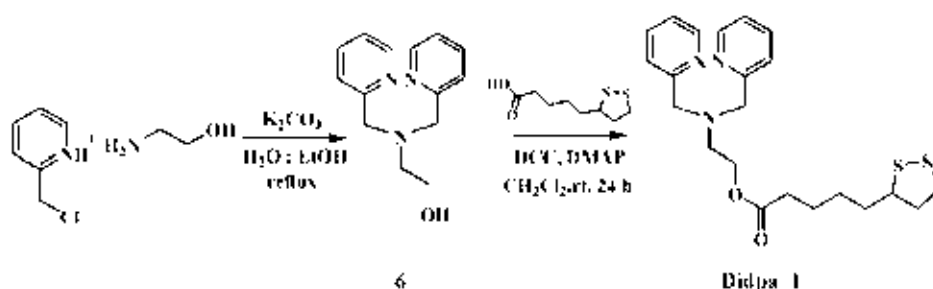
Characterization data for **Didpa**

¹H-NMR spectrum (400 MHz, CDCl₃) : δ (in ppm) = 8.59 (d, 2H, J = 4.8 Hz), 7.63 (t, 2H, J = 8 Hz), 7.25 (d, 2H, J = 10 Hz), 7.14-7.20 (m, 4H), 6.67 (d, 2H, J = 8.8 Hz), 4.96 (s, 2H), 4.83 (s, 4H), 3.45-3.55 (m, 1H), 3.07-3.17 (m, 2H), 2.40-2.46 (m, 1H), 2.30 (t, 2H, J = 7.6 Hz), 1.85-1.94 (m, 2H), 1.62-1.72 (m, 4H), 1.33-1.47 (m, 1H)

^{13}C -NMR spectrum (100 MHz, CDCl_3) : δ (in ppm) = 24.6, 28.7, 34.6, 35.5, 38.4, 40.2, 45.0, 56.4, 68.4, 114.5, 121.9, 123.2, 128.1, 131.7, 136.2, 147.5, 147.6, 156.9, 173.2

MS(ESI): m/z for $\text{C}_{27}\text{H}_{31}\text{N}_3\text{O}_2\text{S}_2$ = 494.114 $[\text{M}+\text{H}]^+$

Preparation of 2-(bis(pyridin-2-ylmethyl)amino)ethyl-5-(1,2-dithiolan-3-yl) penta noate (**Didpa 1**)



• Synthesis of 2-(bis(pyridin-2-ylmethyl)amino)ethanol (**6**)

A mixture of picolyl chloride (11.035 g, 67.27 mmol) and ethylolamine (2 mL, 32.74 mmol) in EtOH: H_2O (20:40 mL) was stirred at room temperature for 5 min. The mixture was added by the portion of potassium carbonate (9.297 g, 67.27 mmol) and refluxed at 80°C for 24 h. The reaction mixture was then cooled to room temperature and treated with sodium hydrogen carbonate (7.0 g) to adjust pH 8. The resulting solution was extracted with ethyl acetate. The organic phase was dried over anhydrous sodium sulfate and the solvent was removed in vacuum. A residue was purified by column chromatography using 10% methanol in ethyl acetate to afford the yellow oil of compound **6** (3.438 g, 42%).

Characterization data for compound **6**

^1H -NMR spectrum (400 MHz, CDCl_3) : δ (in ppm) = 8.53 (d, 2H, J = 4.8 Hz), 7.59 (t, 2H, J = 7.6 Hz), 7.31 (d, 2H, J = 7.6 Hz), 7.14 (t, 2H, J = 5.6 Hz), 3.92 (s, 4H), 3.67 (t, 2H, J = 5.2 Hz), 2.86 (t, 2H, J = 4.8 Hz)

MS(ESI): m/z for $\text{C}_{14}\text{H}_{17}\text{N}_3\text{O}$ = 243.14 $[\text{M}+\text{H}]^+$

• **Synthesis of 2-(bis(pyridin-2-ylmethyl)amino)ethyl-5-(1,2-dithiolan-3-yl)penta noate (Didpa_1)**

A mixture of compound **6** (1.352 g, 5.557 mmol), dicyclohexyl carbodiimide, DCC (1.146 g, 5.557 mmol), and 4-dimethylamino pyridine, DMAP (0.339 g, 2.779 mmol) in 30 mL dichloromethane was stirred at room temperature for 15 min. The (±)- α - lipoic acid (1.146 g, 5.557 mmol) in 20 mL dichloromethane was added dropwise over 30 min into the mixture solution which was, then, stirred at room temperature for 24 h. The solution mixture was extracted with dichloromethane. The combined organic phase was dried over anhydrous sodium sulfate and evaporated under reduced pressure. The residue was subjected to evaporate under vacuum and purified by column chromatography using 10% methanol in ethyl acetate to afford the yellow oil of **Didpa_1** (1.014 g, 42%).

Characterization data for Didpa_1

¹H-NMR spectrum (400 MHz, CDCl₃) : δ (in ppm) = 8.52 (d, 2H, J = 4.8 Hz), 7.66 (t, 2H, J = 7.6 Hz), 7.52 (d, 2H, J = 7.6 Hz), 7.15 (t, 2H, J = 6.6 Hz), 4.20 (t, 2H, J = 5.6 Hz), 3.89 (s, 4H), 3.52-3.56 (m, 1H), 3.08-3.18 (m, 2H), 2.88 (t, 2H, J = 5.6 Hz), 2.40-2.48 (m, 1H), 2.28 (t, 2H, J = 7.2 Hz), 1.86-1.96 (m, 1H), 1.59-1.68 (m, 4H), 1.40-1.48 (m, 2H)

¹³C-NMR spectrum (100 MHz, CDCl₃) : δ (in ppm) = 24.9, 28.7, 34.6, 35.5, 38.4, 40.2, 52.7, 56.4, 60.1, 62.3, 121.7, 123.1, 136.4, 148.7, 156.9, 173.2.

ESI-HRMS:

calcd for C₂₂H₂₉N₃O₂S₂ m/z = 431.1701 [M+H]⁺

Found = 432.1734 [M+H]⁺

- **Complexation of Didpa_1 with Zn(ClO₄)₂·6H₂O**

Zn(ClO₄)₂·6H₂O (0.304 g, 0.816 mmol) in methanol (4 mL) was added dropwise into the solution of **Didpa_1** (0.176 mg, 0.408 mmol) in dichloromethane (2 mL) and the mixture solution was stirred at room temperature for 24 h. The solvent was removed under reduced pressure and the residue was extracted with ethyl acetate. The combined organic phase was dried over anhydrous sodium sulfate and the solvent was removed under reduced pressure to afford the yellow solid of **Didpa_1-Zn** complex.

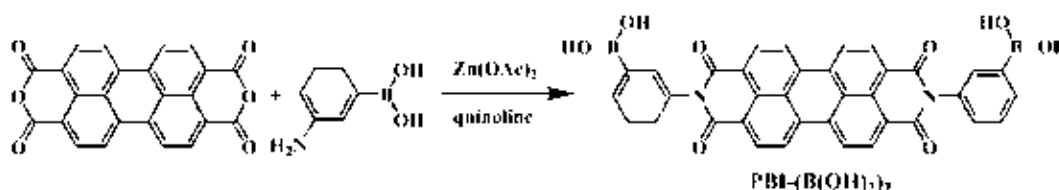
Characterization data for Didpa_1-Zn complex

¹H-NMR spectrum (400 MHz, CDCl₃) : δ (in ppm) = 8.80 (d, 2H, *J* = 5.2 Hz), 8.04 (d, 2H, *J* = 4.8 Hz), 7.61 (d, 2H, *J* = 6.8 Hz), 7.50 (d, 2H, *J* = 8 Hz), 4.25 (t, 2H, *J* = 5.2 Hz), 4.03 (s, 4H), 3.53-3.60 (m, 1H), 3.11-3.22 (m, 2H), 3.08 (t, 2H, *J* = 5.2 Hz), 2.43-2.51 (m, 1H), 2.31-2.36(m, 2H), 1.89-1.92 (m, 3H), 1.46-1.70 (m, 4H)

MS(ESI): m/z for C₂₂H₂₉N₃O₂S₂Zn = 494.836 [M+H]⁺

3.5.1.1.2 Fluorophore as a boronic acid parts

Preparation of PBI-(B(OH)₂)₂



A mixture of perylene-3, 4, 9, 10-tetracarboxylic dianhydride (0.114 g, 0.292 mmol), zinc acetate (0.048 g, 0.22 mmol) and quinoline (15 mL) was stirred at to 100°C for half an hour. 3-aminoboronic acid (0.3 g, 1.46 mmol) was added into the reaction which was heated at 200 °C for 24 h, and then cooled to room temperature. The mixture solution was poured into the cold ethanol (100 ml). The dark red precipitate was slowly formed. The precipitate was filtered and washed with the cold ethanol to give the dark-red solid of 0.156 g (85%).

Characterization data for PBI-(B(OH)₂)₂

¹H-NMR spectrum (400 MHz, CDCl₃) : δ (in ppm) = 8.87 (d, 2H, *J* = 2.8 Hz), 8.12 (d, 2H, *J* = 8 Hz), 8.06 (d, 2H, *J* = 8.4 Hz), 7.77 (d, 2H, *J* = 8 Hz), 7.65-7.68 (m, 2H), 7.50 (t, 2H, *J* = 7.2 Hz), 7.34-7.37 (m, 2H), 7.19 (s, 2H)

¹³C-NMR spectrum (100 MHz, CDCl₃) : δ (in ppm) = 120.0, 121.6, 124.5, 126.5, 127.3, 129.0, 129.3, 129.5, 132.2, 132.7, 133.0, 150.4

MS(ESI): *m/z* for C₃₆H₂₀B₂N₂O₈ = 630.263 [M+H]⁺

3.5.1.1.3 Complexation studies of AuNPs-Didpa \subset Zn²⁺ and PBI-(B(OH)₂)₂ for nucleotides detection

Typically, the stock solutions (1.0×10^{-4} M) of AuNPs-Didpa \subset Zn²⁺ in Milli Q water and PBI-(B(OH)₂)₂ (1.0×10^{-4} M) in DMSO was prepared in 10 mL volumetric flask. The stock solutions (0.001 M) of the sodium salts of PPI, ATP, ADP, AMP, UTP, UDP, UMP, GDP, GMP and CMP were also prepared in 0.01 M HEPES pH 7.4 (shown in Table 3.2).

Table 3.2 The amount of nucleotides were used in fluorescence studies

Nucleotides	Mw	weight (mg)
ATP	551.10	2.76
ADP	449.20	2.25
AMP	365.24	1.83
UTP	586.12	2.93
UDP	404.16	2.02
UMP	368.15	1.84
GDP	443.20	2.22
GMP	407.19	2.04
CMP	367.16	1.84
PPI	265.90	1.33

The 20 μ L of PBI-(B(OH)₂)₂ was putted in cuvette and 20 μ L of modified gold nanoparticles (AuNPs-Didpa \subset Zn²⁺) was added. After that, the solution of each nucleotide (20 μ L) was added into the mixture solution which was, then, diluted to 2 mL with 0.01 M HEPES (pH 7.4). The fluorescence spectra were recorded under excitation wavelength at 450 nm.

3.5.1.1.4 Complexation studies of AuNPs-Didpa_1-Zn and PBI-(B(OH)₂)₂ by fluorescence spectroscopy

In this case, modified gold nanoparticles with **Didpa_1-Zn** were prepared in 10% toluene in DMSO for nucleotides sensing as according in the topic of 3.3.2.1. For the nucleotides detection, the stock solutions (1.0×10^{-4} M) of **AuNPs-Didpa_1-Zn** and **PBI-(B(OH)₂)₂** (1.0×10^{-4} M) in DMSO were prepared and sodium salts of PPI, ATP, ADP, AMP, UTP, UDP, UMP, GDP, GMP and CMP were also prepared in 0.01 M HEPES pH 7.4 (shown in Table 3.2).

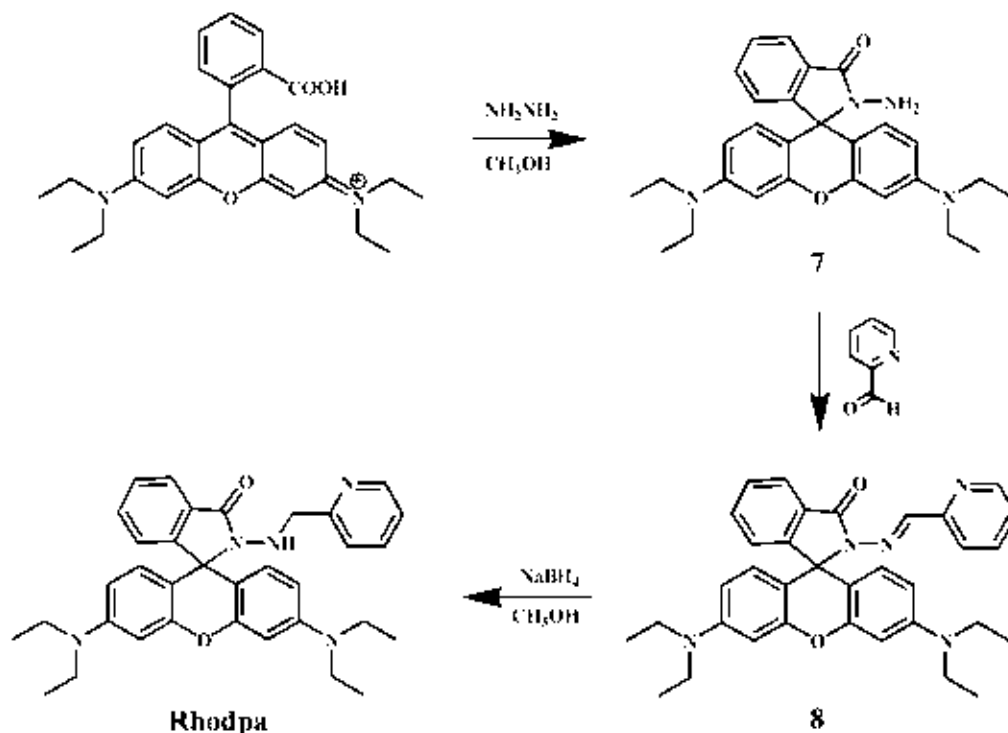
Stock solution of **PBI-(B(OH)₂)₂** (20 μ L) were placed in cuvette and AuNPs-Didpa_1-Zn (20 μ L) was added and stirred for 2 min. Then the solution of nucleotides (20 μ L) was added into the solution which was, then, diluted to 2 mL with 0.01 M HEPES (pH 7.4). The fluorescence spectra were recorded under excitation wavelength at 450 nm.

3.5.1.1.5 Complexation studied between PBI-(B(OH)₂)₂ with nucleotides anions

The stock solution (0.001 M) of various nucleotides such as PPI, ATP, ADP, AMP, UTP, UDP, UMP, GDP, GMP and CMP was prepared in 0.01 M HEPES pH 7.4 in 5 mL volumetric flask (showed in Table 3.2). The 20 μ L of stock solution of **PBI-(B(OH)₂)₂** (1×10^{-4} M) in DMSO was putted into cuvette. The excess of nucleotides (20 μ L) were added in the cuvette. The solution was diluted to 2 mL with 0.01 M HEPES (pH 7.4). The fluorescence spectra were recorded under excitation wavelength at 450 nm.

3.5.1.2 Complexation studies by using replacement procedure

3.5.1.2.1 Synthesis pathway of Rhodpa



• Synthesis of compound 7

Rhodpa was synthesized according to recently reported procedure [58]. Initially, excess hydrazine hydrate was added into the solution of **Rhodamine_B** (0.497 g, 1.0 mmol) in 30 mL methanol. The reaction mixture was refluxed at 90°C for 2 h. The mixture was cooled to room temperature and the solvent was removed under reduced pressure. The residue solution was treated with 1 M HCl (about 10 mL) until the red solution was observed. Aqueous solution of 1 M NaOH (about 30 mL) was added slowly and stirred continuously until the pink precipitate was formed at pH $\sim 8-9$. The pink precipitate was filtered and washed with water to afford the pink solid of compound 7 (0.292 g, 64%).

Characterization data for compound 7

¹H-NMR spectrum (400 MHz, CDCl₃) : δ (in ppm) = 7.92 (dd, 1H, J = 4.8, 7.2 Hz), 7.43 (dd, 2H, J = 4, 6.8 Hz), 7.08 (dd, 1H, J = 3.6, 4.8 Hz), 6.42 (dd, 4H, J = 16.8, 10 Hz), 6.27 (dd, 2H, J = 8.8, 8.8 Hz), 3.59 (bs, 2H), 3.32 (q, 8H, J = 6.8 Hz), 1.14 (t, 12H, J = 7.2 Hz)

MS(ESI): m/z for C₂₈H₃₂N₄O₂ = 456.253 [M+H]⁺

• Synthesis of compound 8

Into the two necked bottom flask, compound 7 (0.5 g, 1 mmol) was dissolved in 5 mL ethanol and the picolyl aldehyde (0.117 g, 1 mmol) was added. For a few minutes, color solution was turned to red and the mixture solution was further stirred at room temperature under nitrogen atmosphere for 2 h until the precipitate was slowly formed. The precipitate was filtered and washed with the cold ethanol to afford the white solid of compound 8 (0.379 g, 64%).

Characterization data for compound 8

¹H-NMR spectrum (400 MHz, CDCl₃) : δ (in ppm) = 8.46 (d, 1H, J = 5.2 Hz), 8.32 (s, 1H), 7.99 (d, 2H, J = 7.6 Hz), 7.61 (t, 1H, J = 7.6), 7.46 (dd, 2H, J = 10.4, 10.4 Hz), 7.12 (d, 2H, J = 13.2, 14 Hz), 6.55 (d, 2H, J = 0.4 Hz), 6.44 (s, 2H), 6.23 (d, 2H, J = 8.8 Hz), 3.31 (q, 8H, J = 7.2 Hz), 1.14 (t, 12H, J = 7.2 Hz)

MS(ESI): m/z for C₃₄H₃₅N₅O₂ = 545.279 [M+H]⁺

• Synthesis of Rhodpa

The solution of compound 8 (0.164 g, 0.3 mmol) in methanol was carefully added to the solution of sodium borohydride (0.227 g, 6 mmol) in methanol which was placed in ice bath and stirred at room temperature for 2 h. The solution mixture

was treated with 3M HCl to adjust pH 7. The solvent was removed under reduced pressure and the residue was extracted with dichloromethane. The organic phase was dried over anhydrous sodium sulfate and evaporated under vacuum. The crude product was purified by column chromatography using 100% ethylacetate to obtain the white solid of **Rhodpa** 0.137 g (83%).

Characterization data for Rhodpa

¹H-NMR spectrum (400 MHz, CDCl₃) : δ (in ppm) = 8.37 (d, 1H, *J* = 4.4 Hz), 7.92 (d, 1H, *J* = 7.2 Hz), 7.45-7.51 (m, 3H), 7.04-7.09 (m, 3H), 6.37-6.44 (m, 4H), 6.23 (d, 2H, *J* = 7.2 Hz), 4.82 (bs, 1H), 3.96 (s, 2H), 3.32 (q, 8H, *J* = 7.2 Hz), 1.15 (t, 12H, *J* = 6.4 Hz)

MS(ESI): *m/z* for C₃₄H₃₇N₅O₂ = 547.295 [M+H]⁺

3.5.1.2.2 Fluorophore replacement studies by fluorescence spectroscopy

For complexation studies of nucleotides sensing, the stock solution (0.001 M) of **Rhodpa-Cu** in DMSO and gold nanoparticles (0.01 M) in 10% toluene in DMSO were prepared in 5 mL volumetric flask. Stock solution (0.001 M) of nucleotides was prepared in 0.01 M HEPES pH 7.4. The mixture solution of **Rhodpa-Cu** (20 μL) and gold nanoparticles (1 mL) were putted in cuvette and stirred for 30 min. After that each of nucleotides (20 μL) was added into the mixture solution which was, then, diluted to 2 mL with 0.01 M HEPES (pH 7.4). The fluorescence spectra were recorded under excitation wavelength at 556 nm.

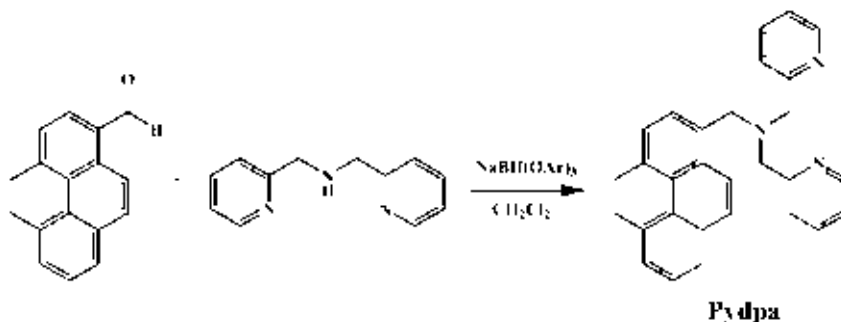
3.5.2 Complexation studies by using Principal Component Analysis (PCA) for discrimination of nucleotides

In this research, we have focused on detection of nucleotides by using the fluorescence spectroscopy and the discrimination studies by the PCA method. Sensory molecules were used in this study are pyrene and coumarin derivatives (**Pydpa** and **Es**). In the case of nucleotides detection, the metal complexation of **Pydpa-Zn**, **Pydpa-Cu**, **Es-Zn**, and **Es-Cu** are used in this study.

Initially, the synthesis of **Pydpa-Zn** and **Pydpa-Cu** were shown in the topic 3.5.2.1. On the other hand, **Es-Zn** and **Es-Cu** were prepared as shown in the topic 3.5.2.2.

3.5.2.1 Synthesis pathway of pyrene derivative

Preparation of **Pydpa**



A mixture of pyrenecarboxaldehyde (0.23 g, 1 mmol), dipicolylamine (0.20 g, 1 mmol) and sodium tris(acetoxy)borohydride (0.28 g, 1.32 mmol) in 10 mL dichloromethane was stirred under N₂ atmosphere at room temperature for 5 h. The mixture was neutralized with sodium hydrogen carbonate and extracted with dichloromethane. The combined organic phase was dried over anhydrous sodium sulfate and evaporated under reduced pressure. The crude product was purified by column chromatography using 5% methanol in dichloromethane to give **Pydpa** as a yellow oil which ultimately solidifies when dried (0.36 g, 88%).

Characterization data for Pydpa

¹H-NMR spectrum (400 MHz, DMSO-d₆) : δ (in ppm) = 8.50 (d, *J* = 4.0 Hz, 2H), 8.37 (d, *J* = 8.8 Hz, 1H), 8.27 (s, 1H), 8.25-8.01 (m, 7H), 7.70 (t, *J* = 7.8 Hz, 2H), 7.48 (d, *J* = 8.0 Hz, 2H), 7.21 (t, *J* = 10.0 Hz, 2H), 4.35 (s, 2H), 3.81 (s, 4H)

ESI-HRMS:

calcd for C₂₉H₂₃N₃ m/z = 414.2048 [M+H]⁺

Found = 414.2022 [M+H]⁺

• Complexation of Pydpa with Zn(ClO₄)₂·6H₂O

Zn(ClO₄)₂·6H₂O (0.171 g, 0.47 mmol) in methanol (5 mL) was added dropwise into solution of **Pydpa** (0.112 g, 0.27 mmol) in methanol (5 mL) and the mixture solution was stirred at room temperature for 24 h. The precipitate was slowly formed. The pale yellow precipitate was filtered and washed with the cold methanol to give **Pydpa-Zn** complex. (0.21 g, 100%)

Characterization data for Pydpa-Zn complex

¹H-NMR spectrum (400 MHz, DMSO-d₆) : δ (in ppm) = 8.71 (s, 2H), 8.42 (s, 1H), 8.37-8.13 (m, 9H), 7.94 (s, 1H), 7.68 (s, 2H), 7.56 (d, *J* = 6.4 Hz, 2H), 4.55 (s, 2H), 4.35 (d, *J* = 15.2 Hz, 2H), 3.69 (d, *J* = 15.6 Hz, 2H)

ESI-HRMS:

calcd for C₂₉H₂₃N₃Cl₃O₁₂Zn m/z = 773.9639 [M+(ClO₄)₃]⁻

Found = 773.9829 [M+(ClO₄)₃]⁻

- **Complexation of Pydpa with CuCl₂·2H₂O**

CuCl₂·2H₂O (0.05 g, 0.29 mmol) in methanol (5 mL) was added dropwise into solution of Pydpa (0.078 g, 0.19 mmol) in methanol (5 mL) and the mixture solution was stirred at room temperature for 24 h. The precipitate was slowly formed. The green solid precipitate was filtered and washed with the cold methanol to give **Pydpa-Cu** complex. (0.90 g, 100%)

Characterization data for Pydpa-Cu complex

MS(ESI): m/z for C₂₉H₂₃Cl₂CuN₃Na = 569.132 [M+H]⁺

3.5.2.2 Complexation studies of Esculetin with metal ions (Zn²⁺ and Cu²⁺) by using UV-vis spectroscopy

3.5.2.2.1 Titration studies of Esculetin with Zn(ClO₄)₂ using UV-visible spectroscopy

A 0.001 M stock solutions of **Esculetin** in DMSO and Zn(ClO₄)₂ in milli Q water were prepared in 5 mL volumetric flask. **Esculetin** (0.2 mL) was placed in cuvette and various concentration of Zn(ClO₄)₂ was added into the solution as shown in Table 3.3. The solution was diluted to 2 mL with DMSO. UV-vis spectra were recorded after adding Zn(ClO₄)₂ in the ratio of Zn²⁺:host from 0:1 to 4:1.(Shown in Table 3.3).

Table 3.3 The concentration of Zn^{2+} ion was used in complexation studies of **Esculetin**

Point	Zn^{2+} / L	[L] mM	$[Zn^{2+}]$ mM	V of Zn^{2+}	V total
1	0.0	0.100000	0.000000	0.000	2.000
2	0.2	0.098039	0.019608	0.004	2.004
3	0.4	0.096154	0.038462	0.008	2.008
4	0.6	0.094340	0.056604	0.012	2.012
5	0.8	0.092593	0.074074	0.016	2.016
6	1.0	0.090909	0.090909	0.020	2.020
7	1.2	0.089286	0.107143	0.024	2.024
8	1.4	0.087719	0.122807	0.028	2.028
9	1.6	0.086207	0.137931	0.032	2.032
10	1.8	0.084746	0.152542	0.036	2.036
11	2.0	0.083333	0.166667	0.040	2.040
12	2.2	0.081967	0.180328	0.044	2.044
13	2.4	0.080645	0.193548	0.048	2.048
14	2.6	0.079365	0.206349	0.052	2.052
15	2.8	0.078125	0.218750	0.056	2.056
16	3.0	0.076923	0.230769	0.060	2.060
17	3.2	0.075758	0.242424	0.064	2.064
18	3.4	0.074627	0.253731	0.068	2.068
19	3.6	0.073529	0.264706	0.072	2.072
20	3.8	0.072464	0.275362	0.076	2.076
21	4.0	0.071429	0.285714	0.080	2.080

3.5.2.2.2 Titration studies of Esculetin with $\text{Cu}(\text{NO}_3)_2$ using UV-visible spectroscopy

The complex preparation in this study was according to the topic of 3.5.2.2.1. A 0.001 M stock solution of **Esculetin** in DMSO and $\text{Cu}(\text{NO}_3)_2$ in milli Q water were prepared in 5 mL volumetric flask. **Esculetin** 0.2 mL was placed in cuvette and various concentration of $\text{Cu}(\text{NO}_3)_2$ was added into the solution as shown in Table 3.4. The solution was diluted to 2 mL with DMSO. UV-vis spectra were recorded after adding $\text{Cu}(\text{NO}_3)_2$ in the ratio of Cu^{2+} :host from 0:1 to 1.5:1 (Shown in Table 3.4)

Table 3.4 The concentration of Cu^{2+} ion was used in complexation studies of **Esculetin**

Point	Cu^{2+}/L	[L] mM	$[\text{Cu}^{2+}]$ mM	V of Cu^{2+}	V total
1	0.0	0.100000	0.000000	0.000	2.000
2	0.1	0.099900	0.000999	0.002	2.002
3	0.2	0.099800	0.001996	0.004	2.004
4	0.3	0.099701	0.002991	0.006	2.006
5	0.4	0.099602	0.003984	0.008	2.008
6	0.5	0.099502	0.004975	0.010	2.010
7	0.6	0.099404	0.005964	0.012	2.012
8	0.7	0.099305	0.006951	0.014	2.014
9	0.8	0.099206	0.007937	0.016	2.016
10	0.9	0.099108	0.008920	0.018	2.018
11	1.0	0.099010	0.009901	0.020	2.020
12	1.1	0.098912	0.010880	0.022	2.022
13	1.2	0.098814	0.011858	0.024	2.024
14	1.3	0.098717	0.012833	0.026	2.026
15	1.4	0.098619	0.013807	0.028	2.028
16	1.5	0.098522	0.014778	0.030	2.030

3.6 Complexation studies of Pydpa-Zn, Pydpa-Cu, Es-Zn and Es-Cu with various nucleotides by fluorescence spectroscopy

3.6.1 Complexation studies of Pydpa-Zn with various nucleotides

Normally, the stock solutions (0.001 M) of sodium salts of PPI, ATP, ADP, AMP, UTP, UDP, UMP, GDP, GMP and CMP were prepared by 0.01 M HEPES pH 7.4 in 5 mL volumetric flask (showed in Table 3.2). Stock solution of **Pydpa-Zn** (1×10^{-3} M) in DMSO was prepared. The 20 μ L **Pydpa-Zn** was placed into cuvette and 10 equiv of each nucleotide (200 μ L) was also added. The solution was diluted to 2 mL with 0.01 M HEPES (pH 7.4). The fluorescence spectra were recorded under excitation wavelength at 347 nm. The sample preparations according to this experiment are also used in the case of the nucleotides detection by using **Pydpa-Cu**, **Es-Zn** and **Es-Cu**.

3.6.2 Titration studies of Pydpa-Zn with PPI using fluorescence spectroscopy

A 0.001 M stock solution of **Pydpa-Zn** in DMSO and PPI in milli Q water were prepared in 5 mL volumetric flask. **Pydpa-Zn** 20 μ L was placed in cuvette and various concentration of PPI was added into the solution as shown in Table 3.5. The solution was diluted to 2 mL with DMSO. Fluorescence spectra were recorded after adding PPI in the ratio of PPI:host from 0:1 to 3:1 (as shown in Table 3.5). The sample preparations in this experiment are also used in the case of titration studies by using **Es-Zn** and **Es-Cu**.

Table 3.5 The concentration of PPI anion was used in complexation studies of **Pydpa-Zn**

Point	PPI/L	[L] mM	[PPI] mM	V of PPI	V total
1	0.0	0.100000	0.000000	0.000	2.000
2	0.1	0.099900	0.000999	0.002	2.002
3	0.2	0.099800	0.001996	0.004	2.004
4	0.3	0.099701	0.002991	0.006	2.006
5	0.4	0.099602	0.003984	0.008	2.008

Point	PPi/L	[L] mM	[PPi] mM	V of PPi	V total
6	0.5	0.099502	0.004975	0.010	2.010
7	0.6	0.099404	0.005964	0.012	2.012
8	0.7	0.099305	0.006951	0.014	2.014
9	0.8	0.099206	0.007937	0.016	2.016
10	0.9	0.099108	0.008920	0.018	2.018
11	1.0	0.099010	0.009901	0.020	2.020
12	1.1	0.098912	0.010880	0.022	2.022
13	1.2	0.098814	0.011858	0.024	2.024
14	1.3	0.098717	0.012833	0.026	2.026
15	1.4	0.098619	0.013807	0.028	2.028
16	1.5	0.098522	0.014778	0.030	2.030
17	1.6	0.098423	0.015755	0.032	2.032
18	1.7	0.098325	0.016729	0.034	2.034
19	1.8	0.098227	0.017703	0.036	2.036
20	1.9	0.098129	0.018677	0.038	2.038
21	2.0	0.098031	0.019651	0.040	2.040
22	2.1	0.097933	0.020625	0.042	2.042
23	2.2	0.097835	0.021599	0.044	2.044
24	2.3	0.097737	0.022573	0.046	2.046
25	2.4	0.097639	0.023547	0.048	2.048
26	2.5	0.097541	0.024521	0.050	2.050
27	2.6	0.097443	0.025495	0.052	2.052
28	2.7	0.097345	0.026469	0.054	2.054
29	2.8	0.097247	0.027443	0.056	2.056
30	2.9	0.097149	0.028417	0.058	2.058
31	3.0	0.097051	0.029391	0.06	2.060

3.6.3 Complexation studies of **Pydpa-Zn** and **Es-Zn** with various nucleotides by fluorescence spectroscopy

Normally, 0.001 M stock solutions of **Pydpa-Zn** and 5×10^{-4} M of **Es-Zn** in DMSO and 0.001 M sodium salts of PPI, ATP, ADP, AMP, UTP, UDP, UMP, GDP, GMP and CMP were prepared in 0.01 M HEPES pH 7.4 in 5 mL volumetric flasks. **Pydpa-Zn** (20 μ L) and **Es-Zn** (40 μ L) were putted in cuvette. Each nucleotide (200 μ L) was added into the mixture solution. The solution was, then, diluted to 2 mL with 0.01 M HEPES (pH 7.4). The fluorescence spectra were recorded under excitation wavelength at 347 nm. The sample preparation according to this experiment was used for the study of the nucleotides detection by using **Pydpa-Zn** and **Es-Cu**.

3.7 Job's plot study

3.7.1 Job's plot study of **Esculetin** with Zn^{2+} ion

Typically, stock solution (0.001 M) of **Esculetin** in DMSO was prepared in 25 mL volumetric flask. A solution of Zn^{2+} cation (0.001 M) was prepared in milli Q water in 10 mL volumetric flask.

Fluorescence spectra of **Esculetin** with Zn^{2+} cation were monitored from 400-700 nm upon excitation at 380 nm at ambient temperature. Firstly, the solution of Zn^{2+} ion was added directly to 3 mL **Esculetin** in a 1-cm quartz cuvette and stirred for 5 minute. Fluorescence spectra were recorded after each experiment. Table 3.6 showed $[\text{Zn}^{2+}]/([\text{Zn}^{2+}]+[\text{Esculetin}])$ ratios utilized in the manipulation. The sample preparation according to this experiment was used for the stoichiometry complexation between **Esculetin** with Cu^{2+} ion.

Table 3.6 Amounts of **Esculetin** and Zn^{2+} cation and HEPES buffer pH 7.4 were used in Job's plot experiment.

Ratio	Esculetin	Zn^{2+}	V total (mL)
0.0	3.0	0.0	3.0
0.1	2.8	0.2	3.0
0.2	2.5	0.5	3.0
0.3	2.3	0.7	3.0
0.4	2.0	1.0	3.0
0.5	1.8	1.2	3.0
0.6	1.5	1.5	3.0
0.7	1.0	2.0	3.0
0.8	0.8	2.2	3.0
0.9	0.2	2.8	3.0
1.0	0.0	3.0	3.0

3.7.2 Job's plot study of **Pydpa-Zn** with **PPi**

Typically, stock solution (0.001 M) of **Pydpa-Zn** in DMSO was prepared in 25 mL volumetric flask. A solution of Zn^{2+} cation (0.001 M) was prepared in milli Q water in 10 mL volumetric flask.

Fluorescence spectra of **Pydpa-Zn** with **PPi** anion were monitored from 400-700 nm upon excitation at 380 nm at ambient temperature. Firstly, the solution of **PPi** anion was added directly to 2 mL **Pydpa-Zn** in a 1-cm quartz cuvette and stirred for 2 minute. Fluorescence spectra were recorded after each experiment. Table 3.7 showed $[\text{PPi}]/([\text{PPi}]+[\text{Pydpa-Zn}])$ ratios utilized in the manipulation. The sample preparation according to this experiment was used for the stoichiometry complexation between **Pydpa-Zn** with **PPi**.

Table 3.7 Amounts of **Pydpa-Zn** and PPI anion and HEPES buffer pH 7.4 were used in Job's plot experiment.

Ratio	Esculetin	Zn²⁺	V total (mL)
0.0	2.0	0.0	2.0
0.1	1.8	0.2	2.0
0.2	1.6	0.4	2.0
0.3	1.4	0.6	2.0
0.4	1.2	0.8	2.0
0.5	1.0	1.0	2.0
0.6	0.8	1.2	2.0
0.7	0.6	1.4	2.0
0.8	0.4	1.6	2.0
0.9	0.2	1.8	2.0
1.0	0.0	2.0	2.0

CHAPTER IV

RESULTS AND DISCUSSION

A major target of this research aims to design and synthesize sensor for nucleotide detections. A nucleotide consists of nucleobase, sugar and phosphate groups. A fundamental knowledge of transition metal ions (Zn^{2+} and Cu^{2+}) can coordinate with phosphate anions. In this research, the nucleotides sensing has been studied by the use of two different systems: i) using the gold nanoparticles and ii) using the Principal Component Analysis (PCA). The conceptually sensing purposes used in this research were shown in Figure 4.1.

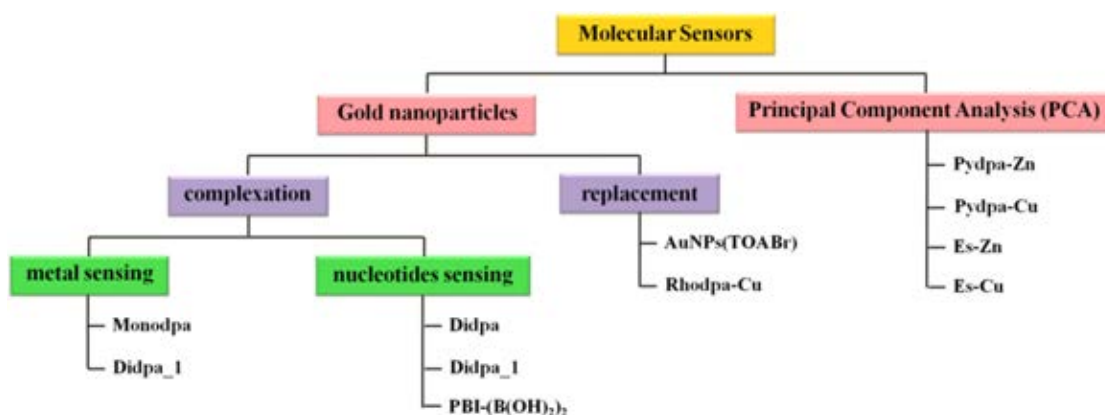


Figure 4.1. Diagram of the conceptually sensing purposes used in this research.

4.1. Optical properties of gold nanoparticles

Gold nanoparticles used in these researches were prepared by two methods as following:

- i) Gold nanoparticles in H_2O using citrate as a stabilizer.
- ii) Gold nanoparticles in toluene using tetraalkylammonium bromide (TOABr) as a stabilizer.

4.4.1 Gold nanoparticles in H₂O

Gold nanoparticles were synthesized by sodium borohydride and citrate as a reducing agent and stabilizer, respectively. Typically, aqueous solution of hydrogen tetrachloroaurate and sodium citrate were mixed and stirred for 5 min. Then sodium borohydride was added in portions to reduce Au³⁺ to Au⁰ resulting in the color changes from pale yellow to red. Gold nanoparticles were purified by centrifugation at 10000 rpm to get rid of the sodium borohydride affording the gold nanoparticles with the negative charge of citrate as stabilizer. The gold nanoparticles were characterized by UV-visible spectroscopy. The characteristic of absorption band of gold nanoparticles was observed at 520 nm implying the average particle diameter at 14.9 nm [63] as shown in Figure 4.2.

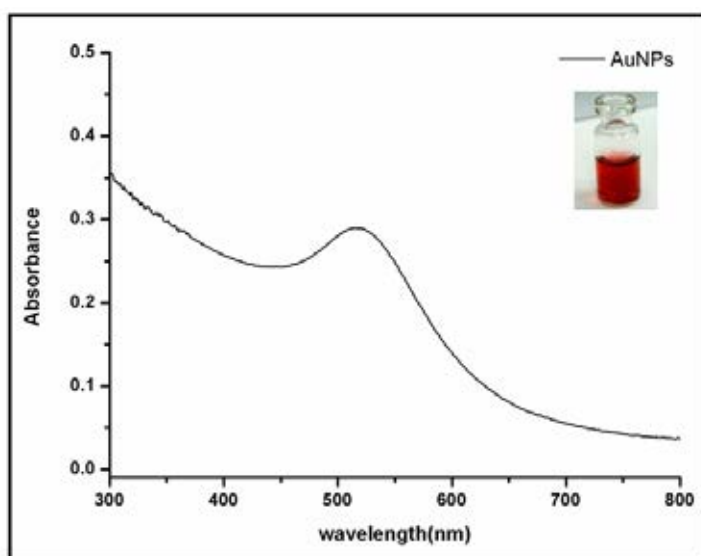


Figure 4.2. UV-visible spectrum of gold nanoparticles using citrate as stabilizer in H₂O.

4.4.2 Gold nanoparticles in toluene

Gold nanoparticles were synthesized via phase-transfer of tetraalkylammonium bromides (TOABr). Typically, aqueous solution of hydrogen tetrachloroaurate and TOABr in toluene were mixed and vigorously stirred for 30 min. Tetrachloroaurate was transferred to the organic phase resulting in the

occurrence of deep orange color in the organic phase. Then the aqueous solution of sodium borohydride (0.4 M) was added slowly in portions to reduce Au^{3+} to Au^0 . The color of the solution was slowly changed from deep orange via colorless to ruby red. Gold nanoparticles were purified by extraction with 3 M HCl and washed five times with Milli Q water to afford gold nanoparticles with TOABr as stabilizer. The gold colloid characterized by UV-visible spectroscopy displayed the maximum absorption band at 523 nm implying an average diameter of ca. 20 nm [64] as shown in Figure 4.3.

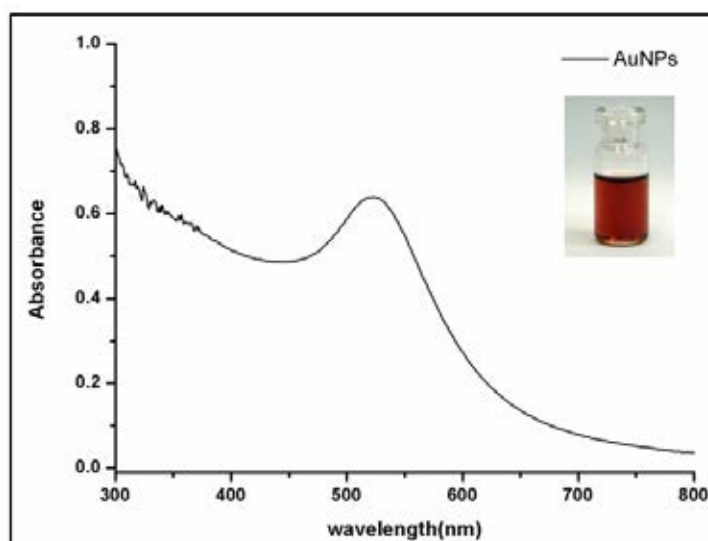


Figure 4.3. UV-visible spectrum of gold nanoparticles was synthesized in toluene.

4.2. Modification of gold nanoparticles

4.2.1 Modification of gold nanoparticles in H_2O with Monodpa, Didpa, Didpa_1 and Didpa_1-Zn

Functionalized gold nanoparticles with organic molecules (**Monodpa**, **Didpa**, **Didpa_1** and **Didpa_1-Zn**) were prepared by phase-transfer process and synthesis pathway of these sensors was shown in the topic of 3.5.1.1.1. Gold nanoparticles in aqueous and organic molecules in dichloromethane were mixed together and vigorously stirred for 2 h. The modified gold nanoparticles were characterized by UV-visible spectroscopy. The result showed the absorption band of 332, 264, 336 and 346

nm corresponding to the characteristic of π - π^* transition of **Monodpa**, **Didpa**, **Didpa_1** and **Didpa_1-Zn**, respectively. From Figure 4.4A, B and C, the modified gold nanoparticles with **Monodpa**, **Didpa** and **Didpa_1** showed the shifts of the surface plasmon band of gold nanoparticles from 520 nm to 521, 529 and 530 nm, respectively. This result showed a strong evidence of the successful modification of gold nanoparticles upon an aggregation of gold nanoparticles through hydrophobic interaction. Interestingly, the observation of the blue color change in the case of **Didpa_1-Zn** modified gold nanoparticles revealed the occurrence of high aggregation of gold nanoparticles. This can be explained that Zn^{2+} in **AuNPs-Didpa_1-Zn** preferred to bind with citrate anion as a stabilizer on gold nanoparticles (as shown in Figure 4.4D).

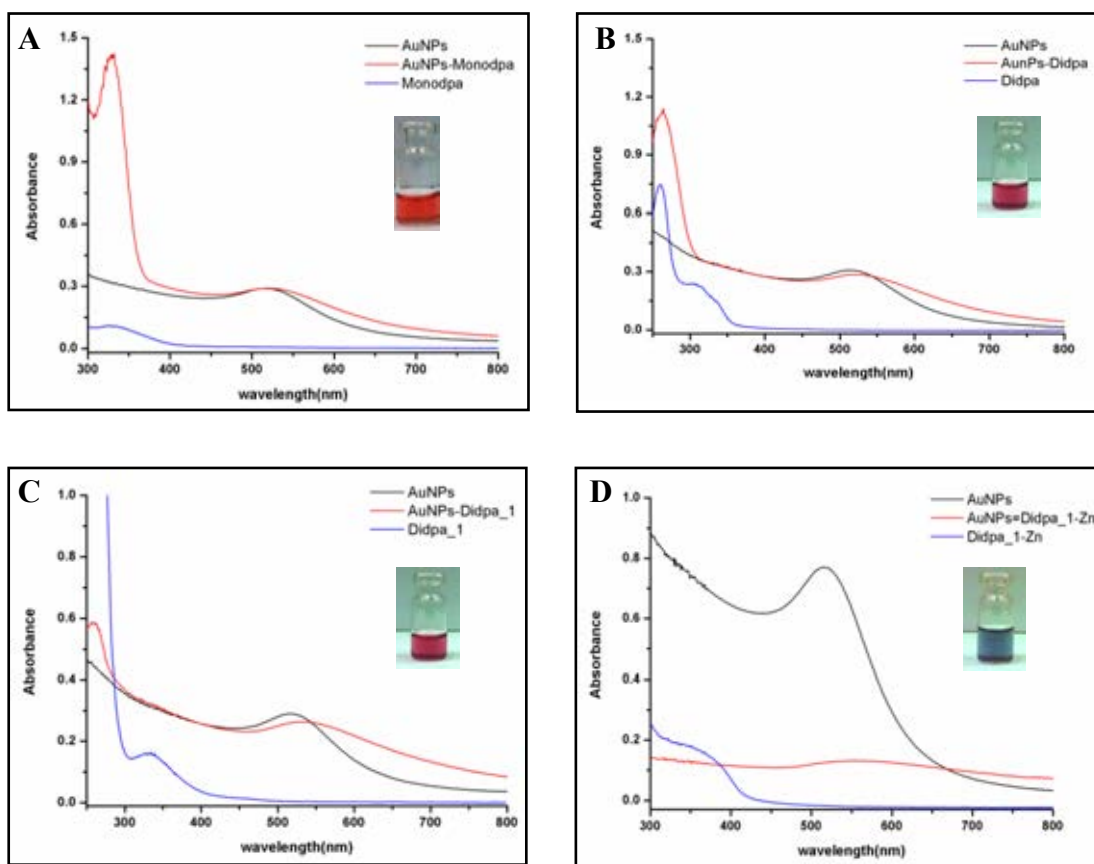


Figure 4.4. UV-visible spectra of functionalized gold nanoparticles with **Monodpa** (A), **Didpa** (B), **Didpa_1** (C) and **Didpa_1-Zn** (D)

4.3. Study on the metal sensing by using modified gold nanoparticles with Monodpa and Didpa_1

Metal sensing ability of **AuNPs-Monodpa** and **AuNPs-Didpa_1** was investigated by UV-visible spectroscopy. **AuNPs-Monodpa** displayed an extinction band at 521 nm and it was shifted to 535 nm upon the addition of Co^{2+} ions, whereas other metal ions (Cd^{2+} , Cu^{2+} , Zn^{2+}) give the unchanged absorption band at 521 nm. Moreover, the color of solution was changed from red to purple due to the complexation of **AuNPs-Monodpa** and Co^{2+} through the chelation and/or electrostatic interactions [65] as shown in Figure 4.5. This approach induces the aggregation of gold nanoparticles resulting in the color change.

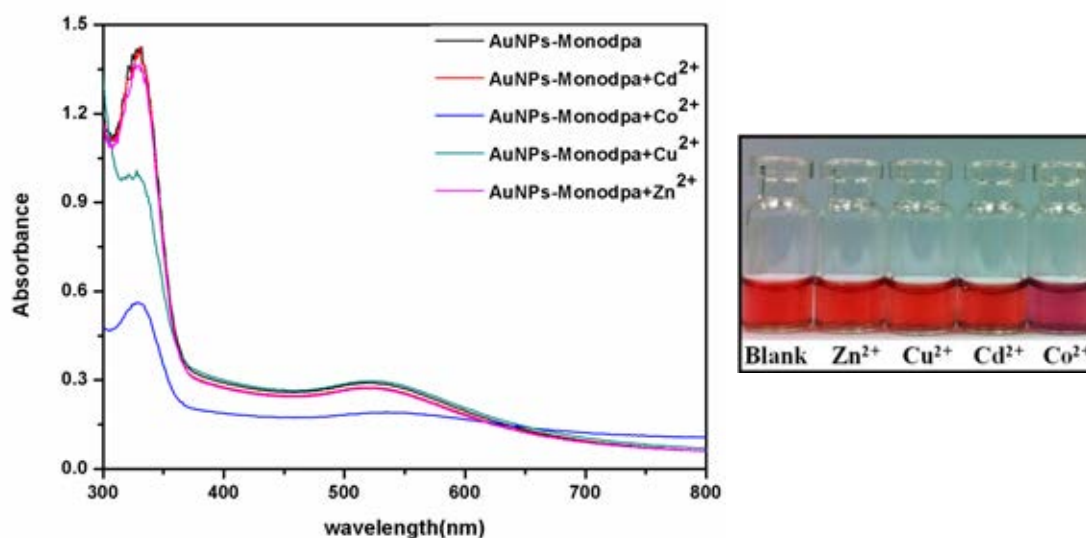


Figure 4.5. UV-visible absorption spectra of **AuNPs-Monodpa** before and after adding various metal ions.

In the case of **AuNPs-Didpa_1**, the absorption spectra in aqueous solution displayed the plasmon band at 530 nm. The presence of metal ions such as Zn^{2+} , Cu^{2+} and Cd^{2+} into the solution of the AuNPs-Didpa_1 caused a large shift ($\Delta\lambda = 20$ nm) of the absorption band to 550 nm. Furthermore, the color change of the solution was observed from red to blue solution (Figure 4.6) and then, the precipitate was slowly formed to give a clear colorless solution. The results suggested that dipicolylamine of **Didpa_1** based gold nanoparticles preferentially coordinated with a given metal ions of Zn^{2+} , Cu^{2+} and Cd^{2+} inducing a large aggregation of gold nanoparticles [66].

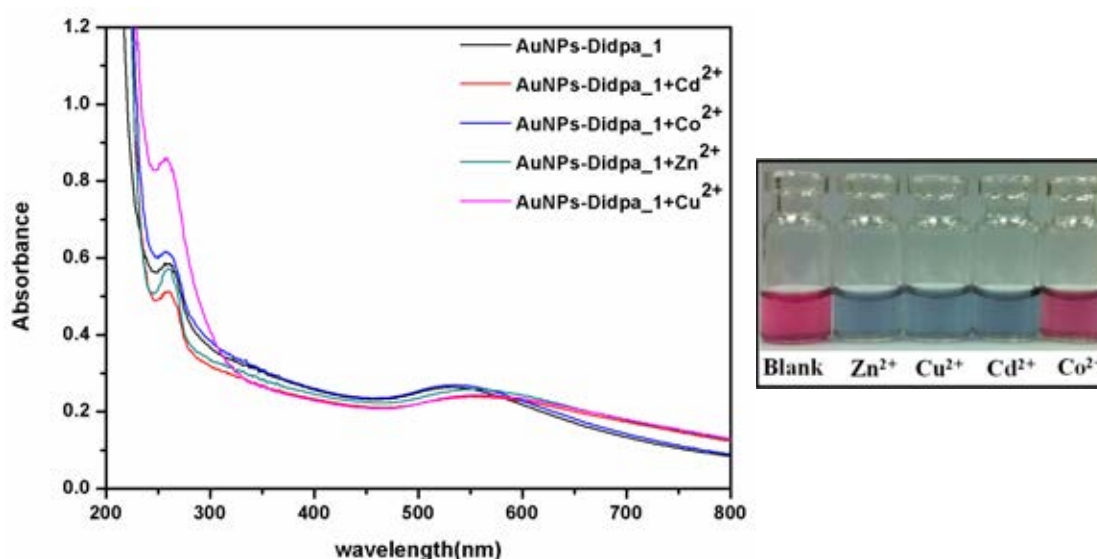


Figure 4.6. UV-visible absorption spectra of **AuNPs-Didpa_1** before and after adding various metal ions.

4.4. Nucleotides detection

In this research, we have focused on studying the nucleotides detection using fluorescence spectroscopy upon two concepts: i) the energy transfer process of sensory molecules to gold nanoparticles and ii) the discrimination of the similarity of nucleotides by Principal Component Analysis (PCa).

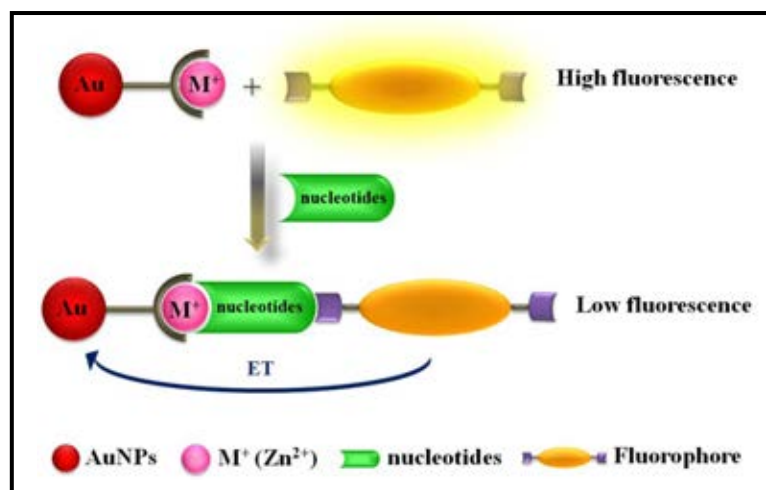
In our basic knowledge, gold nanoparticles have a large absorption band capable to overlap the emission band of the suitable fluorophore upon packing on nanoparticles surfaces resulting in the fluorescence quenching. We have applied this performance of gold nanoparticles for nucleotides sensing with two methodologies as following:

- i) Nucleotides complexation between fluorophore and gold nanoparticles
- ii) Fluorophore replacement with nucleotides

4.4.1 Application of gold nanoparticles for nucleotides detection

4.4.1.1 Complexation between fluorophore and gold nanoparticles for nucleotides sensing

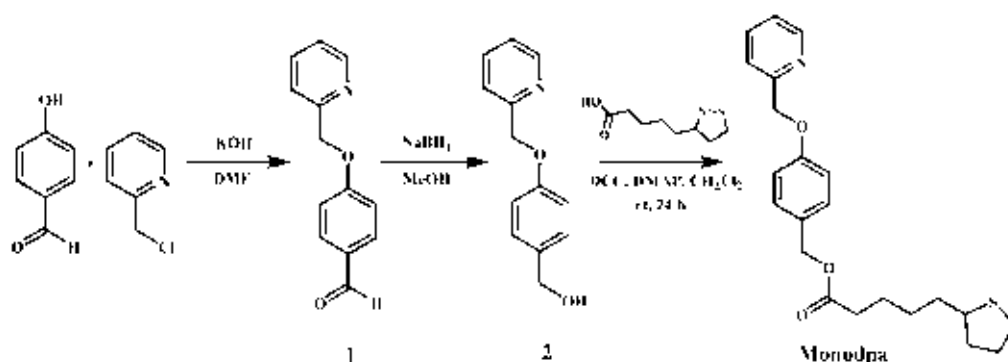
From our concept shown below, we hypothesized that the fluorescence quenching was observed after the suitable nucleotides formed the complex with the modified gold nanoparticles and fluorophore. This approach stemmed from the nucleotides as a linkage between the modified gold nanoparticles and fluorophore inducing the energy transfer from fluorophore to gold nanoparticles (as shown in Scheme 4.1). Herein, we modified the gold nanoparticles with the picolyl unit acting a Zn-chelated part for binding with phosphate unit based nucleotides and synthesized the boronic acid based fluorophore.



Scheme 4.1. Concept of nucleotides sensing by gold nanoparticles via energy transfer process.

4.4.1.1.1. Modification of gold nanoparticles part of Monodpa, Didpa and Didpa_1

- **Synthesis and characterization of Monodpa**



Scheme 4.2. Synthesis pathway of **Monodpa**

The **Monodpa** was prepared through the nucleophilic addition reaction shown in Scheme 4.2. Firstly, the hydroxy group of 4-hydroxybenzaldehyde was deprotonated by potassium hydroxide (1 equiv) in DMF under nitrogen atmosphere for 1 hour. Then, a solution of 2-(chloromethyl) pyridine hydrochloride was added into the reaction mixture and stirred at room temperature for 24 hour until the reaction completed. The reaction was extracted with ethyl acetate and then washed with

saturated sodium chloride to give the yellow solid of compound **1** in 83 %yield. The $^1\text{H-NMR}$ spectrum of compound **1** (Figure 4.7) displayed the characteristic peaks of aldehyde proton ($-\text{CHO}$) at 9.88 ppm. Compared to 4-hydroxyl benzaldehyde, the hydroxyl proton disappeared and the aromatic protons shifted to downfield at 7.84-7.10 ppm. The pyridine protons of compound **1** showed the upfield shift at 8.62 -7.28 ppm and the downfield shifts of the methylene protons ($-\text{CH}_2-$) appeared at 5.29 ppm due to the influence of the electron withdrawing group by the oxygen atom. The $^1\text{H-NMR}$ spectrum corresponds to the structure of **Monodpa**.

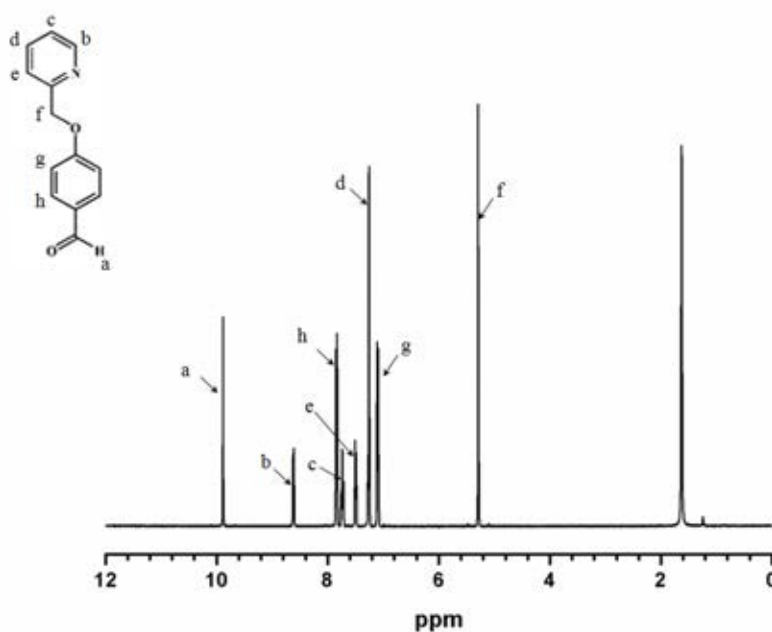


Figure 4.7. $^1\text{H-NMR}$ spectrum of compound **1**.

The aldehyde group of compound **1** was reduced to primary alcohol by sodium borohydride in cold methanol under nitrogen atmosphere. After the reaction completed, the reaction was neutralized by 3 M HCl. Then, the product was purified by extraction with dichloromethane to afford the yellow solid of compound **2** in 90 %yield. The $^1\text{H-NMR}$ spectrum of compound **2** shows the characteristic peak of primary alcohol proton ($-\text{CH}_2-\text{OH}$) at 4.62 ppm and the disappearance of aldehyde proton at 9.88 ppm as shown in Figure 4.8. The protons in the range of 8.59-6.96 ppm were assigned to the aromatic protons and pyridine protons.

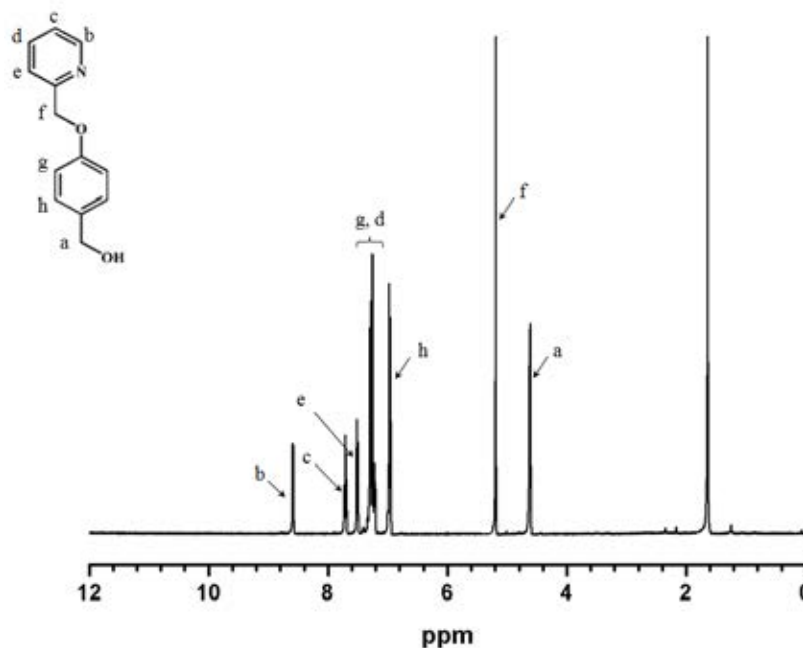


Figure 4.8. $^1\text{H-NMR}$ spectrum of compound **2**.

Finally, **Monodpa** was synthesized through esterification reaction between compound **2** and (\pm)- α - lipoic acid by using DCC and DMAP as a catalyst. The reaction was treated with 3 M HCl for neutralization and purified by column chromatography using 20% ethyl acetate in dichloromethane as eluent to give the yellow oil of **Monodpa** in 32 %yield. The $^1\text{H-NMR}$ spectrum of **Monodpa** (Figure 4.9) displayed the characteristic peaks at 3.57-1.38 ppm corresponding to 13 protons of lipoic alkyl chain which performed the upfield shift compared to (\pm)- α - lipoic acid. The methylene protons of $\text{Ar-CH}_2\text{O}$ shifted to downfield at 5.04 ppm. The $^1\text{H-NMR}$ spectrum showed a singlet proton at 5.21 ppm assigned to the methylene protons of $\text{py-CH}_2\text{-OR}$ and the aromatic and pyridine protons were observed at 8.59-6.96 ppm.

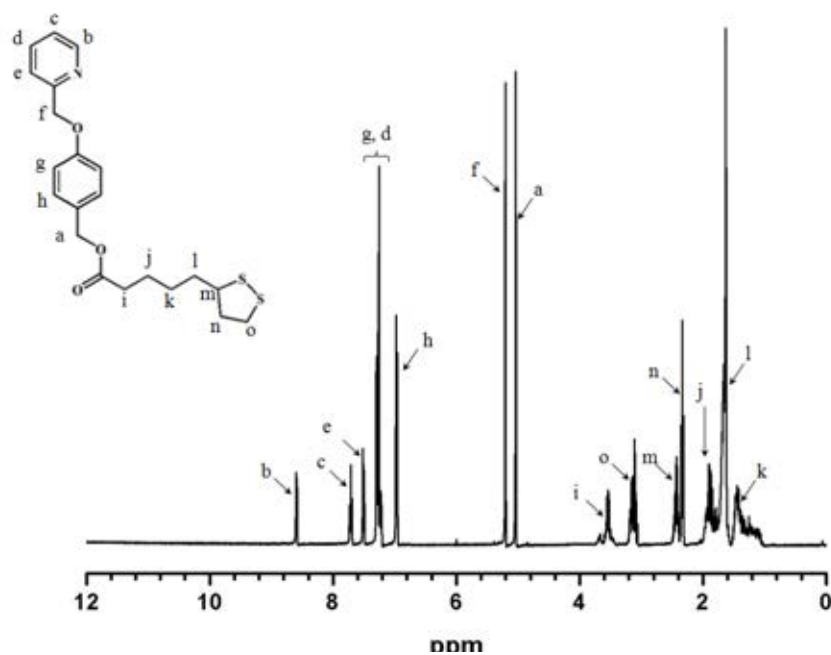
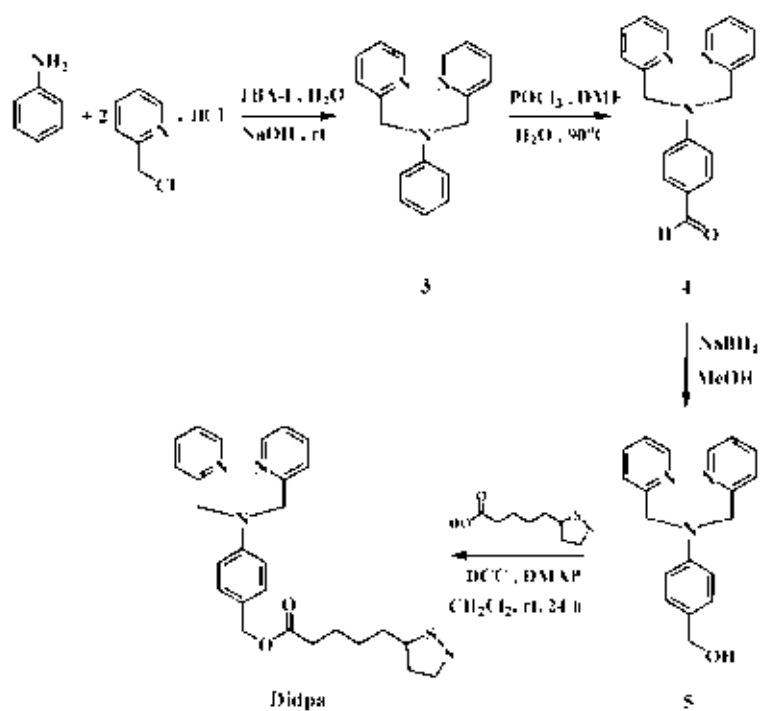


Figure 4.9. ¹H-NMR spectrum of Monodpa.

• Synthesis and characterization of Didpa



Scheme 4.3. Synthesis pathway of Didpa.

The **Didpa** was synthesized by four steps demonstrated in Scheme 4.3. Initially, compound **3** was prepared through the reaction between aniline and picolyl chloride by using tetrabutylammonium iodide (TBA-I) as catalyst for exchanging chloroide to iodide. After reaction completed, the reaction mixture was extracted with dichloromethane and purified by column chromatography using 20% ethyl acetate in dichloromethane as eluent to afford a white solid of compound **3** in 29 %yield. The $^1\text{H-NMR}$ spectrum of compound **3** (Figure 4.10) displayed the characteristic peaks at 4.83 ppm assigned to 4 protons of $-\text{CH}_2\text{-pyridine}$ upon the upfield shift due to the electron donating of nitrogen atom. The addition of 13 aromatic protons corresponding to the pyridine and aniline protons were observed at 8.59-6.71 ppm. This $^1\text{H-NMR}$ results suggested the structure of compound **3**.

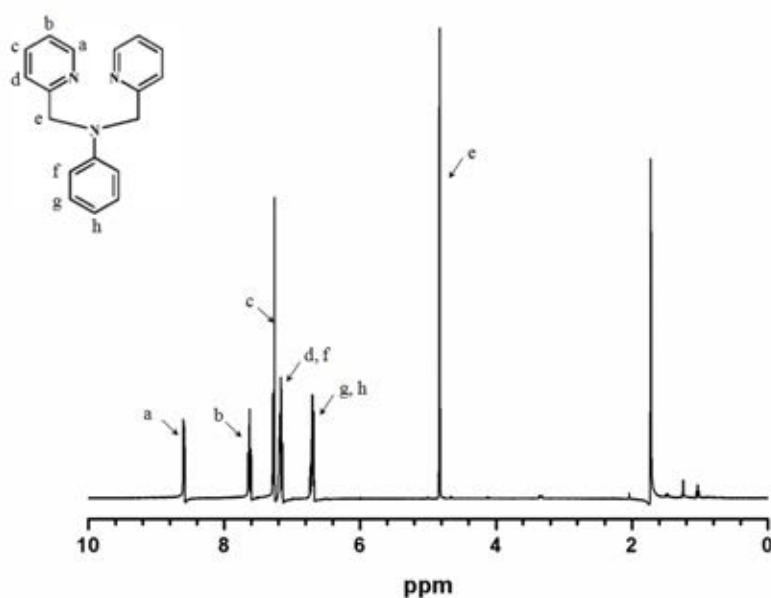


Figure 4.10. $^1\text{H-NMR}$ spectrum of compound **3**.

Compound **4** was synthesized by Vilsmerier-Haack reaction between POCl_3 and compound **3** in dimethyl formaldehyde. The completed reaction was neutralized by potassium carbonate to give the pH 6-8. The reaction mixture was extracted with dichloromethane to give the yellow oil of compound **4** in 85 %yield. The $^1\text{H-NMR}$ spectrum of compound **4** (Figure 4.11) displayed the characteristic peaks of aldehyde

proton ($-CHO$) at 9.73 ppm indicating that the attachment of aldehyde group to aromatic ring of compound **3** was achieved. The $-CH_2$ -pyridine was observed at 4.91 ppm. Moreover, the pyridine and aromatic protons of compound **4** showed the downfield shift at 8.61-6.78 ppm compared to these protons of compound **3**.

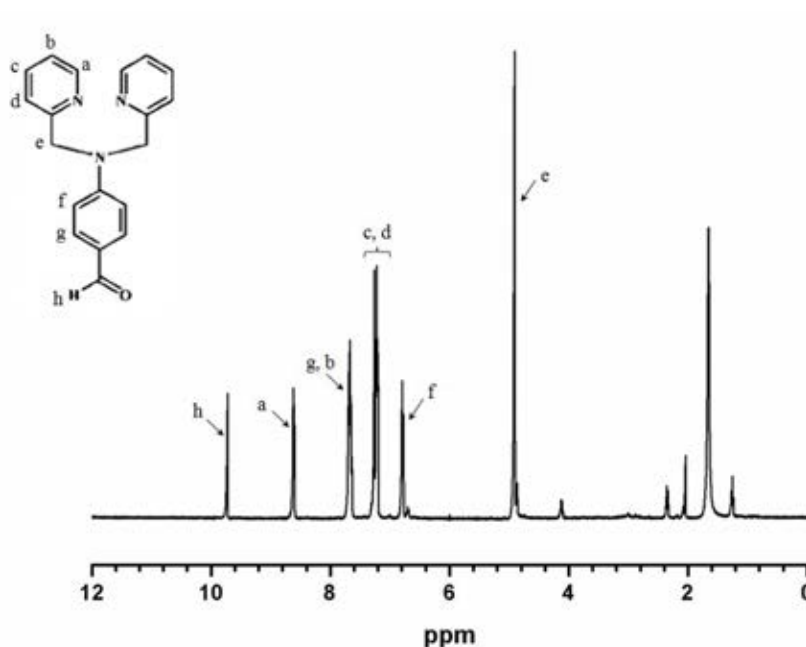


Figure 4.11. 1H -NMR spectrum of compound **4**.

The aldehyde moiety of compound **4** was reduced to a primary alcohol by sodium borohydride in cold methanol under nitrogen atmosphere. The product was purified by extraction with dichloromethane to afford the yellow solid of compound **5** in 80 %yield. The 1H -NMR spectrum of compound **5** displayed the characteristic peak of primary alcohol proton ($-CH_2-OH$) at 4.53 ppm with a concomitant of the disappearance of aldehyde proton at 9.73 ppm as shown in Figure 4.12. The $-CH_2$ -pyridine was observed at 4.82 ppm. The proton peaks at 8.58-6.67 ppm were assigned to aromatic and pyridine protons.

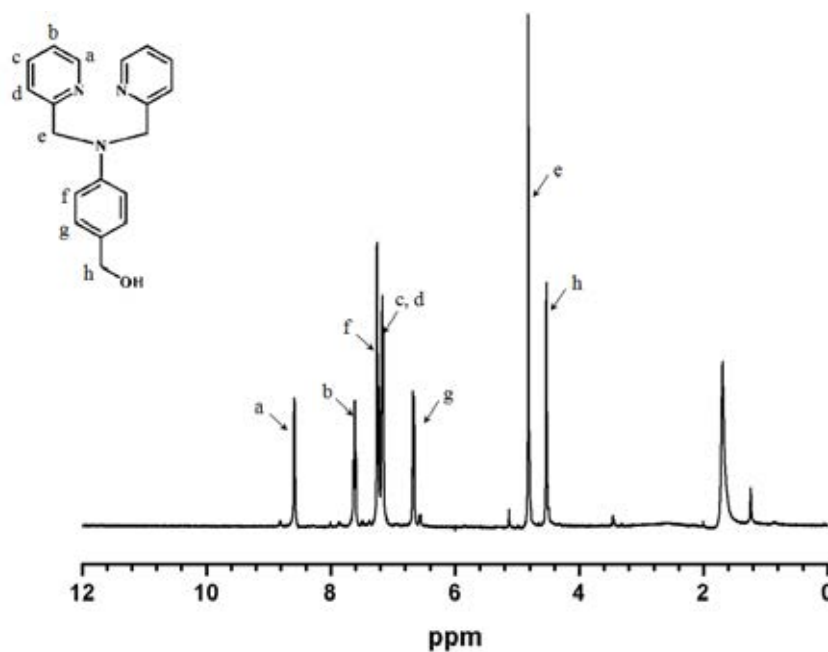


Figure 4.12. ^1H -NMR spectrum of compound **5**.

Didpa was synthesized through the esterification reaction between compound **5** and (\pm)- α -lipotic acid by using DCC and DMAP as catalysts. The product was purified by column chromatography using 10% methanol in ethyl acetate as eluent to give the yellow oil of **Didpa** in 29 %yield. The ^1H -NMR spectrum of **Didpa** (Figure 4.13) displayed the characteristic protons of lipotic alkyl chain with upfield shift at 3.55-1.33 ppm. The proton peaks of $\text{Ar-CH}_2\text{O}$ shifted to downfield at 4.96 ppm due to influence of electron withdrawing group by the oxygen atom. Additionally, the $-\text{CH}_2$ -pyridine and aromatic protons of pyridine were observed at 4.83 ppm and 8.59-6.66 ppm, respectively.

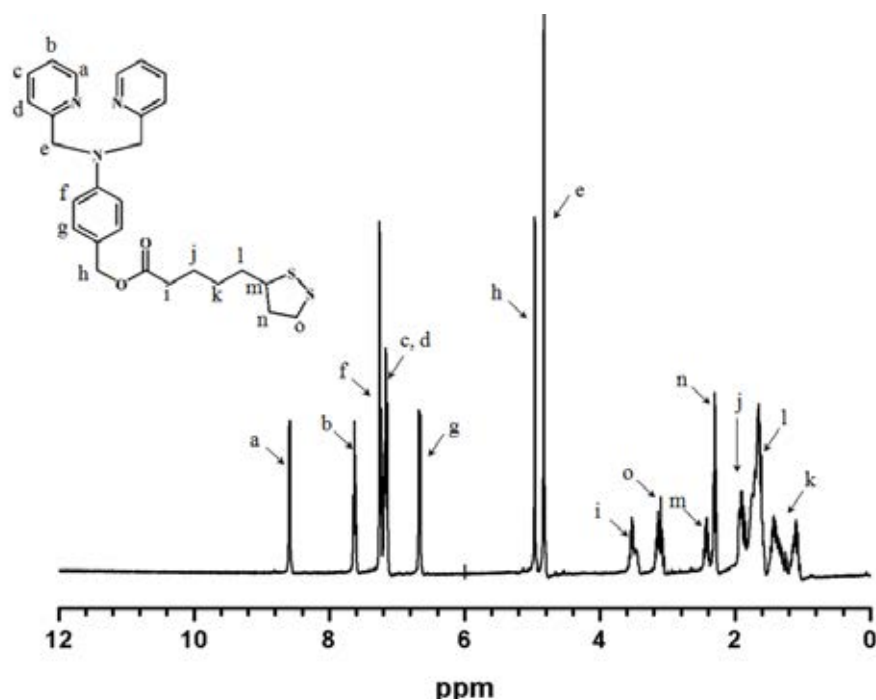
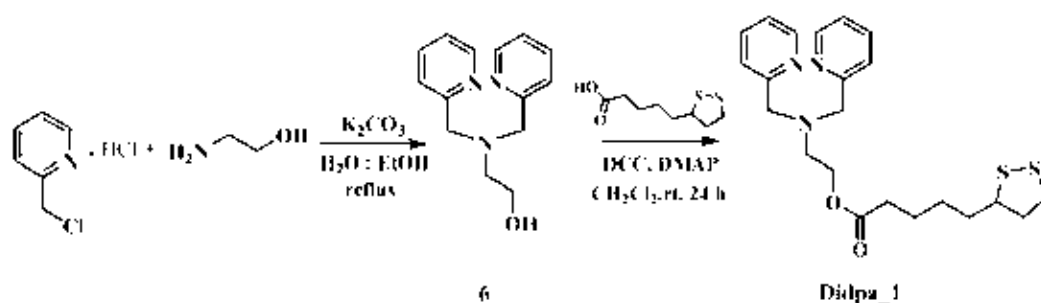


Figure 4.13. $^1\text{H-NMR}$ spectrum of **Didpa**.

• **Synthesis and characterization of Didpa_1**



Scheme 4.4. Synthesis pathway of **Didpa_1**.

Compound **6** was synthesized by the nucleophilic substitution between ethanolamine and picolyl chloride by using potassium carbonate as base. After the reaction completed, the pH of the solution mixture was adjusted to pH 8 by sodium hydrogen carbonate. The reaction mixture was purified by column chromatography using 80% ethyl acetate in dichloromethane to afford the yellow oil of compound **6** in 42 %yield. The $^1\text{H-NMR}$ spectrum of compound **6** showed the characteristic peak of

primary alcohol ($-CH_2-OH$) at 3.66 ppm (Figure 4.14). The proton of CH_2 -pyridine was shifted to upfield at 3.92 ppm upon the influence of the electron donating group of nitrogen atom. The $-CH_2N-$ of ethanolamine was shift from 2.82 to 2.86 ppm and the disappearance of amine proton was observed. In addition, pyridine protons were showed the upfield shifts at 8.53-7.14 ppm.

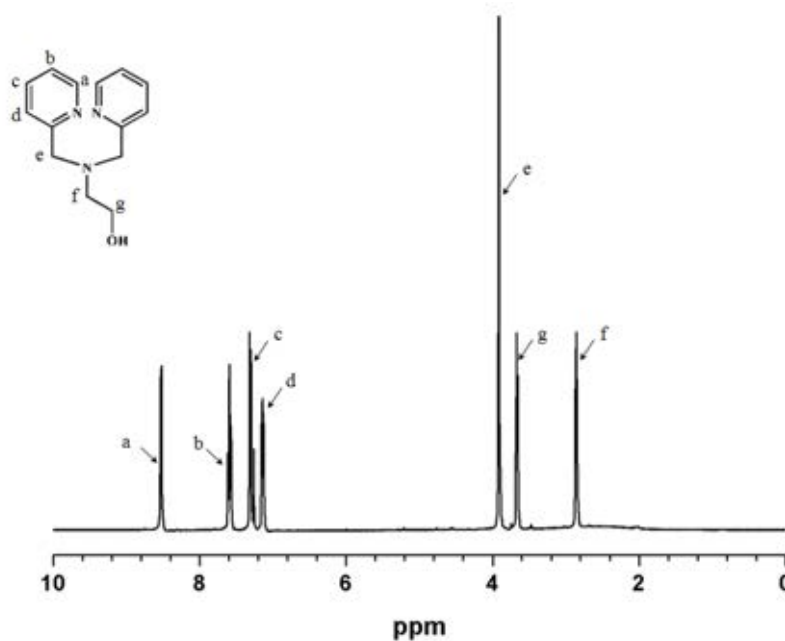


Figure 4.14. 1H -NMR spectrum of compound **6**.

Didpa_1 was obtained by an esterification reaction of compound **6** and (\pm)- α -lipoic acid in the presence of DCC and DMAP as catalyst in dichloromethane. The product was purified by column chromatography using 10% methanol in ethyl acetate to give the yellow oil of **Didpa_1** in 62 %yield. 1H -NMR spectrum of **Didpa_1** showed the characteristic protons of lipoic alkyl chain at 3.56-1.40 ppm (Figure 4.15). The $-CH_2$ -pyridine was observed at 3.89 ppm. The triplet protons at 2.88 and 4.20 ppm corresponded to the methylene protons of $-N-CH_2-$ and $-O-CH_2-$, respectively. The pyridine protons were observed at 8.52-7.15 ppm. The 1H -NMR assignments agreed with the structure of **Didpa_1**.

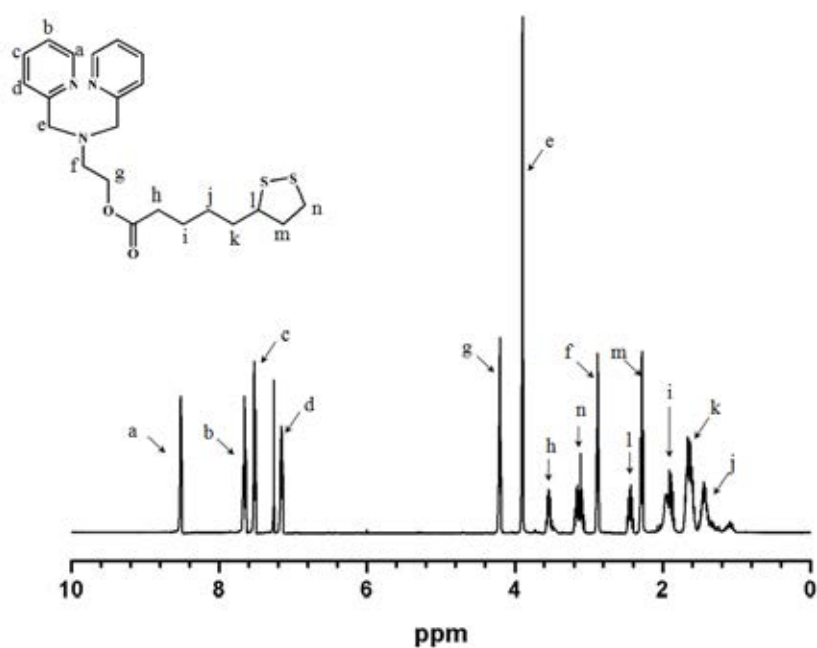
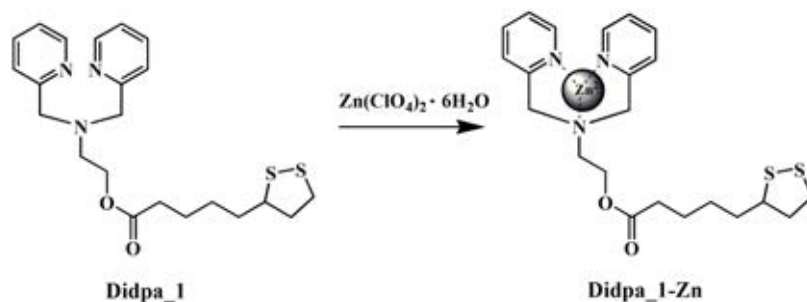


Figure 4.15. $^1\text{H-NMR}$ spectrum of **Didpa_1**.

• **Synthesis and characterization of *Didpa_1-Zn***



Scheme 4.5. Synthesis pathway of **Didpa_1-Zn**.

Didpa_1-Zn complex was obtained from the reaction between **Didpa_1** and $\text{Zn}(\text{ClO}_4)_2 \cdot 6\text{H}_2\text{O}$. When $\text{Zn}(\text{ClO}_4)_2 \cdot 6\text{H}_2\text{O}$ was added into the solution of **Didpa_1**, the color solution was changed immediately from pale yellow to orange. The corresponding solution was stirred at room temperature for 24 h to ensure a complete reaction giving the yellow solid of **Didpa_1-Zn** complex in 58 %yield. The $^1\text{H-NMR}$ spectrum of **Didpa_1-Zn** (Figure 4.16) displayed the downfield shift of pyridine protons at 8.79-7.49 ppm because the nitrogen atom coordinated toward Zn^{2+} .

Furthermore, lipotic alkyl chain was observed at 3.60-1.46 ppm. Compared to ^1H -NMR spectrum of **Didpa_1**, all assignments of complex were changed significantly. Therefore, the **Didpa_1-Zn** was successfully obtained. Moreover, **Didpa_1-Zn** was confirmed by ESI MS with the intense peak of 531.124 m/z.

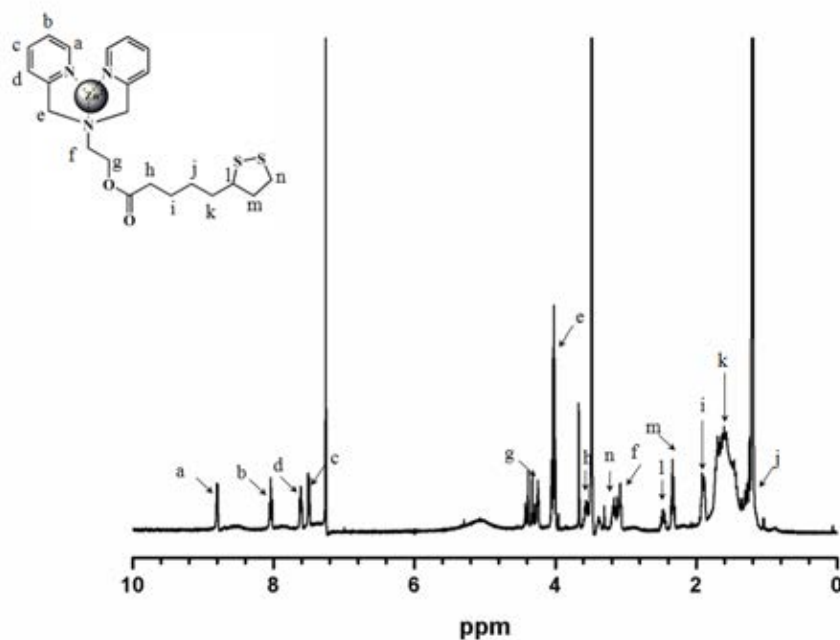
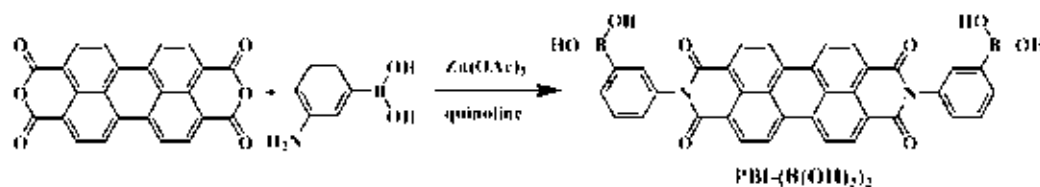


Figure 4.16. ^1H -NMR spectrum of **Didpa_1-Zn**.

4.4.1.1.2. Synthesis of boronic acid based fluorophore part.

- Synthesis and characterization of $\text{PBI-(B(OH)}_2)_2$



Scheme 4.6. Synthesis pathway of $\text{PBI-(B(OH)}_2)_2$.

$\text{PBI-(B(OH)}_2)_2$ was obtained from the reaction between perylene-3,4,9,10-tetracarboxylic dianhydride and 3-aminoboronic acid in the presence of zinc acetate as catalyst. The dark red precipitate was filtrated and washed with cold ethanol to give the dark-red solid of $\text{PBI-(B(OH)}_2)_2$ in 85 %yield. $^1\text{H-NMR}$ spectrum of $\text{PBI-(B(OH)}_2)_2$ showed the upfield shift of aromatic proton at 8.86-7.19 (Figure 4.17).

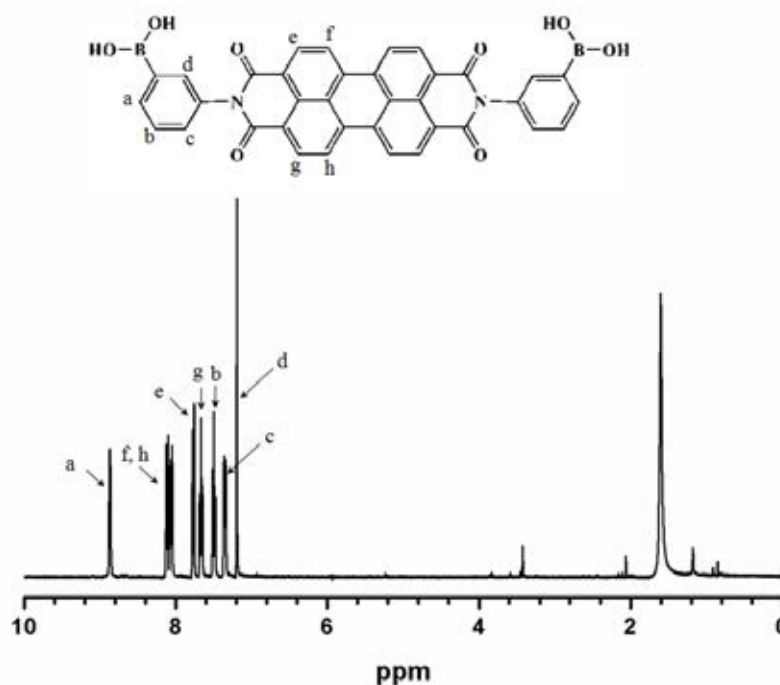


Figure 4.17. $^1\text{H-NMR}$ spectrum of $\text{PBI-(B(OH)}_2)_2$.

The **PBI-(B(OH)₂)₂** was designed and synthesized for nucleotides detection consisting of perylene as a sensory unit and the boronic acid as a receptor unit for binding with diol group of ribose based nucleotides. The absorption band of **PBI-(B(OH)₂)₂** was showed in the range of 450-550 nm and the fluorescence spectrum was displayed in the range of 460-575 nm (shown in Figure 4.18).

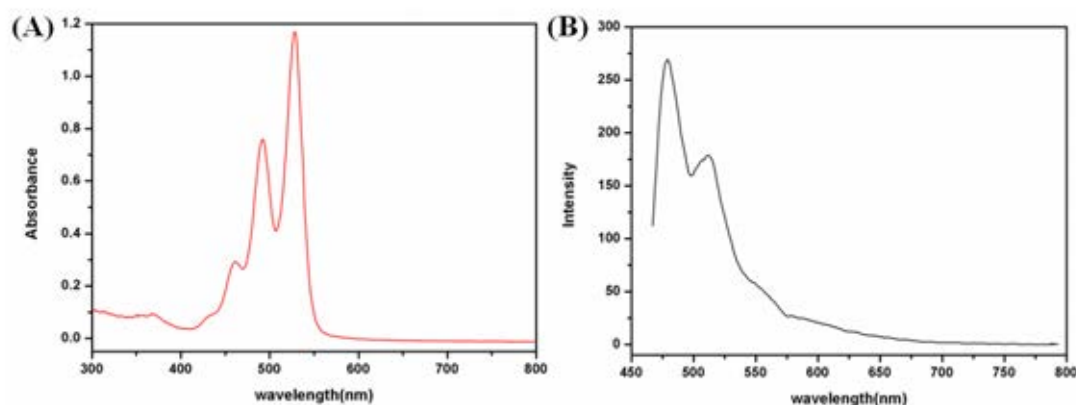


Figure 4.18. (A) Absorption (1×10^{-4} M) and (B) emission (1×10^{-5} M) spectrum of **PBI-(B(OH)₂)₂** in DMSO ($\lambda_{\text{ex}} = 450$ nm).

4.4.1.1.3. Complexation studies of nucleotides detection by using AuNPs-Didpa \subset Zn²⁺ with **PBI-(B(OH)₂)₂**

The application of gold nanoparticles for nucleotides sensing according to the Scheme 4.1 was investigated by using fluorescence spectroscopy. The gold nanoparticles used in this study were synthesized using citrate as a stabilizer. The modified gold nanoparticles were prepared according to the topic of 3.2.1 and 3.3. Considering the fluorescence quenching of **PBI-(B(OH)₂)₂** in the presence of the modified gold nanoparticles, it suggested that the interaction between both receptors in HEPES buffer solution at pH 7.4 induced the fluorescence resonance energy transfer process. Compared to the solution of **PBI-(B(OH)₂)₂** and AuNPs-Didpa \subset Zn²⁺, the addition of ATP to AuNPs-Didpa \subset Zn²⁺+ **PBI-(B(OH)₂)₂** did not give the influence of fluorescence change (Figure 4.19). This indicated that ATP did

not be allow to form complex with **AuNPs-Didpa** \subset **Zn²⁺** and **PBI-(B(OH)₂)₂**. This system, thus, was not suitable for nucleotides sensing purpose.

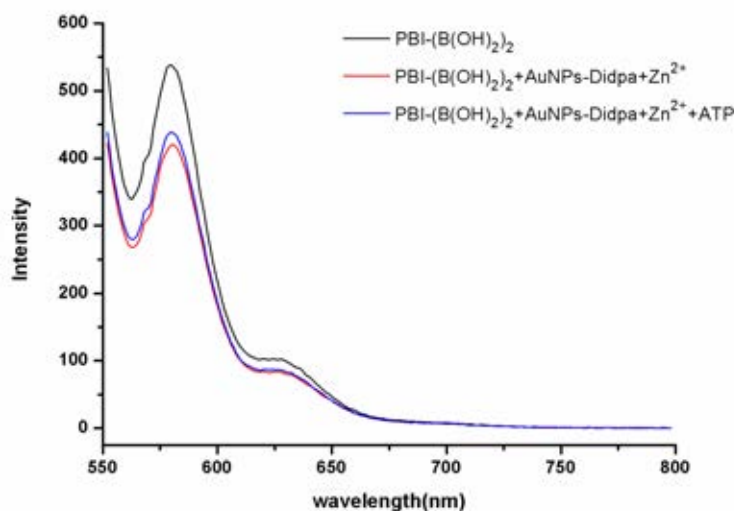


Figure 4.19. Complexation of **PBI-(B(OH)₂)₂** and **AuNPs-Didpa** \subset **Zn²⁺** upon adding various nucleotides ($\lambda_{\text{ex}} = 525 \text{ nm}$).

From the previous report in our group, **Didpa** is able to bind with **Zn²⁺** with a weak interaction since the lone pair electron of nitrogen atom adjacent to aromatic ring prefer to delocalize into the aromatic ring resulting in a weak coordination with **Zn²⁺**. To solve this problem, we have designed the **Didpa_1** possessing the nitrogen atom adjacent to aliphatic chain to avoid the delocalization of lone pair electron on the nitrogen atom.

In the preliminary, we have examined the binding properties of **Didpa_1** and **Zn²⁺**. Considering the complex of **Didpa_1-Zn**, the absorption band of **Didpa_1-Zn** showed the characteristic peak at 336 nm in the attribution of π - π^* transition of pyridine. Observing, the absorption band was shifted to 350 nm upon the addition of **Zn²⁺** as shown in Figure 4.20.

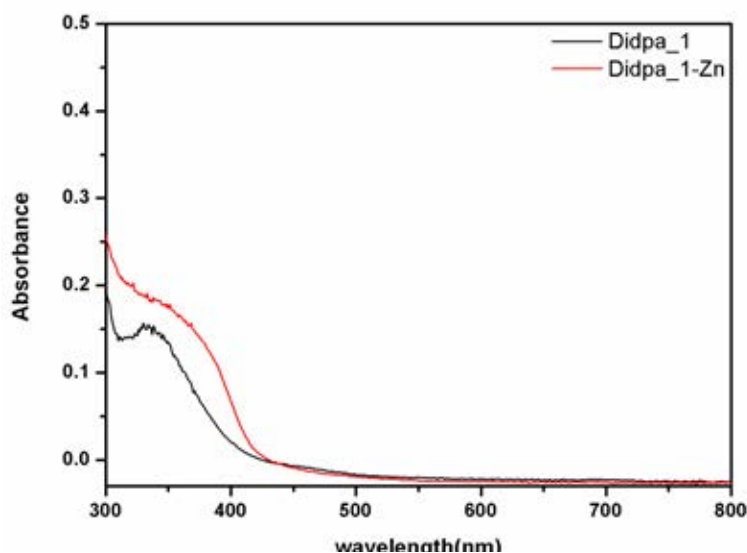


Figure 4.20. Absorption spectra of **Didpa_1** and **Didpa_1-Zn** in DMSO (1×10^{-4} M).

To avoid the aggregation of **Didpa_1-Zn** modified on the gold nanoparticles in aqueous, therefore, **Didpa_1-Zn** modified on gold nanoparticles was prepared by a new method using tetraalkylammonium bromide (TOABr) as a stabilizer. In preparation, the solution of **Didpa_1-Zn** complex, gold nanoparticles with TOABr dissolved in the 10% toluene in DMSO was stirred vigorously. The absorption spectrum of the modified gold nanoparticles exhibited two absorption bands at 353 and 526 nm correspond to π - π^* transition of **Didpa_1-Zn** and the surface Plasmon band of gold nanoparticles, respectively. A small red shift ($\Delta\lambda = 3$ nm) of the absorption band is indicative of a slight aggregation of **AuNPs-Didpa_1-Zn** (Figure 4.21).

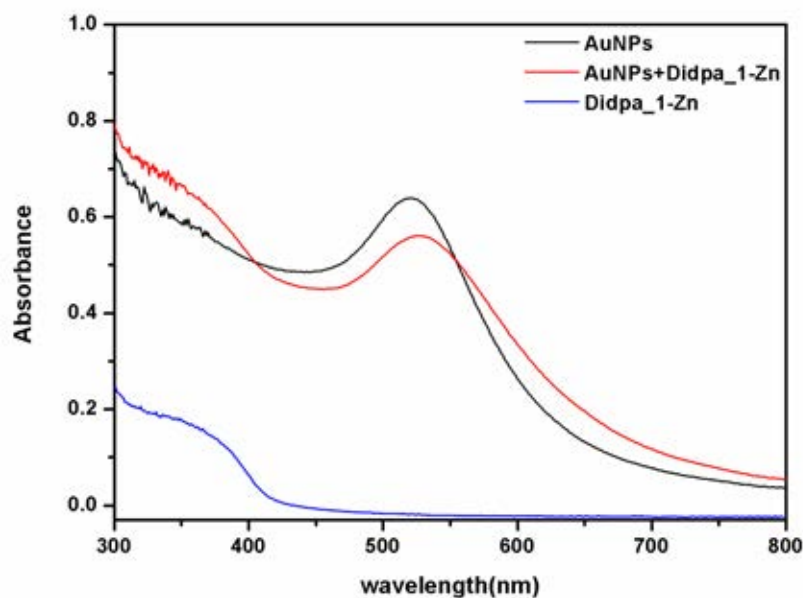


Figure 4.21. UV-visible spectra of **Didpa_1-Zn**-functionalized gold nanoparticles (red).

4.4.1.1.4. Complexation studies between AuNPs-Didpa_1-Zn and PBI-(B(OH)₂)₂ for nucleotides detection

Gold nanoparticles used in this case were prepared by TOABr in toluene. Thus, the detection of nucleotides using **AuNPs-Didpa_1-Zn** was studied in 10% toluene in DMSO. From Figure 4.22, the strong fluorescence quenching of **PBI-(B(OH)₂)₂** was observed upon the addition of **AuNPs-Didpa_1-Zn** indicating that packing of **PBI-(B(OH)₂)₂** was coated on the surface of gold nanoparticles probably by hydrophobic interaction. Unfortunately, the addition of the various nucleotides did not induce the fluorescence spectral change of **PBI-(B(OH)₂)₂**. It is possibly caused by no interaction between **PBI-(B(OH)₂)₂** and nucleotides. To verify the binding ability of **PBI-(B(OH)₂)₂** with nucleotides, the fluorescence responses of **PBI-(B(OH)₂)₂** and nucleotides were displayed in Figure 4.23. After adding nucleotides, no fluorescence changes were observed. From all results in this part, we found that our hypothesized concept has not been achieved in the nucleotides sensing purpose.

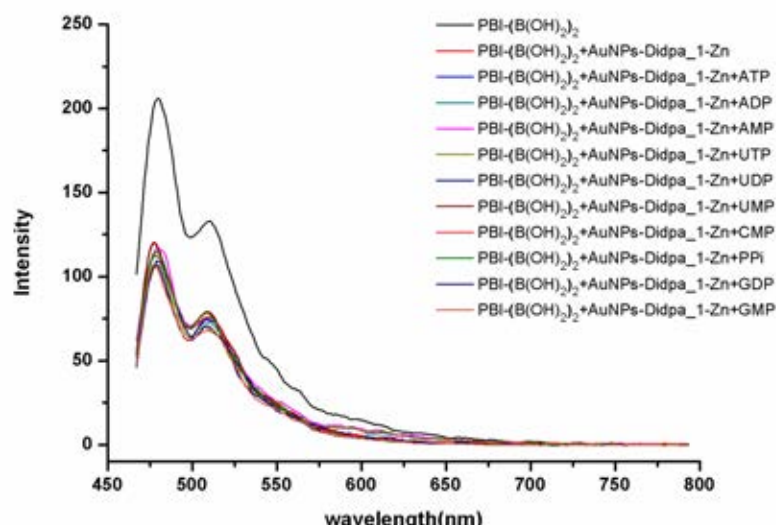


Figure 4.22. Complexation of **PBI-(B(OH)₂)₂** and **AuNPs-Didpa_1-Zn** upon adding various nucleotides ($\lambda_{\text{ex}} = 450 \text{ nm}$).

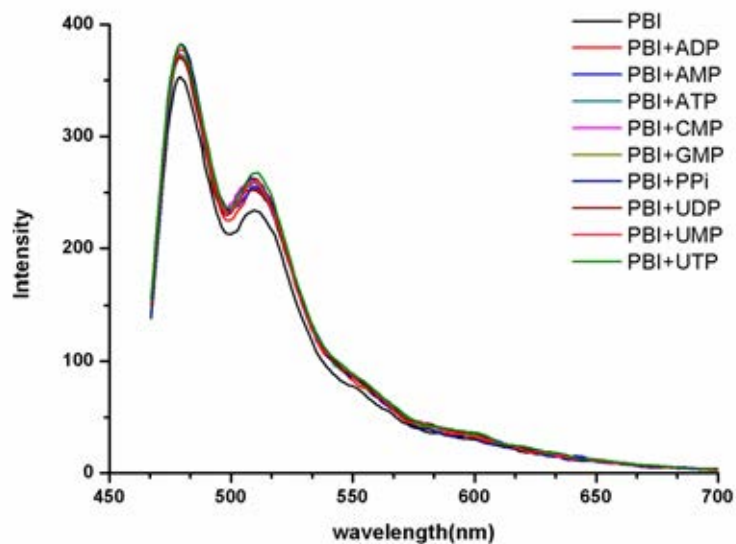
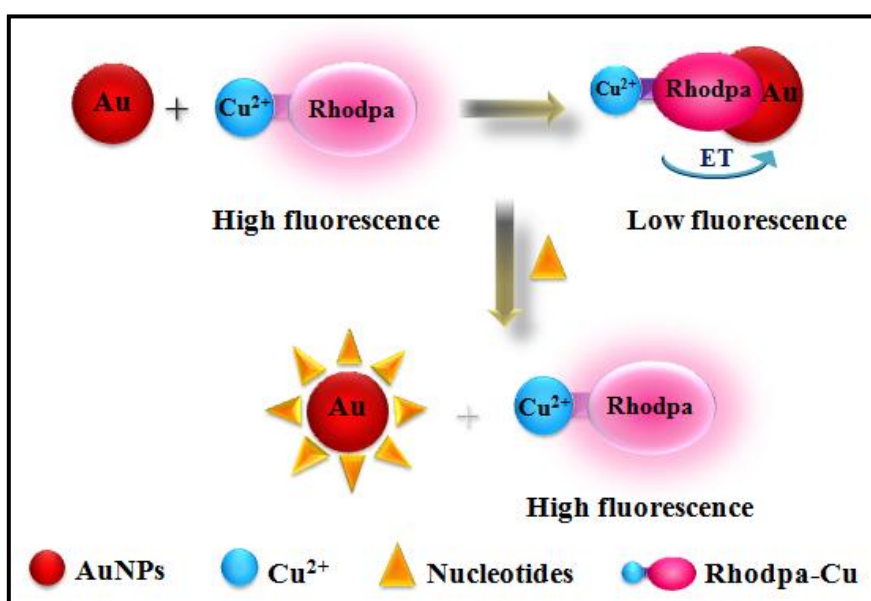


Figure 4.23. Fluorescence spectra of **PBI-(B(OH)₂)₂** before and after adding various nucleotides in aqueous solution of 0.01 M HEPES (pH 7.4) ($\lambda_{\text{ex}} = 450 \text{ nm}$).

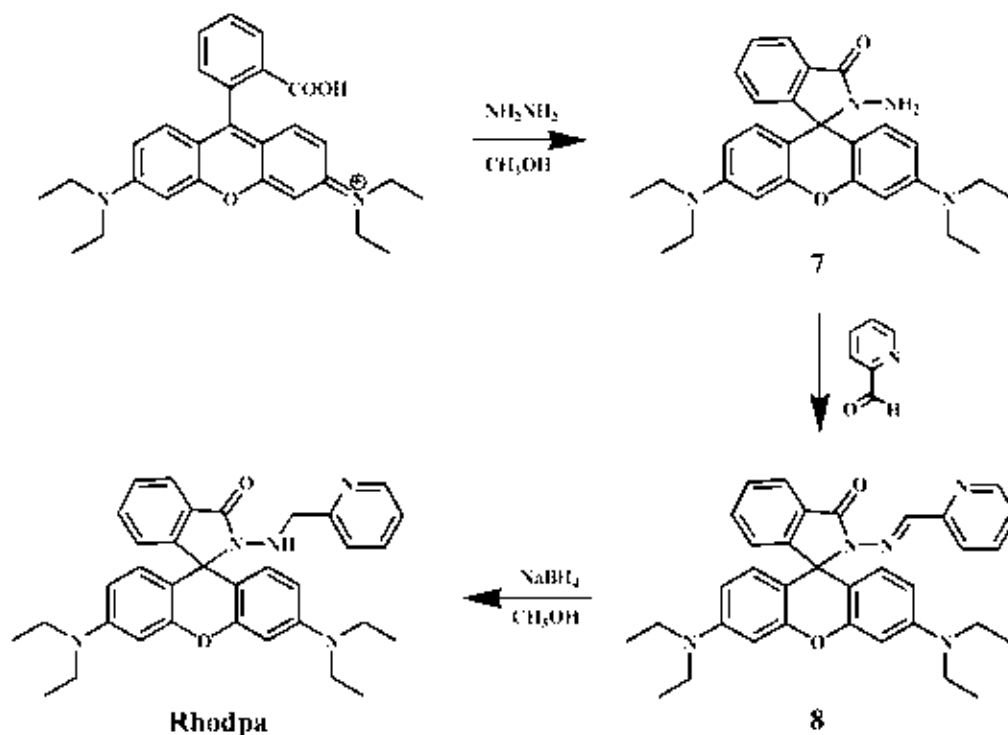
4.4.1.2 Fluorophore replacement with nucleotides using gold nanoparticles and Rhodpa-Cu

From the previous report in literature review [67], nucleotides were used as stabilizer of gold nanoparticles. Zhao reported that each of gold nanoparticles exhibited the different stabilizer properties upon coating on the surface of gold nanoparticles. In our knowledge, the suitable fluorophore compound showed the fluorescence quenching upon complexation with gold nanoparticles [68]. Herein, we attempted to combine two knowledges of nucleotides as stabilizer of gold nanoparticles and the fluorescence change upon the complexation of fluorophore and gold nanoparticles in order to explore the novel nucleotides-sensing system. In our hypothesis, fluorescence intensity of fluorogenic compound was quenched upon packed on gold nanoparticles surfaces through fluorescence energy transfer process. Conceptually, we expected that when the fluorogenic compound on the gold nanoparticles surfaces was replaced by nucleotides, the fluorescence intensity of the fluorogenic compound turned to increase as shown in the scheme 4.7. Molecular sensor used in this study was **Rhodpa-Cu** and the synthesis pathway was shown in scheme 4.8.



Scheme 4.7. Concept of nucleotides sensing by fluorophore replacement with nucleotides

4.4.1.2.1 Synthesis and characterization of Rhodpa



Scheme 4.8. Synthesis pathway of **Rhodpa**.

Compound **7** was synthesized by the cyclization reaction between **rhodamine_B** and hydrazine as shown in Scheme 4.8. The reaction mixture was heated at 90°C for 2 h. The color solution changed from dark purple to pale yellow. The red clear solution was obtained after adding with 1 M HCl (10 mL) and then 1 M NaOH (30 mL) was added to adjust pH 6-8. The precipitate was immediately formed to afford compound **7** as pink solid in 64% yield. The $^1\text{H-NMR}$ spectrum of compound **7** (Figure 4.24) showed the disappearance of $-\text{COOH}$ assignment at 12.79 ppm. The aromatic protons of compound **7** shifted to upfield at 6.27-7.92 ppm. The single board proton of $-\text{NH}_2$ was observed at 3.59 ppm. In addition, the proton peaks at 3.32 and 1.14 assigned to $-\text{N-CH}_2-$ and $-\text{N-CH}_2-\text{CH}_3$, respectively, were appeared.

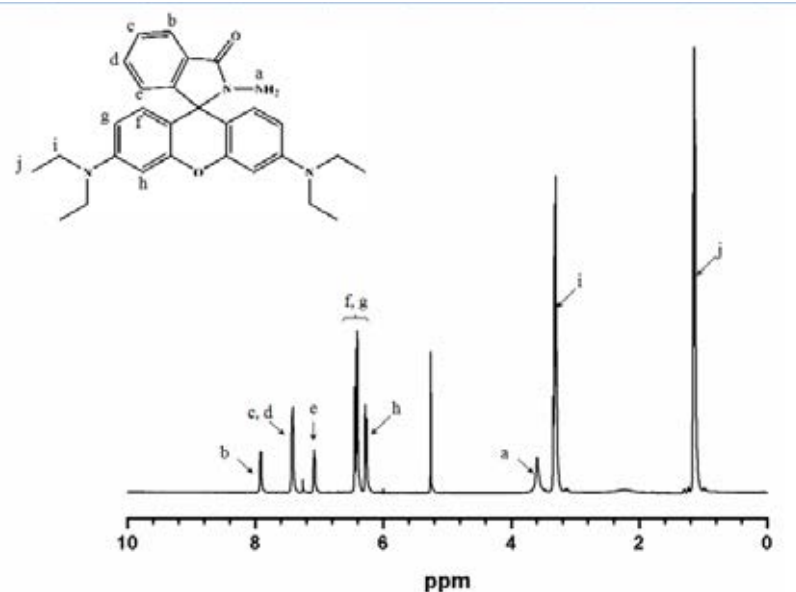


Figure 4.24. ^1H -NMR spectrum of compound 7.

Compound **8** was synthesized through Schiff base reaction between compound **7** and 2-(chloromethyl) pyridine hydrochloride in methanol for 2 h. After that, the precipitate was slowly formed to afford the white solid of compound **7** in 64 %yield. The ^1H -NMR spectrum of compound **8** (Figure 4.25) displayed the characteristic peak of $-\text{N}=\text{CH}$ -pyridine at 8.32 ppm and the disappearance of amine proton at 3.59 ppm. The proton peaks at 3.31 and 1.14 ppm were assigned to $-\text{N}-\text{CH}_2-$ and $-\text{N}-\text{CH}_2-\text{CH}_3$, respectively. The aromatic protons were observed at 8.46-6.23 ppm corresponding to 14 protons of rhodamine and pyridine.

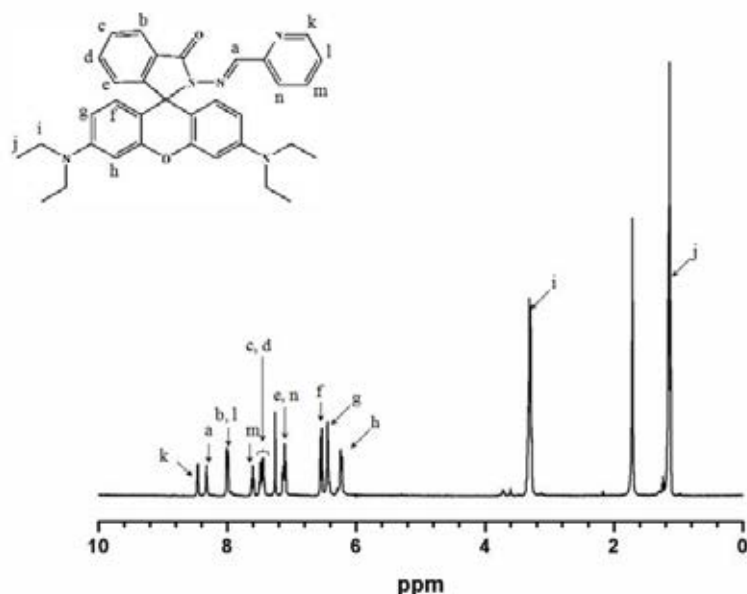


Figure 4.25. ^1H -NMR spectrum of compound **8**.

Rhodpa was synthesized through the reduction reaction of compound **8** using sodium borohydride as reducing agent in cold methanol for 2 hr. After the reaction completed, the mixture was extracted with 3 M HCl for neutralization and purified by column chromatography using ethyl acetate to give the **Rhodpa** as a white solid in 83.44 %yield. The ^1H -NMR spectrum of **Rhodpa** (Figure 4.26) displayed the characteristic peak of $-\text{CH}_2\text{-pyridine}$ at 3.96 ppm and $-\text{NH-}$ proton of **Rhodpa** at 4.815 ppm. The aromatic and pyridine protons showed the upfield shift at 8.374-6.228 ppm. The proton peaks at 3.319 and 1.154 ppm were assigned to $-\text{N-CH}_2\text{-}$ and $-\text{N-CH}_2\text{-CH}_3$, respectively. All assignments are consistent with the structure of the desired compound (**Rhodpa**).

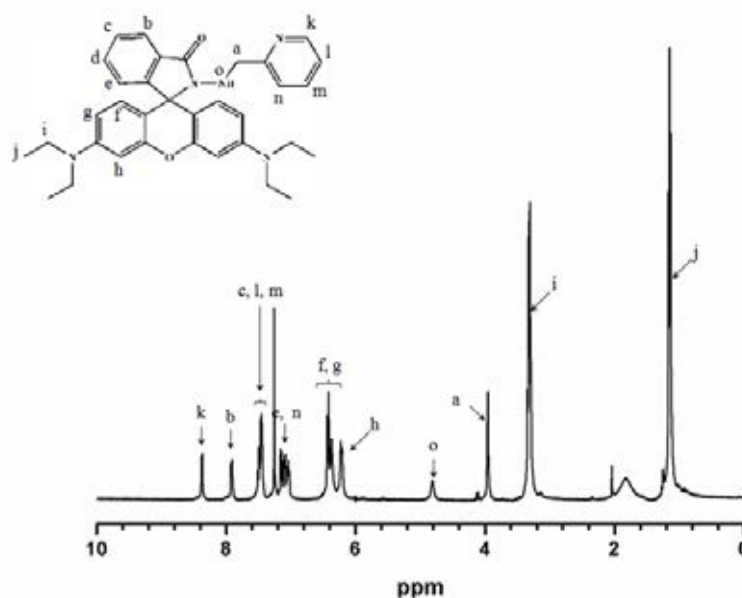


Figure 4.26. ^1H -NMR spectrum of **Rhodpa**.

The **Rhodpa** was prepared for nucleotides sensing task according to the literature procedure [58]. The absorption spectrum of **Rhodpa** was observed at 318 nm (Figure 4.28A) assigned to the ring-closing form of rhodamine_B. Upon the addition of Cu^{2+} , the absorption bands at 315 nm and 556 nm was observed. The characteristic peak at 556 nm indicated the ring-opening form of **Rhodpa** due to Cu^{2+} complexation at the nitrogen atom of pyridine and oxygen atom of Rhodamine part (Figure 4.27). Moreover, upon the addition of Cu^{2+} , **Rhodpa-Cu** exhibited the emission band at 583 nm corresponding to the ring-opening form of **Rhodpa** which possessed a high conjugate system.

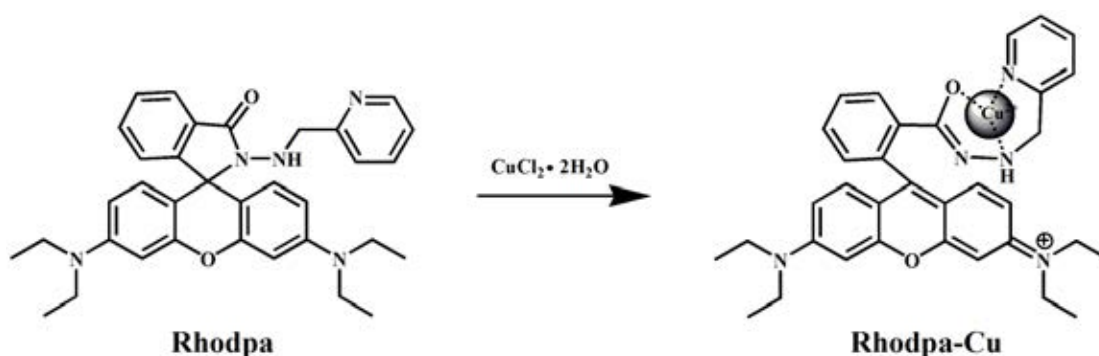


Figure 4.27. Model of **Rhodpa** bound Cu^{2+} ion.

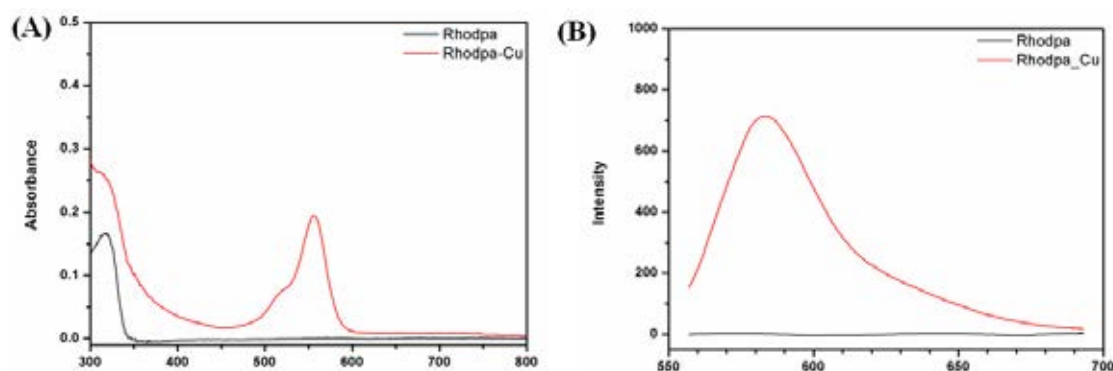


Figure 4.28. (A) Absorption ($1 \times 10^{-5} \text{M}$) and (B) emission ($1 \times 10^{-6} \text{M}$) spectra of **Rhodpa** and **Rhodpa-Cu** in DMSO ($1 \times 10^{-4} \text{M}$).

4.4.1.3 Complexation studies of fluorophore replacement with nucleotides

A ligand-exchanged reaction is a general phenomenon which the chemical change occurs when one ligand is replaced with other ligands. The concept of nucleotides sensing of ligand-exchanged studies is illustrated in Scheme 4.7. In this research, the system consists of gold nanoparticles of 10% toluene in DMSO and **Rhodpa-Cu** as a signaling unit. From the Figure 4.29, **Rhodpa-Cu** demonstrated strong fluorescence intensity at 590 nm. On the other hand, in the presence of AuNPs, fluorescence of **Rhodpa-Cu** was quenched due to packing on the surface of gold nanoparticles via hydrophobic interaction causing the fluorescence resonance energy transfer process. After adding ATP was added into the mixture solution of AuNPs and **Rhodpa-Cu**, a small fluorescence enhancement of **Rhodpa-Cu** was monitored. Unlikely, upon addition of HEPES buffer solution, a fluorescence spectrum of **Rhodpa-Cu** was enhanced at the same as the case of the added ATP. This clearly indicated that a ligand-exchanged reaction between **Rhodpa-Cu** and ATP cannot perform in this approach. Possibly, AuNPs have a better binding with HEPES buffer than ATP because HEPES buffer possessing a long carbon chains is more hydrophobicity than ATP.

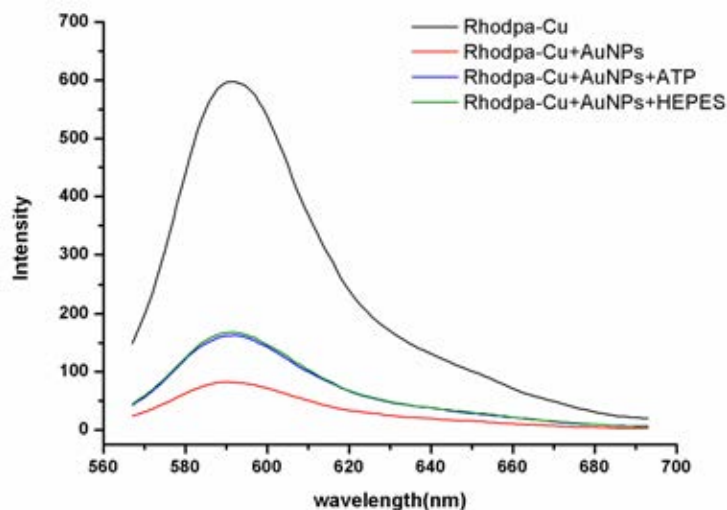


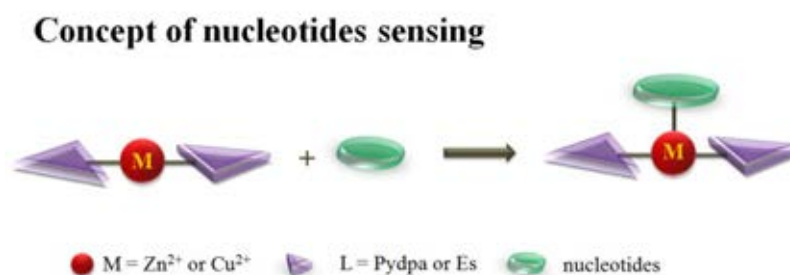
Figure 4.29. Fluorescence spectra of **Rhodpa-Cu** and **AuNPs** upon adding various nucleotides ($\lambda_{\text{ex}} = 550 \text{ nm}$).

From all data related the gold nanoparticles, our concepts of the nucleotides sensing purposes has not been successfully designed. Then experienced many problems about the aggregation of gold nanoparticles and the interfere of organic buffer. Thus, we took an alternative concept related to the statistical technique for nucleotides sensing tasks using several sensory molecules. The Principal Component Analysis (PCA) is a statistical procedure, which is an effective tool in discriminating the similarity of analytes.

4.4.2 Nucleotides sensing by using Principal Component Analysis (PCA)

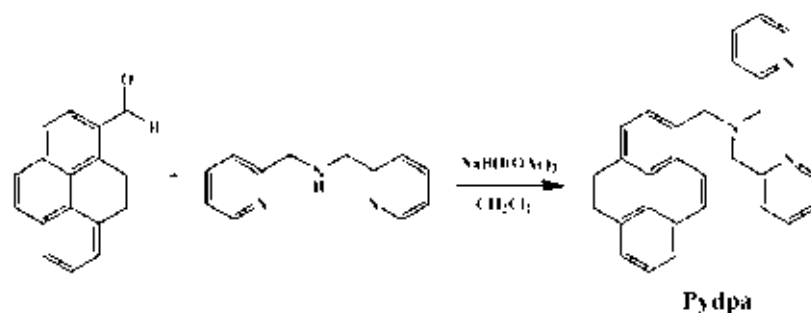
In the previous section, we reported that gold nanoparticles cannot be used for the nucleotide detection. To overcome this limitation, we have an attention to lead another strategy to provide the best procedure to analyze the nucleotides detection. Currently, Principal Component Analysis (PCA) is a useful mathematical procedure that has been found in several applications by reducing the dimensionality of number of data set into a new coordinate system called “Principal Components (PCs)”. To identify patterns in the data, a principal component (PC) axis is calculated to lie in the direction of maximum amount of variance in the original data. The coordinates of the sample relative to the PC axes are termed scores. The first principal component (PC1) represents the greatest variance and the second greatest variance is projected to the second principal component (PC2) and so on. All data analysis using PCA method were performed in MATLAB version 7.11 (R2011a).

In this research, we aim to design and synthesize the fluorescence sensors for the nucleotide detections. The complexation of **Pydpa-Zn**, **Pydpa-Cu**, **Es-Zn**, and **Es-Cu** were prepared as the sensory molecules in purpose to coordinate with phosphate anion based nucleotides undergone the electrostatic interaction (Scheme 4.9). Initially, the complexation studies of sensors were carried out by fluorescence spectrophotometry. The opportunity to obtain the similar results was often happening. Thus, these problems could be solved by using PCA procedure. The prominent point of PCA is showing the great discrimination of the identical data. Molecular sensors of **Pydpa-Zn** and **Pydpa-Cu** were synthesized as shown below.



Scheme 4.9. Concept of nucleotides sensing by Principal Component Analysis (PCA).

4.4.2.1 Synthesis and characterization of Pydpa



Scheme 4.10. Synthesis pathway of **Pydpa**.

The **Pydpa** was synthesized through Schiff base reaction which is a nucleophilic addition reaction between amine and aldehyde groups to generate an imine (as shown in Scheme 4.10) [69]. The **Pydpa** was prepared between pyrenecarboxaldehyde and dipicolylamine. The resulting imine was reduced in situ by sodium tris(acetoxy)borohydride under N₂ atmosphere at room temperature for 5 hr. The product was purified by column chromatography using 5% methanol in dichloromethane as eluent to give the yellow solid of **Pydpa** in 88 %yield. The ¹H-NMR spectrum of **Pydpa** (Figure 4.30) displayed the characteristic proton at 4.35 ppm corresponding to 2 protons of –CH₂-pyrene and the singlet proton at 3.81 ppm corresponding to 4 protons of –CH₂-pyridine with upfield shift. Moreover, the range of proton region at 8.50-7.21 ppm was assigned to aromatic and pyridine protons.

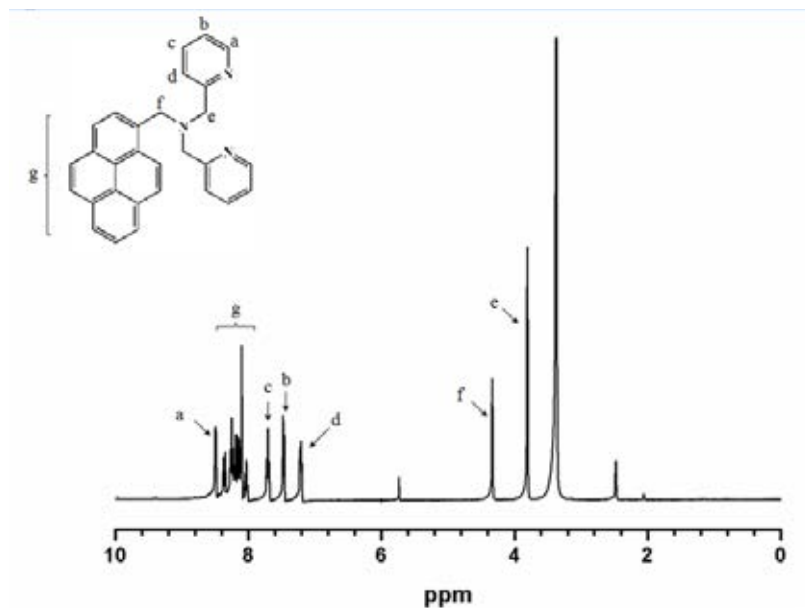


Figure 4.30. $^1\text{H-NMR}$ spectrum of **Pydpa**.

4.4.2.2 Synthesis and characterization of **Pydpa-Zn**



Scheme 4.11. Synthesis pathway of **Pydpa-Zn**.

The **Pydpa-Zn** complex was obtained from the reaction between **Pydpa** and $\text{Zn}(\text{ClO}_4)_2 \cdot 6\text{H}_2\text{O}$. When $\text{Zn}(\text{ClO}_4)_2 \cdot 6\text{H}_2\text{O}$ was added into the solution of **Pydpa**, the yellow precipitate was slowly formed in the solution to give the pale yellow solid of **Pydpa-Zn** in quantitative yield. The $^1\text{H-NMR}$ spectrum of **Pydpa-Zn** complex (Figure 4.31) displayed the characteristic protons at 4.55 and 3.69 ppm assigned to $-\text{CH}_2\text{-pyrene}$ and $-\text{CH}_2\text{-pyridine}$, respectively. The aromatic and pyridine proton of **Pydpa-Zn** were shifted to downfield at 8.71-7.56 ppm because the nitrogen atom coordinated with Zn^{2+} . Moreover, the downfield shifts of methylene protons of

pyrene- CH_2 were observed at 4.55 ppm. The changes of the proton assignments supported the complexation between **Pydpa** and Zn^{2+} . In addition, the optical properties of **Pydpa-Zn** showed the absorption band in the range of 305-358 nm (Figure 32A) and the emission band at 365-430 nm (Figure 32B), corresponding to monomeric pyrene. The fluorescence spectrum of **Pydpa-Zn** showed the identical fluorescence spectrum of **Pydpa** whereas the absorption spectrum showed the hypsochromic effect. From the absorption spectroscopy, the result suggested the formation of **Pydpa** and Zn^{2+} . Moreover, **Pydpa-Zn** was confirmed by ER-ESI MS showing the intense peak at 414.2022 m/z.

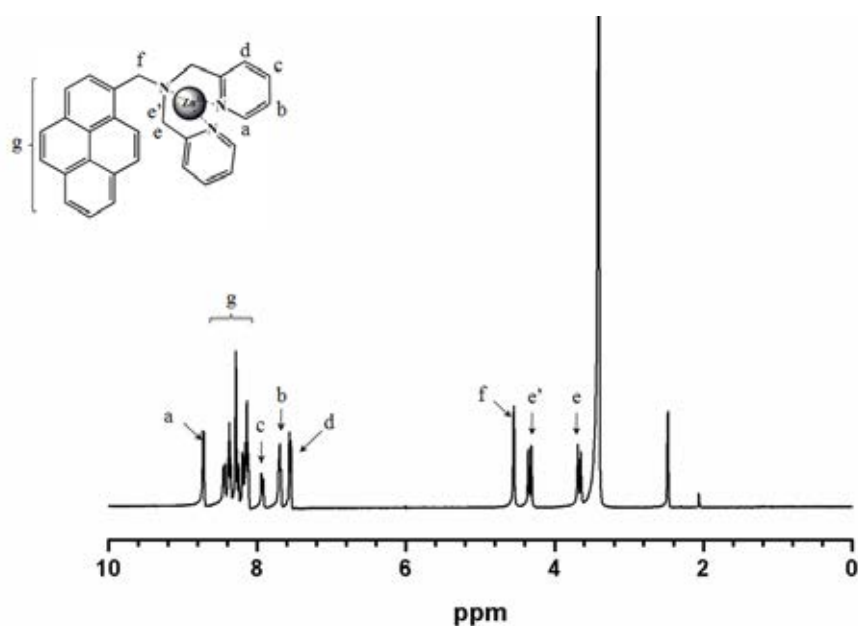


Figure 4.31. 1H -NMR spectrum of **Pydpa-Zn** complex.

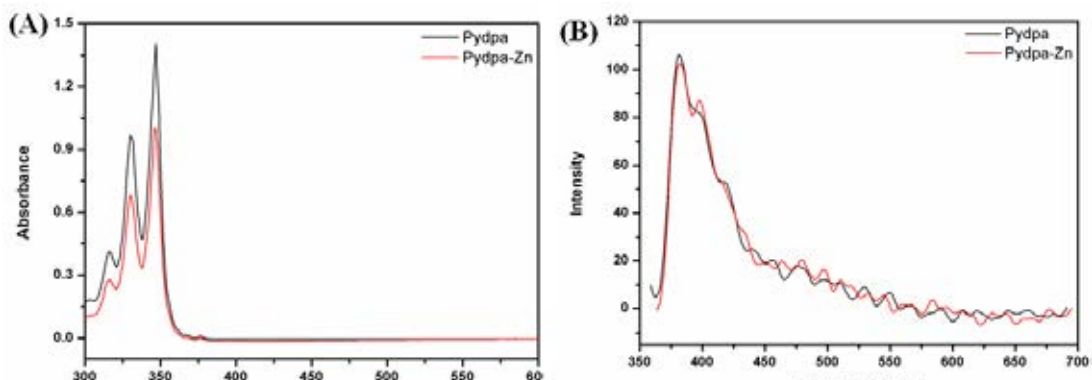
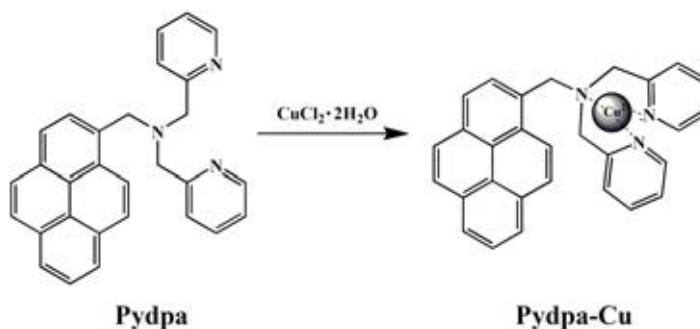


Figure 4.32. (A) Absorption spectra of sensor at 1×10^{-4} M and (B) emission spectra of sensor at 1×10^{-5} M in DMSO.

4.4.2.3 Synthesis and characterization of Pydpa-Cu



Scheme 4.12. Synthesis pathway of **Pydpa-Cu**.

The **Pydpa-Cu** complex was synthesized from **Pydpa** and $\text{CuCl}_2 \cdot 2\text{H}_2\text{O}$. The green precipitate was formed after adding $\text{CuCl}_2 \cdot 2\text{H}_2\text{O}$ into the solution of **Pydpa**. The precipitate was filtrated and washed with cold methanol to give the green solid of **Pydpa-Cu** in quantitative yield. The complexation was characterized by UV-visible and fluorescence spectroscopy. The absorption band of **Pydpa-Cu** showed the bathochromic shift from 346, 330 and 315 nm to 350, 332 and 319 nm, respectively (Figure 4.33A). Moreover, the observation of the emission band at 475 nm was assigned to pyrene excimer emission as shown in Figure 4.33B.

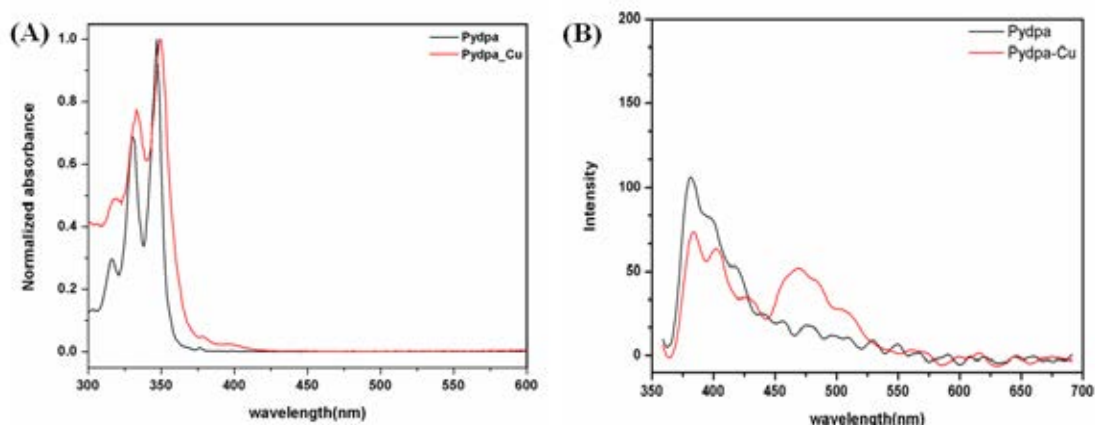


Figure 4.33. (A) Normalized absorption spectra of **Pydpa** and **Pydpa-Cu** complex at 1×10^{-4} M and (B) emission spectra of **Pydpa** and **Pydpa-Cu** complex at 1×10^{-5} M in DMSO.

The complexation of **Es-Zn** and **Es-Cu** were prepared by the addition of Zn^{2+} or Cu^{2+} into the solution of **Esculetin** according reported procedure [70]. From, the UV-visible spectroscopy, the characteristic peak of **Es-Zn** and **Es-Cu** showed a red-shift from 380 nm to 398 and 387 nm, respectively (Figure 4.34A). The results indicated that, metal ions (Zn^{2+} and Cu^{2+}) can deprotonate the diol of **Esculetin** inducing the decrease of the energy gap between the HOMO and LUMO of π - π^* transition. Figure 4.34B showed the fluorescence quenching of **Es-Zn** and **Es-Cu** because the unpair electron of metal ions was transferred to **Esculetin** affecting to electron delocalized into the aromatic ring. Moreover, Job's plot analysis between **Esculetin** and metal ions (Zn^{2+} and Cu^{2+}) were demonstrated the ratio 2:1 stoichiometry as shown in Figure 4.35 and 4.36, respectively.

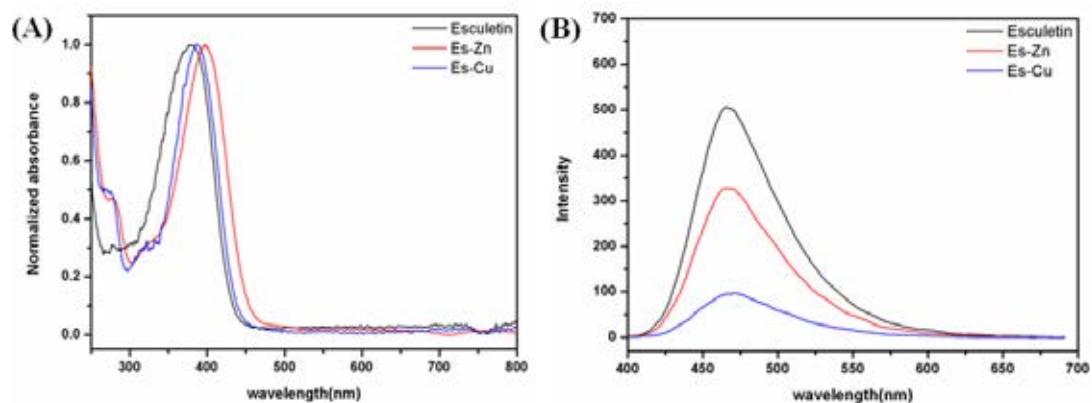


Figure 4.34. (A) Normalized absorption spectra of 1×10^{-4} M of sensors in DMSO and (B) emission spectra of 1×10^{-5} M of sensors in DMSO.

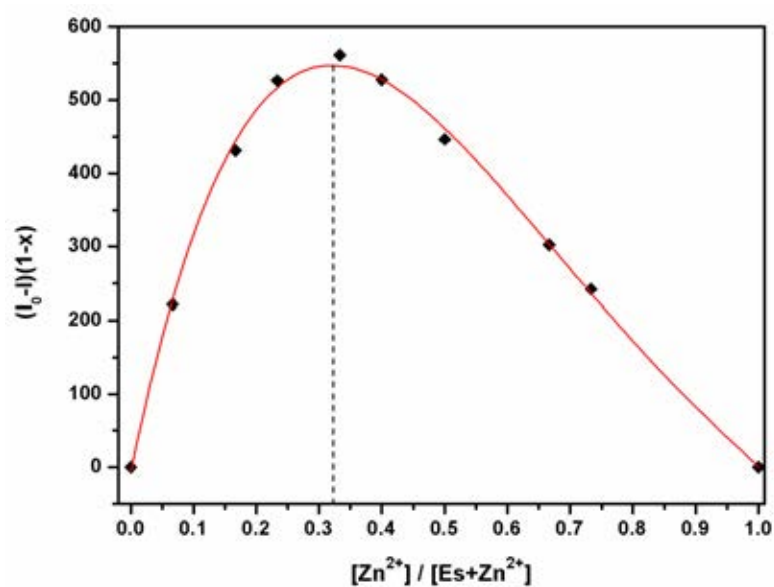


Figure 4.35. Job's plot of **Esculetin** and Zn^{2+} using fluorescence intensity at 470 nm suggests 2:1 stoichiometry.

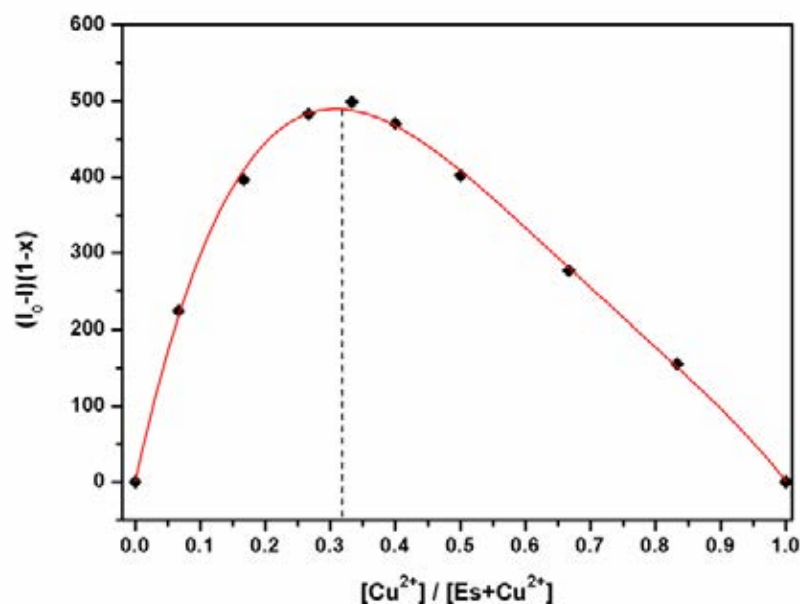


Figure 4.36. Job's plot of Esculetin and Cu²⁺ using fluorescence intensity at 470 nm suggests 2:1 stoichiometry.

4.4.2.4 Complexation studies of Pydpa-Zn, Pydpa-Cu, Es-Zn and Es-Cu with nucleotides by using fluorescence spectroscopy

The complex of **Pydpa-Zn** showed a weak fluorescence band at 384 nm due to photo-induced electron transfer (PET) process (Figure 4.37). The fluorescence responses of **Pydpa-Zn** toward various nucleotides were examined in HEPES buffer solution at pH 7.4. The results showed that the fluorescence behavior of **Pydpa-Zn** exhibited the greatest fluorescence enhancement at 384 nm upon the addition of PPI and the slight changes of fluorescence intensity in the case of ATP, ADP and GDP. Moreover, the nucleoside monophosphate did not induce the significant changes of emission spectrum. The significant fluorescence enhancement might be attributed to the electrostatic interaction between two oxygen atoms of PPI and Zn²⁺ which reduced the magnitude of electron donating of Zn²⁺ resulting in an inhibition of PET process. The binding ability of **Pydpa-Zn** with PPI was performed by using fluorescence titration technique as shown in Figure 4.38. The log *K* value of **Pydpa-Zn** with PPI was 8.83 calculated by specfit 32 program showing the best fit curve in Figure 4.39.

Moreover, the stoichiometry between **Pydpa-Zn** with PPi was evaluated by Job's continuous variation method. From Figure 4.40, the maximum of the corresponding Job's plot shown at 0.3 suggested that the stoichiometry complexation of **Pydpa-Zn** with PPi was 2:1. The proposed binding of **Pydpa-Zn** and PPi was showed in Figure 4.41 which Zn^{2+} could coordinate with two oxygen atoms of PPi [71]. To verify the discrimination of the structural similarity of nucleotides, the PCA method has been applied using fluorescence spectrophotometry. First of all, the fluorescence data of the complexation between **Pydpa-Zn** and various nucleotides were transformed by using statistical technique of PCA method. The PCA score plot of **Pydpa-Zn** shown in Figure 4.42 composed of the variable variance with clustering of 11 clusters in HEPES buffer solution at pH 7.4. The results showed the significant separation of PPi clustering on the right hand side. This PCA result of **Pydpa-Zn** represented 99.54% variance along PC1 and 0.12% variance along PC2.

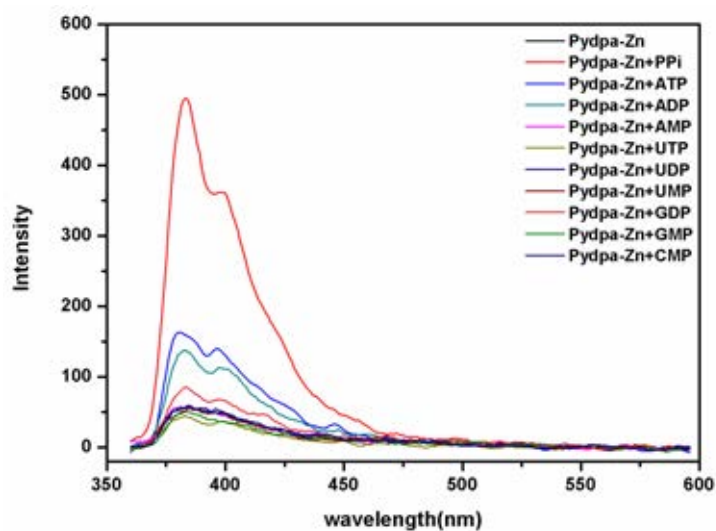


Figure 4.37. Fluorescence emission spectra of **Pydpa-Zn** (1×10^{-5} M) upon the addition of various nucleotide anions (10 equiv) in aqueous solution of HEPES buffer 0.01 M, pH 7.4. ($\lambda_{\text{ex}} = 346$ nm)

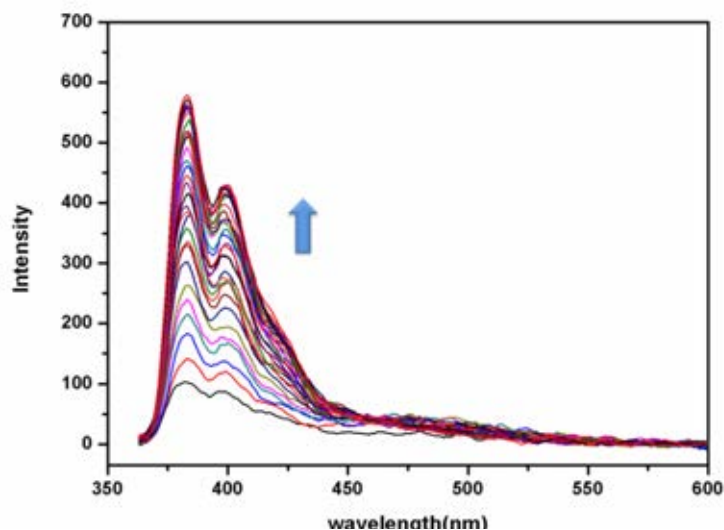


Figure 4.38. Fluorescence titration spectra of **Pydpa-Zn** (1×10^{-5} M) in aqueous solution (0.01M HEPES buffer, pH 7.4) upon the incremented addition of PPI. ($\lambda_{\text{ex}} = 346$ nm)

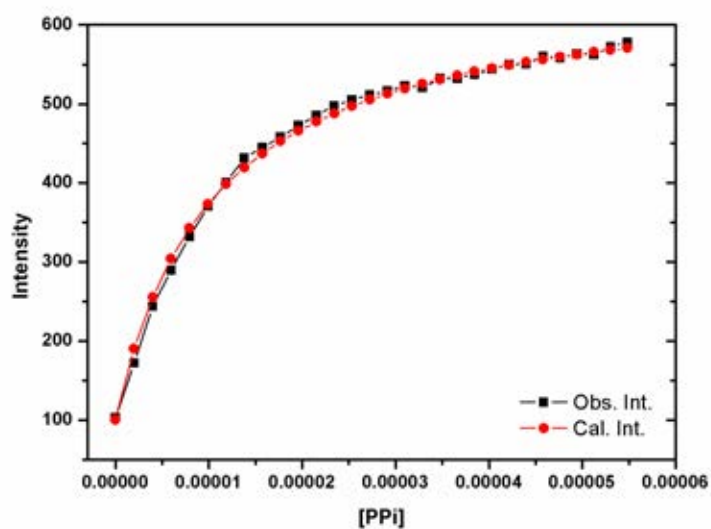


Figure 4.39. Comparing experimental data and calculated data of **Pydpa-Zn** and PPI using fluorescence titration at 384 nm for calculation of the association constant (K). ($\lambda_{\text{ex}} = 346$ nm)

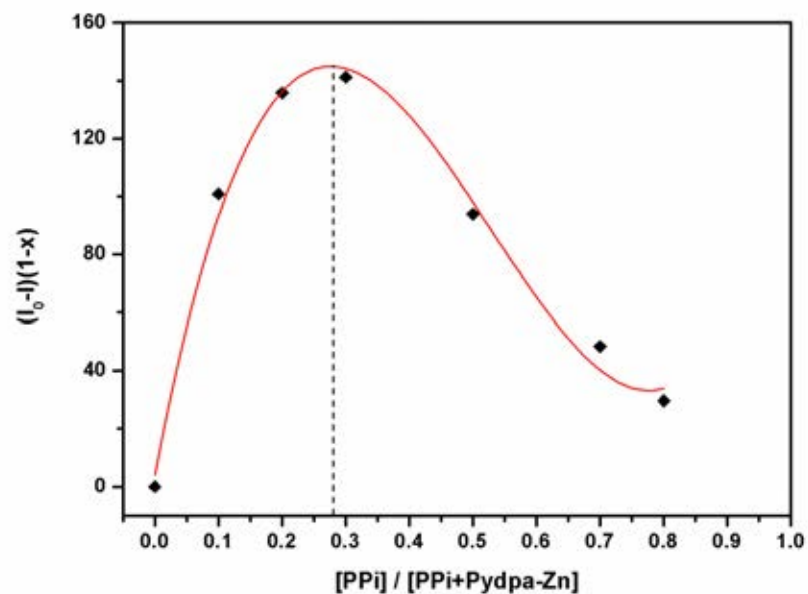


Figure 4.40. Job's plot of **Pydpa-Zn** and PPI using fluorescence intensity at 386 nm under excitation wavelength at 346 nm.

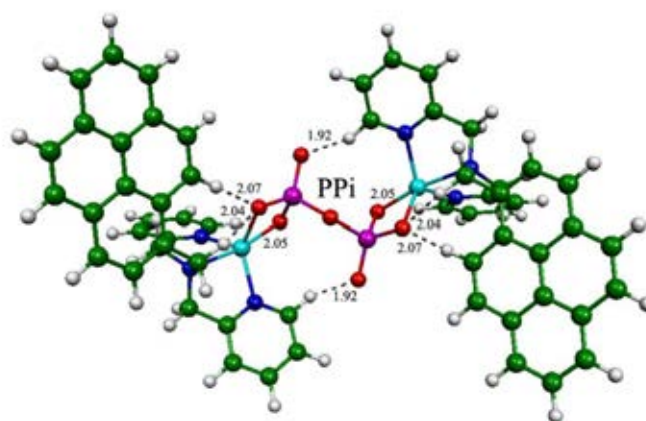


Figure 4.41. The proposed structures of **Pydpa-Zn-PPI** complexes.

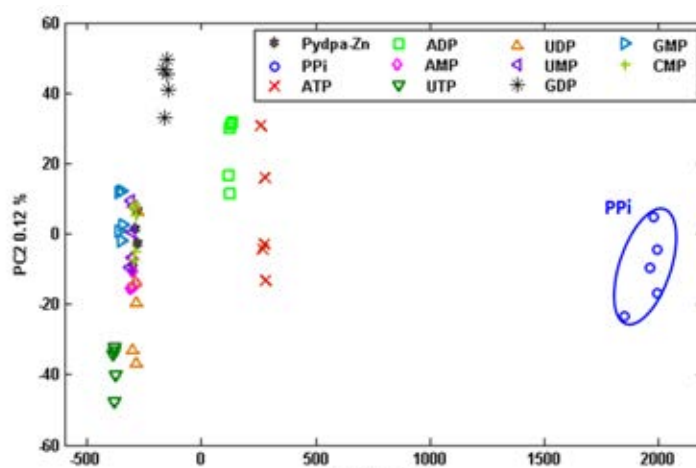


Figure 4.42. PCA score plot of **Pydpa-Zn** upon the addition of various nucleotide anions (10 equiv) in aqueous solution of HEPES buffer 0.01 M, pH 7.4. PCA score plot shows clustering for all 11 samples.

In the case of **Pydpa-Cu**, the emission band was observed at 475 nm assigned to pyrene excimer emission. As depicted in Figure 4.44, the fluorescence responses of **Pydpa-Cu** remained unchanged upon the addition of various nucleotides. This result may be rationalized that no vacant site of Cu^{2+} ion could coordinate with phosphate based nucleotides [72-74]. The proposed structure of **Pydpa-Cu** was depicted in Figure 4.43. Alternatively, we utilized the statistical technique of PCA method to differentiate the similarity of nucleotides. Unfortunately, the result shown in Figure 4.45 suggested that the PCA score plot of **Pydpa-Cu** cannot differentiate the structural similarity of nucleotides.



Figure 4.43. Possibility structure of **Pydpa-Cu**.

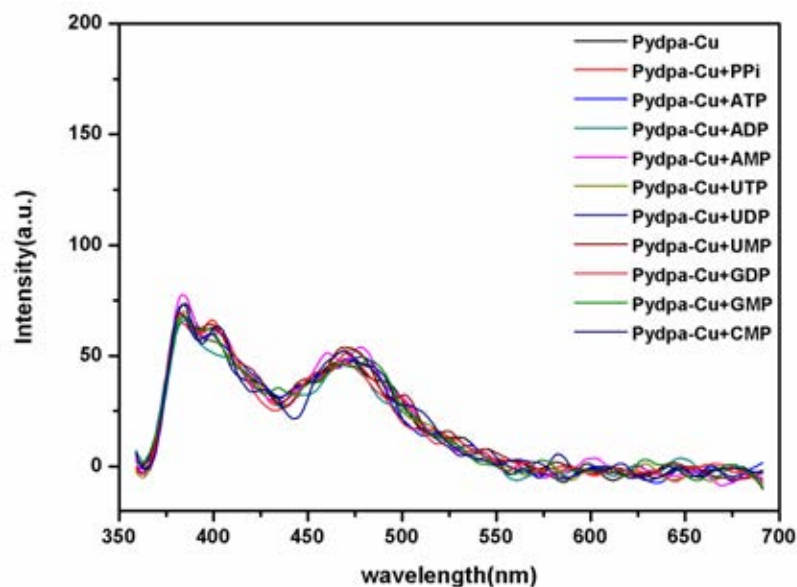


Figure 4.44. Fluorescence emission spectra of **Pydpa-Cu** (1×10^{-5} M) upon the addition of various nucleotide anions (10 equiv) in aqueous solution of HEPES buffer 0.01 M, pH 7.4. ($\lambda_{\text{ex}} = 346$ nm)

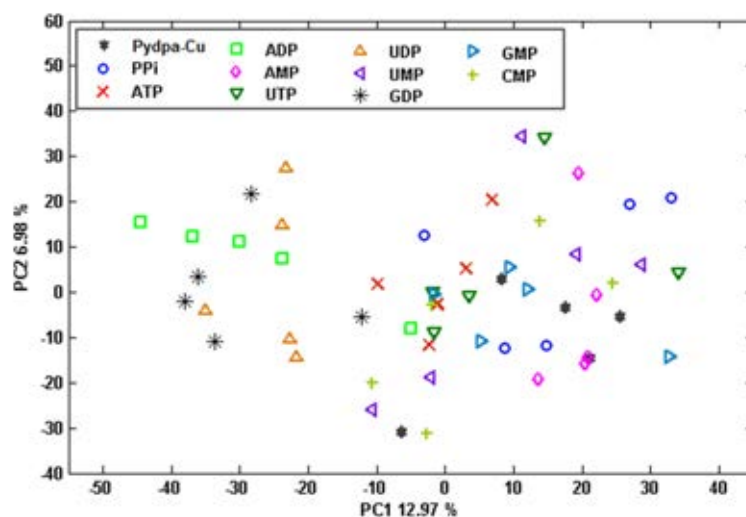


Figure 4.45. PCA score plot of **Pydpa-Cu** upon the addition of various nucleotide anions (10 equiv) in aqueous solution of HEPES buffer 0.01 M, pH 7.4. PCA score plot shows clustering for all 11 samples.

Furthermore, we have studied the binding affinity of **Es-Zn** toward nucleotides using the fluorescence spectroscopy and applied the PCA method to discriminate the species of nucleotides. As shown in Figure 4.46, the fluorescence spectra of **Es-Zn** displayed the maximum emission band at 470 nm (excitation at 380 nm). The fluorescence intensity of **Es-Zn** was enhanced upon the addition of nucleotide in aqueous solution. The fluorescence enhancement may be explained by the suppression of PET process via electrostatic interaction between Zn^{2+} and two oxygen atoms of phosphate based nucleotides. Considering, all of the fluorescence spectral changes of **Es-Zn** in the presence of various nucleotides cannot differentiate the type of nucleotides. However, a large spectral change was observed in the case of PPI. Therefore, the binding ability of **Es-Zn** toward PPI was investigated by using fluorescence titration as shown in Figure 4.47. The $\log K$ value of **Es-Zn** with PPI was 5.23 calculated by equation 4.1 showing the best fit curve in Figure 4.48. The Job's plot analysis described the complexation between **Es-Zn** and PPI in 1:1 binding mode as shown in Figure 4.49.

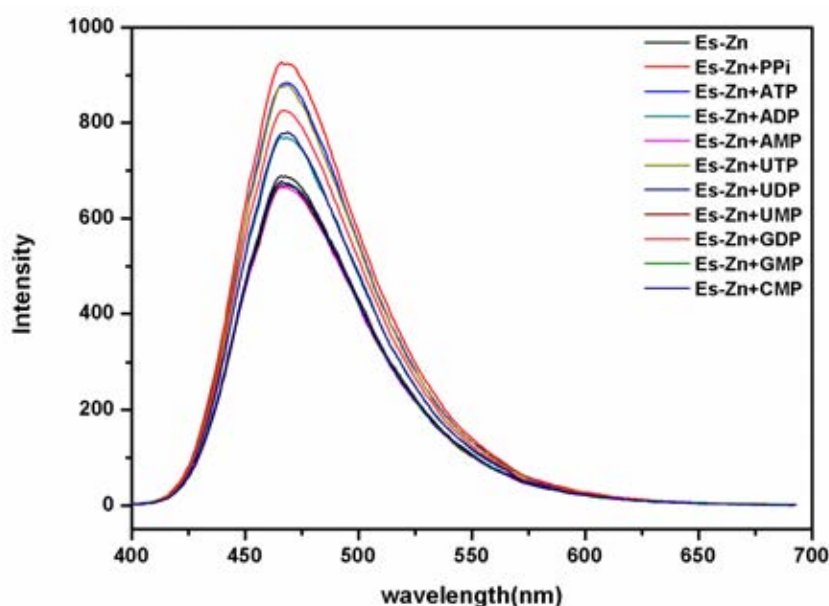


Figure 4.46. Fluorescence emission spectra of **Es-Zn** (1×10^{-5} M) upon the addition of various nucleotide anions (10 equiv) in aqueous solution of HEPES buffer 0.01 M, pH 7.4. ($\lambda_{\text{ex}} = 380$ nm)

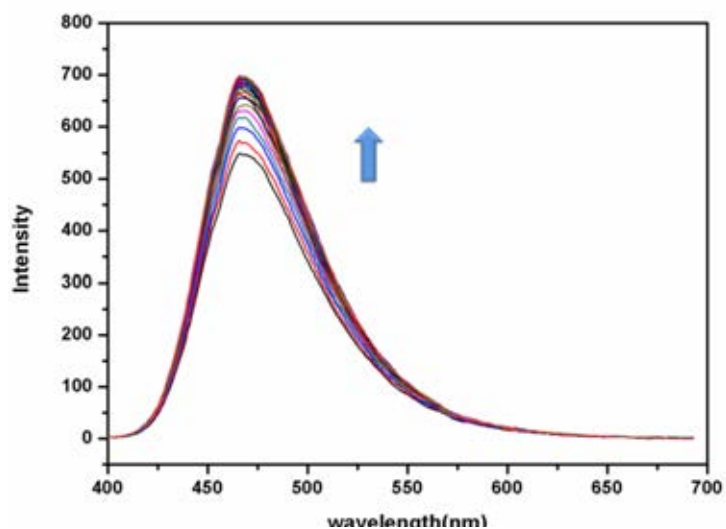


Figure 4.47. Fluorescence titration spectra of **Es-Zn** (1×10^{-5} M) in aqueous solution (0.01M HEPES buffer, pH 7.4) upon gradually adding of PPI. ($\lambda_{\text{ex}} = 380$ nm)

$$I = \frac{(I_0 + I_{\text{lim}} \beta [\text{guest}])}{(1 + \beta [\text{guest}])} \quad 4.1$$

I = intensity of a particular concentration of guest

I_0 = initial intensity

I_{lim} = limiting (final) intensity

β = stability constant of the receptor with the guest

$[\text{guest}]$ = concentration of guest

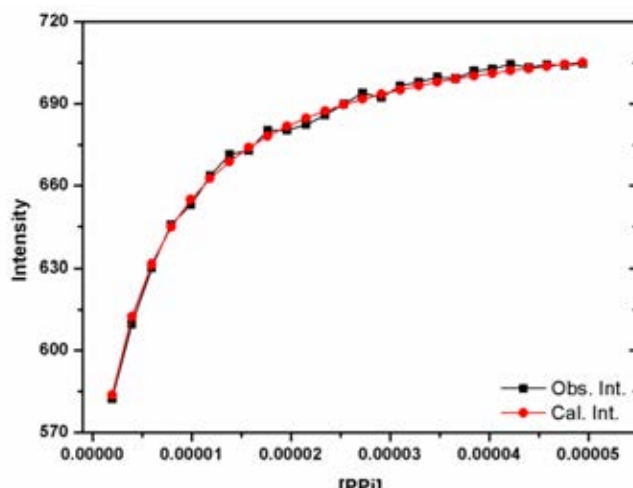


Figure 4.48. Comparing experiment data and calculated data of **Es-Zn** and PPI using fluorescence titration at 470 nm for calculation of association constant (K). ($\lambda_{\text{ex}} = 380$ nm)

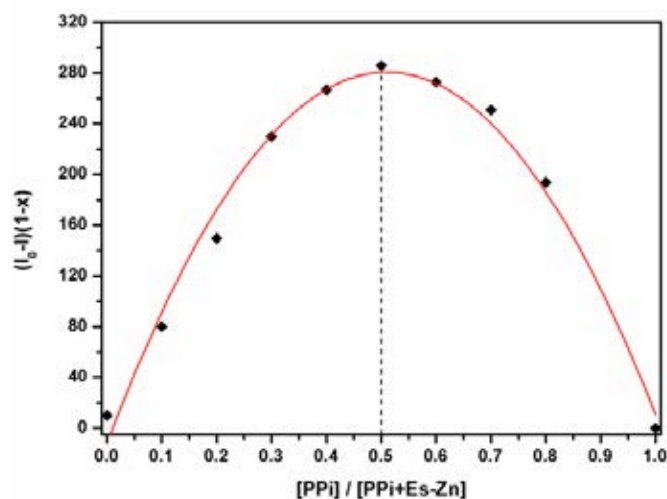


Figure 4.49. Job's plot of **Es-Zn** and PPI using fluorescence intensity at 470 nm under excitation wavelength 380 nm.

In our attempts for discrimination of the structural similarity of analytes, the binding affinity of **Es-Zn** toward nucleotides was classified by PCA method. The results depicted in Figure 4.50 exhibited the clustering discrimination of PPI, ATP and UTP, ADP and UDP, and GDP. The clustering of nucleoside monophosphates existed

an identical group of **Es-Zn**. This implied that **Es-Zn** cannot bind to monophosphate nucleotide. The PCA score plot of **Es-Zn** in HEPES buffer solution showed the horizontal PC1 axis with 99.88% of variance and 0.01% of variance along PC2. However, the distribution of clustering along PC2 for each analyte showed a poor discrimination with a wide-ranged distribution.

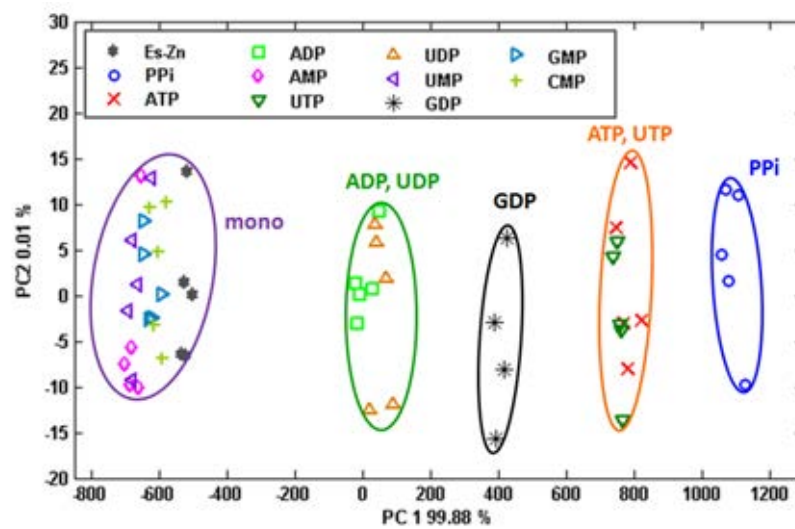


Figure 4.50. PCA score plot of **Es-Zn** upon the addition of various nucleotide anions (10 equiv) in aqueous solution of HEPES buffer 0.01 M, pH 7.4. PCA score plot shows clustering for all 11 samples.

Moreover, **Es-Cu** was employed for nucleotide phosphate sensing. From Figure 4.51, the highly fluorescence enhancement of **Es-Cu** at 470 nm was observed upon binding PPi. The spectral results suggested that the positive charge of Cu^{2+} interacted to the negative charge of oxygen on PPi via the electrostatic interaction resulting in the fluorescence changes. The small changes of fluorescence intensity were observed in the case of ATP, ADP and UTP. Therefore, the order of the binding affinity of **Es-Cu** toward nucleotides was $\text{PPi} \gg \text{ATP} > \text{UTP} > \text{ADP}$. In expectation for high differentiation of nucleotides, the PCA score plot shown in Figure 4.51 was used to classify the cluster of nucleotide in this issue. The PCA plot displayed excellent separation of PPi on the right hand side. For other nucleotides, PCA plot showed a poor discrimination. The PCA results are consistent with the fluorescence

responses in Figure 4.52. The PCA score plot of **Es-Cu** with various nucleotide anions shows 99.94% variance along PC1, while the vertical PC2 axis displays 0.01% variance (Figure 4.52). Both results of fluorescence spectrum and PCA plot indicated that **Es-Cu** demonstrated the selective binding to PPI over other phosphate based nucleotides. Therefore, we have focused on studying the binding ability of **Es-Cu** and PPI by using the fluorescence titrations (shown in Figure 4.53). The log K value of **Es-Cu** with PPI was 4.64 calculated by equation 4.1 showing the best fit curve in Figure 4.54. The Job's plot analysis described the complexation between **Es-Zn** and PPI in 1:1 binding mode as shown in Figure 4.55.

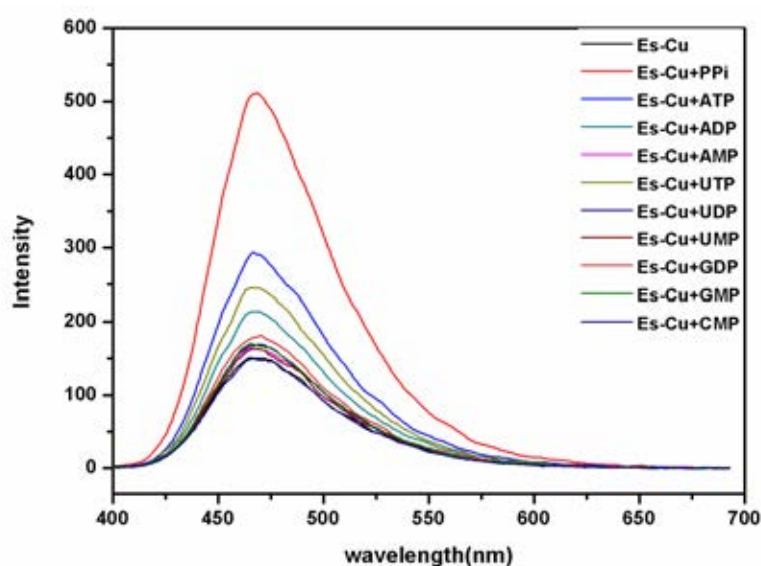


Figure 4.51. Fluorescence emission spectra of **Es-Cu** (1×10^{-5} M) upon the addition of various nucleotide anions (10 equiv) in aqueous solution of HEPES buffer 0.01 M, pH 7.4. ($\lambda_{\text{ex}} = 380$ nm)

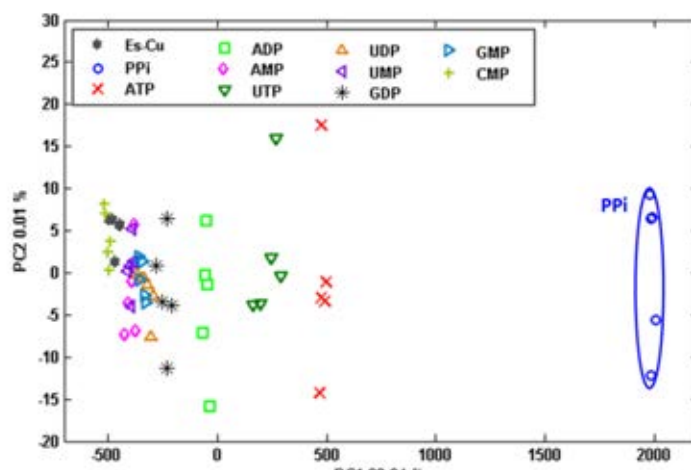


Figure 4.52. PCA score plot of **Es-Cu** upon the addition of various nucleotide anions (10 equiv) in aqueous solution of HEPES buffer 0.01 M, pH 7.4. PCA score plot shows clustering for all 11 samples.

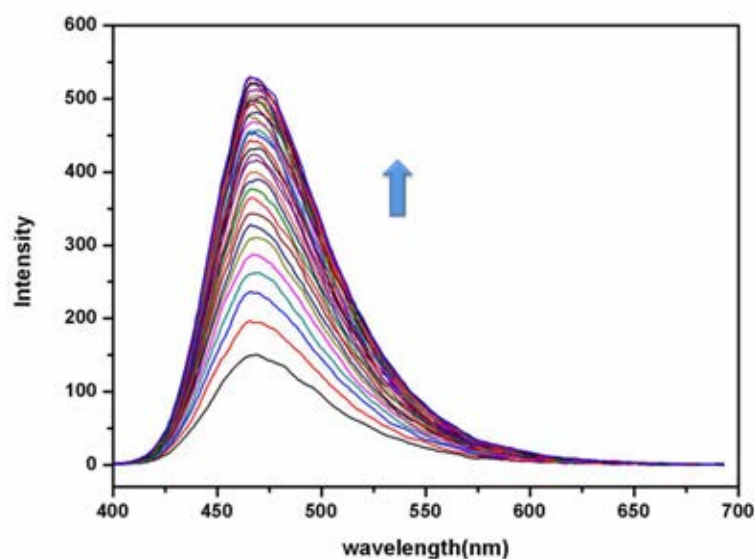


Figure 4.53. Fluorescence titration spectra of **Es-Cu** (1×10^{-5} M) in aqueous solution (0.01M HEPES buffer, pH 7.4) upon gradually adding of PPI. ($\lambda_{\text{ex}} = 380$ nm)

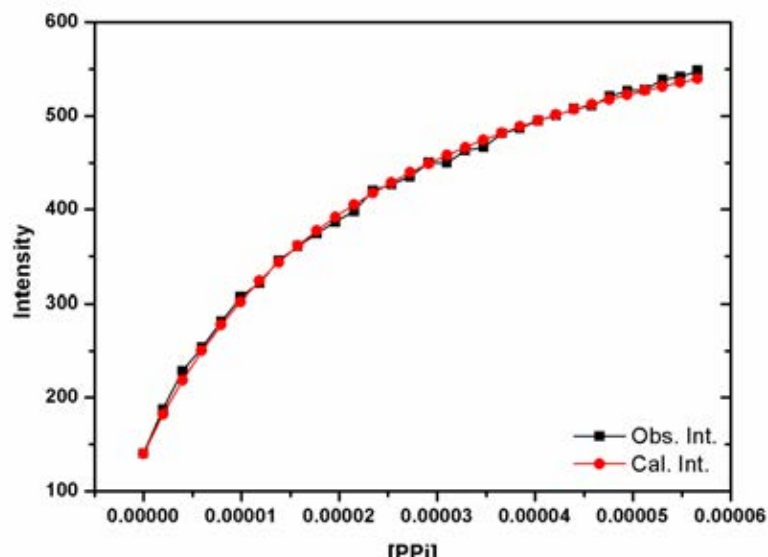


Figure 4.54. Comparing experiment data and calculated data of **Es-Zn** and PPI using fluorescence titration at 470 nm for calculation of association constant (K). ($\lambda_{\text{ex}} = 380$ nm)

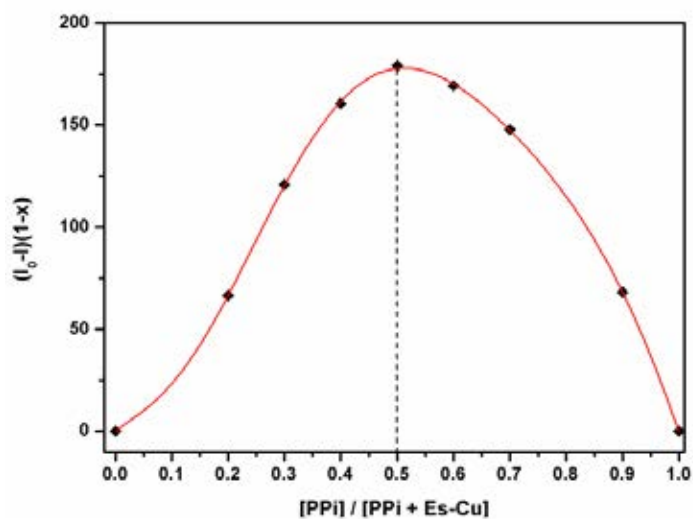


Figure 4.55. Job's plot of **Es-Cu** and PPI using fluorescence intensity at 470 nm under excitation wavelength at 380 nm.

The preliminary results of fluorescence spectroscopy and PCA method revealed that **Pydpa-Zn**, **Es-Zn** and **Es-Cu** show a highly selective sensing for PPI in

aqueous solution. Other nucleotides cannot demonstrate the clustering discrimination by PCA method. Then, new strategy was lead to discriminate the ambiguous data by combinatorial sensor arrays patterns based on Principle Component Analysis (PCA) method. Interestingly, these sensors (**Pydpa-Zn**, **Es-Zn** and **Es-Cu**) upon binding with various nucleotides exhibited the different recognition patterns relied on the fluorescence responses. To verify the discrimination of various nucleotides, the sensor arrays and the combination of/or **Pydpa-Zn**, **Es-Zn**, **Es-Cu** were constructed. We hypothesized that the sensor arrays relied on these sensory molecules would show a high potential for differentiation of various nucleotides. The classification diagram of sensor arrays was demonstrated in Figure 4.56.

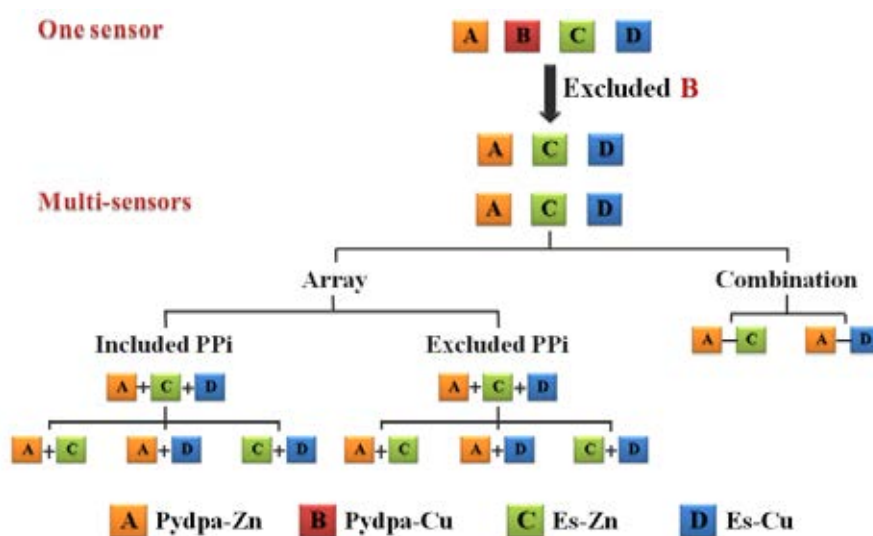


Figure 4.56. The classification of nucleotide by using Principal Component Analysis (PCA).

4.5. Sensor Arrays

A sensor array based on PCA method was investigated using a combinatorial data set of the fluorescence responses between sensor and various nucleotides. Due to the selective binding affinity of all sensors with PPI, thus, we have investigated the clustering discrimination of phosphate anions based nucleotides including and excluding PPI. The combinatorial data was assigned as a "/".

4.5.1 Study on the clustering discrimination of all sensors with nucleotides including PPI

The combinatorial data of three sensors generated by the sensor array in terms of **Pydpa-Zn / Es-Zn / Es-Cu** showed two dimensions score plot for PC1 and PC2 representing 98.85 %variance (Figure 4.57). This PCA pattern showed a highly potential discrimination of PPI in quadrant IV. The appearance of triphosphate (ATP and UTP) cluster in quadrant I was remarkably differentiated from di- and monophosphate. On the other hand, the cluster of UDP and GDP appeared in quadrant II. Furthermore, nucleoside monophosphate appeared in quadrant III. To quantify the classification performance, Linear Discriminant Analysis (LDA) with leave-one-out cross validation approach was used to express the discrimination of the nucleotides. Cross-validated LDA shows 88% accuracy of overall prediction for 10 nucleotides. The classified prediction of PPI, tri- and di- phosphate illustrated a perfect discrimination in 100% accuracy, whereas nucleoside monophosphate displayed 70% accuracy.

Pydpa-Zn / Es-Zn / Es-Cu

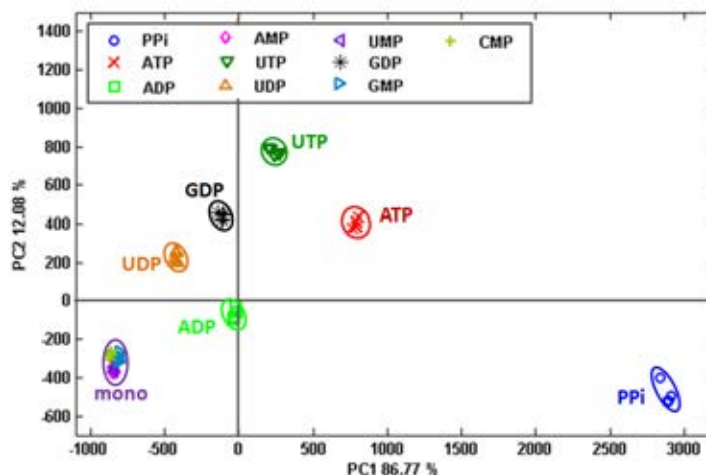


Figure 4.57. PCA score plot of sensor arrays of **Pydpa-Zn / Es-Zn / Es-Cu** upon addition of various nucleotide anions (10 equiv) in aqueous solution of HEPES buffer 0.01 M, pH 7.4.

The recognition pattern of sensor array **Pydpa-Zn / Es-Zn / Es-Cu** can obviously separate only PPI. For sensor arrays, if the number of sensing elements can be reduced with the maintenance of discrimination performance, its application will be of interests. Therefore, we attempt to reduce the sensing elements by using two selected sensing elements as the following:

1. **Pydpa-Zn / Es-Zn**
2. **Pydpa-Zn / Es-Cu**
3. **Es-Zn / Es-Cu**

For all manipulation of the sensor array, the loading plots were obtained from the measurement of the entire fluorescent spectrum in the range of 350 nm to 700 nm. The sensor array of **Pydpa-Zn / Es-Zn** showed two dimension score plot for the first two PCs representing 99.63 %variance (Figure 4.58A). This pattern can classify PPI in quadrant IV and the cluster of ATP, UTP and GDP existing in quadrant I, whereas

UDP cluster was observed in quadrant II. The nucleoside monophosphate and ADP cluster appeared together in quadrant III at the original point. Moreover, cross-validation LDA showed 88% accuracy of overall prediction for 10 nucleotides. The discrimination of PPi, tri- and di- phosphate illustrated in 100% accuracy, while monophosphate groups showed 70% accuracy. In comparison to the three fluorophore arrays which provided 98.85 %variance and an analog accuracy, these suggested the similarity of discrimination ability with the two selected sensing elements.

In the case of **Pydpa-Zn / Es-Cu**, the PCA results showed 97.10% variance belonging to PC1, while the vertical PC2 axis displayed 2.68% variance (Figure 4.58B). Clearly, it can classify the PPi cluster from other nucleotides and appeared on the border line between quadrant I and quadrant IV. Interestingly, the appearance of ATP cluster in quadrant I was remarkably separated from the UTP cluster which appeared in quadrant II. Unfortunately, the ADP, GDP, UDP and monophosphate was observed in the same quadrant III with very poor separation compared to the discrimination performance of **Pydpa-Zn / Es-Zn** and the three sensing element of **Pydpa-Zn / Es-Zn / Es-Cu**. Considering, the individual fluorescence spectra of **Pydpa-Zn** (Figure 4.37) and **Es-Cu** (Figure 4.51) remained unchanged upon the addition of UDP and monophosphate groups. Therefore, the loading plot of two sensing array of **Pydpa-Zn / Es-Cu** was consistent with the fluorescence spectrum of the individual sensing element. Furthermore, cross validation LDA showed 88% corrected classification for all 10 nucleotides. The classified prediction of PPi and triphosphate illustrated a perfect discrimination in 100% accuracy, whereas di- and monophosphate showed 93.33% and 75% accuracy, respectively.

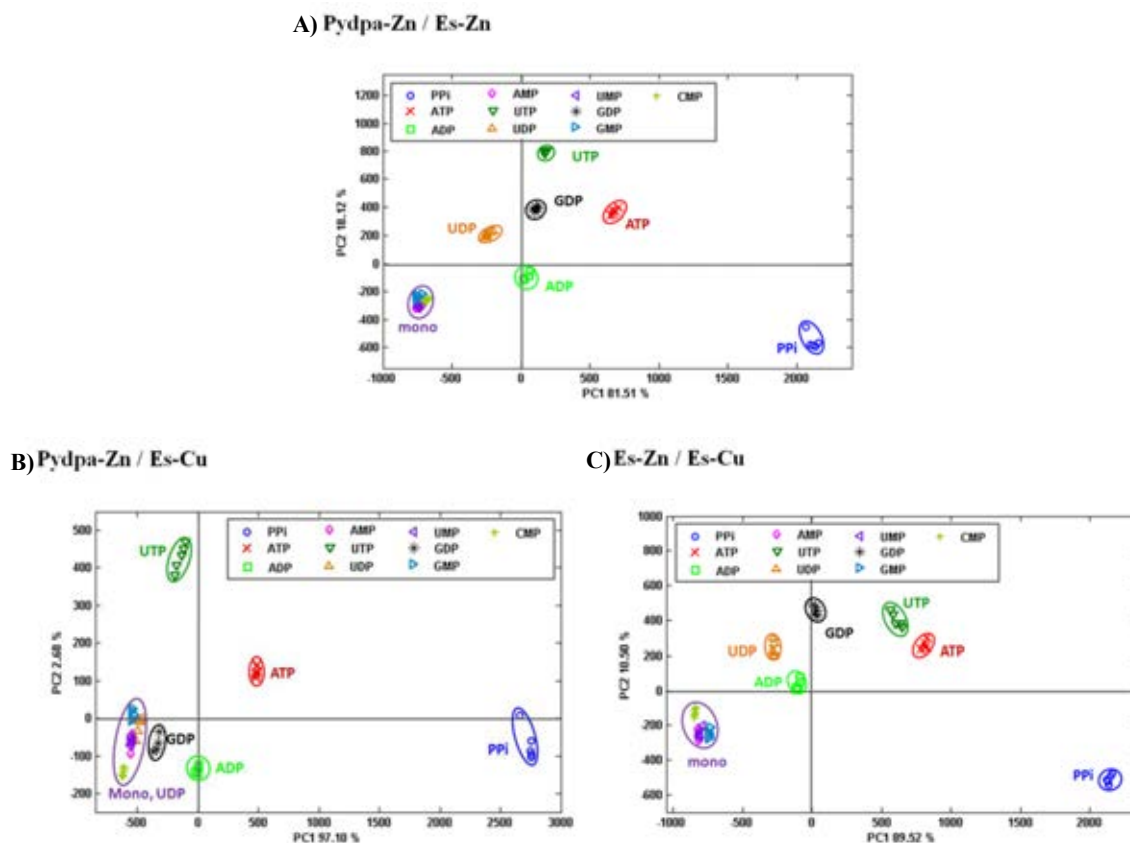


Figure 4.58. PCA score plots of sensor arrays (A) **Pydpa-Zn / Es-Zn**, (B) **Pydpa-Zn / Es-Cu** and (C) **Es-Zn / Es-Cu** upon the addition of various nucleotide anions (10 equiv) in aqueous solution of HEPES buffer 0.01 M, pH 7.4. Sensor array including the fluorescence data of PPI anion for determining of PCA analysis.

Finally, the PCA results of combinatorial data of **Es-Zn / Es-Cu** showed two dimensions score plot for PC1 and PC2 representing 100% variance (Figure 4.58C). The PPI cluster showed a highly potential differentiation in quadrant IV. In quadrant I, the ATP cluster is close to UTP cluster while GDP, UDP and ADP were observed separately in quadrant II. Each species of nucleoside monophosphate cannot be discriminated. Furthermore, cross-validated LDA for the classified prediction showed 86% correct classification for all 10 nucleotides. The PPI, tri- and di- phosphate demonstrated a perfect discrimination in 100% accuracy, whereas the discrimination of monophosphate gave a poor value with 65% classification accuracy.

Considering, the sensor arrays including PPI showed a highly potential discrimination of PPI. The results were consistent with the fluorescence spectra of the sensors and the nucleotides. On the other hand, other nucleotides cannot be clearly classified. In comparison to the three fluorophore array which provided the similar accuracy and %variance, this suggested the similarity of discrimination ability with two selected sensing elements. However, the combinatorial data inducing PPI of three or two selected sensing elements gave a worse discrimination performance for other nucleotides differentiation. Therefore, the further PCA plots for discrimination of other nucleotides were carried out with the excluded PPI. In our expectation, the sensor arrays excluding PPI would show a highly discrimination compared to the sensor arrays including PPI.

4.5.2 Study on the clustering discrimination of all sensors with nucleotides the excluded PPI

The combinatorial data of **Pydpa-Zn / Es-Zn / Es-Cu** with the excluded PPI was shown in Figure 4.59. This system showed two dimensions score plot for PC1 and PC2 representing 96.55 %variance. The PCA results showed that ATP and ADP clusters appeared in quadrant I, whereas the UTP and GDP appeared in quadrant IV and UDP cluster was found in the borderline between quadrant III and IV. On the other hand, the each species of nucleoside monophosphate cannot be classified and existed together on the border line between quadrant II and quadrant III. Additionally, the recognition pattern was optimized for accuracy prediction by Linear Discriminant Analysis (LDA) with leave-one-out cross validation. Cross-validated LDA showed 86.67% classification accuracy. The classified prediction of tri- and di- phosphate demonstrated a perfect discrimination in 100% accuracy, whereas the monophosphate group exhibited 70% classification accuracy.

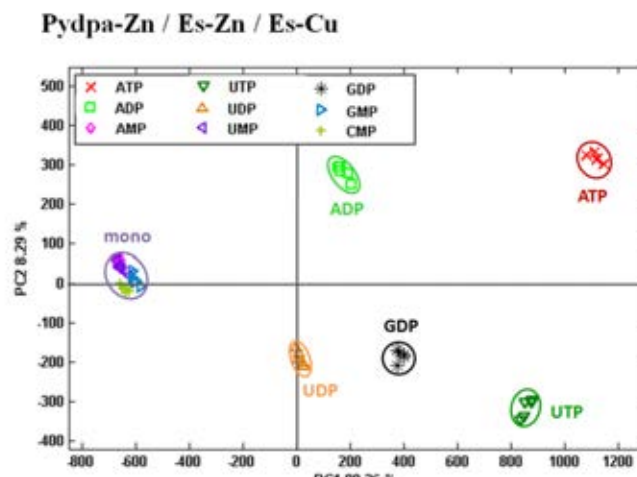


Figure 4.59. PCA score plot of sensor arrays **Pydpa-Zn / Es-Zn / Es-Cu** upon the addition of various nucleotide anions (10 equiv) in aqueous solution of HEPES buffer 0.01 M, pH 7.4. Sensor array excluding fluorescence data of PPI anion for determining of PCA analysis.

Interestingly, the sensor array, **Pydpa-Zn / Es-Zn / Es-Cu** excluding PPI, showed a better discrimination of the cluster of ATP, ADP, UTP, UDP and GDP. As the previous reports, the number of sensing elements can be reduced for the discrimination studies. The selected sensing elements used for this studied were categorized as the following:

1. **Pydpa-Zn / Es-Zn**
2. **Pydpa-Zn / Es-Cu**
3. **Es-Zn / Es-Cu**

The PCA score plot of the combinatorial data of **Pydpa-Zn** and **Es-Zn** has been shown in Figure 4.60A. It illustrated a good resolution for separation of ATP, UTP, ADP, UDP, and GDP clusters which showed a two dimensional score plot of the first two principal components (PC1 and PC2) representing variance of 99.42%. This PCA score plot of **Pydpa-Zn / Es-Zn** showed the similar patterns to **Pydpa-Zn / Es-Zn / Es-Cu** system. Clearly, ATP and ADP clusters can be obviously separated

from the other nucleotides in quadrant I, while UTP, UDP and GDP clusters appeared together in quadrant IV. At the same results, this pattern cannot discriminate the nucleoside monophosphate clusters including AMP, UMP, GMP and CMP which located on the border line between quadrant II and quadrant III. Moreover, cross-validate LDA showed a total accuracy of 93.33%. The classified prediction of tri- and di- phosphate displayed a perfect discrimination in 100% accuracy, whereas the monophosphate gave 85% classification accuracy.

In the case of **Pydpa-Zn / Es-Cu**, the two dimensions score plot of the first two principal components (PC1 and PC2) represented the variance of 98.73% (Figure 4.60B). It can definitely discriminate ATP and ADP clusters in quadrant I and the cluster of UTP in quadrant IV. Considering the fluorescence responses, the results were consistent with the individual sensing element of **Pydpa-Zn** (Figure 4.37) and **Es-Cu** (Figure 4.51). The fluorescence spectrum remained unchanged upon adding UDP and monophosphate based nucleotides. In the case of PCA plot, UDP and monophosphate based nucleotides appeared at the same cluster. Furthermore, the GDP in quadrant II cannot be clearly separated from monophosphate groups. The accuracy prediction of **Pydpa-Zn / Es-Cu** showed a total accuracy of 93.33% for 10 nucleotides. Prediction of clustering for tri- and di- phosphate displayed excellent discrimination in 100% accuracy, whereas monophosphate groups demonstrated 85% accuracy.

Finally, the PCA score plot for sensor array of **Es-Zn / Es-Cu** showed 94.95% variance belonging to PC1 and the PC2 axis displayed 4.88% variance as shown in Figure 4.60C. The discrimination pattern of this system is similar to sensor array of **Pydpa-Zn / Es-Zn**. This system depicted the clusters of ATP and ADP in quadrant I, while UDP and GDP clusters appeared in quadrant IV. Considering, the UTP cluster displayed on the border line between quadrant I and quadrant IV. Additionally, each nucleoside monophosphate cannot be identified by this sensor array. Furthermore, cross validation LDA for all 10 nucleotides showed 84.44% classification accuracy. The classified prediction of tri- and di- phosphate illustrated a perfect discrimination in 100% accuracy, whereas monophosphate showed 65% accuracy.

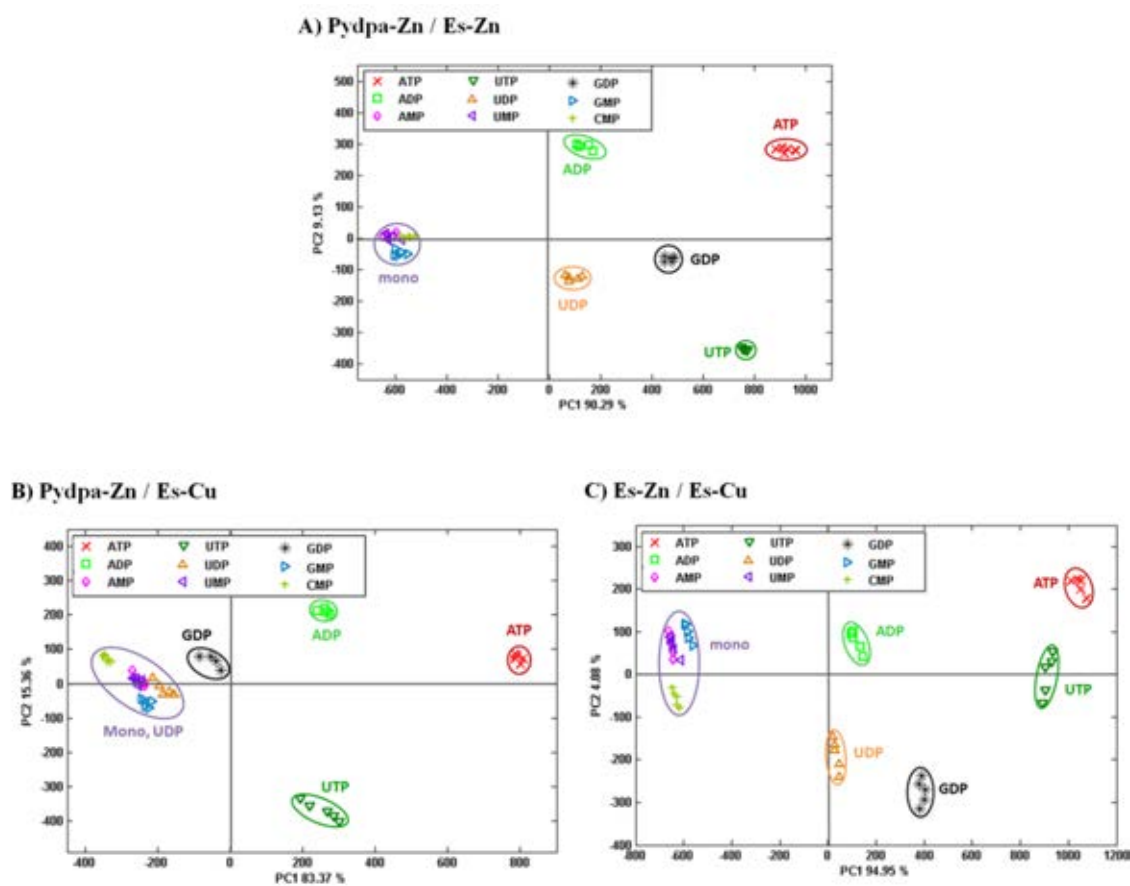


Figure 4.60. PCA scores plot of sensor arrays of nucleotides sensors upon the addition of various nucleotide anions (10 equiv) in aqueous solution of HEPES buffer 0.01 M, pH 7.4. Sensor array excluded the fluorescence data of PPI anion for determining of PCA analysis.

From the preliminary results, the classified prediction of 10 nucleotides demonstrated the % accuracy of all systems by cross-validation LDA as listed in Table 4.1. Comparison between the sensor arrays including PPI and excluding PPI, the discrimination ability of system excluding PPI allowed a better discrimination with 93.33% accuracy of a total nucleotides in particular of **Pydpa-Zn / Es-Zn** and **Pydpa-Zn / Es-Cu**.

Table 4.1 % accuracy of both sensor arrays for 10 nucleotides by cross-validation LDA

Classification	%accuracy							
	Including PPI				Excluding PPI			
	Pydpa-Zn / Es-Zn / Es-Cu	Pydpa-Zn / Es-Zn	Pydpa-Zn / Es-Cu	Es-Zn / Es-Cu	Pydpa-Zn / Es-Zn / Es-Cu	Pydpa-Zn / Es-Zn	Pydpa-Zn / Es-Cu	Es-Zn / Es-Cu
PPi	100	100	100	100	-	-	-	-
Triphosphate	100	100	100	100	100	100	100	100
Diphosphate	100	93	100	100	100	100	100	100
Monophosphate	70	70	75	65	70	85	85	65
Total	88	88	88	86	86	93	93	84

Deeply considering, the binding ability of sensory molecules (**Pydpa-Zn**, **Es-Zn** and **Es-Cu**) toward nucleotides displayed the different recognition patterns of the fluorescence responses and **Pydpa** and **Es** exhibited the different emission bands at 384 nm and 470 nm, respectively, upon excitation at 346 nm. Therefore, we applied PCA to transform the differentiable pattern of the fluorescence responses into the principal component (PC) score by using the fluorescence data obtained from the mixture solution of two selected sensing elements to identify the nucleotides. The combinatorial sensor systems created to study the discrimination of nucleotides were assigned as a “+” and the selected combinatorial systems used in this study were listed as the following:

Combinatorial Sensor

1. **Pydpa-Zn+Es-Zn**
2. **Pydpa-Zn+Es-Cu**

Since **Es-Zn+Es-Cu** patterns showed an identical emission spectrum at 470 nm corresponding to **Es** after adding various nucleotides, the discrimination performance of **Es-Zn+Es-Cu** toward nucleotides has not been investigated in this study.

Considering, the combinatorial sensor between **Pydpa-Zn** and **Es-Zn** (**Pydpa-Zn+Es-Zn**) showed emission bands at 384 and 470 nm assigned to **Pydpa-Zn** and **Es-Zn**, respectively (excited at 346 nm). Figure 4.61, showed the fluorescence spectral changes of **Pydpa-Zn+Es-Zn** upon the addition of various nucleotides. Among these nucleotides, the fluorescence intensity of **Pydpa-Zn** and **Es-Zn** were enhanced differently upon the addition of analytes. Observing, the emission band at 384 nm belonging to **Pydpa-Zn** displayed a small fluorescence enhancement for ATP, ADP, GDP, UTP and UDP, while the nucleoside monophosphates remained unchanged. In contrast, the case of ATP, ADP, GDP, UTP and UDP can remarkably enhance the fluorescence intensity of **Es-Zn** at 470 nm. Considering the different recognition pattern, PCA score plot of **Pydpa-Zn+Es-Zn** with various nucleotides in HEPES buffer pH 7.4 showed two dimension score plot of PC1 and PC2 representing the 99.76 %variance as shown in Figure 4.62. This PCA pattern allows the classification of nucleotides into 3 groups including the appearance of P_{Pi} cluster on the right upper corner in quadrant I, tri and di phosphate (ATP, ADP, UTP, UDP, GDP) in quadrant IV and monophosphate groups (AMP, UMP, GMP, CMP) on the left lower corner in quadrant II. Furthermore, cross-validated LDA for classified prediction demonstrated a perfect discrimination of P_{Pi}, tri- and di- phosphate in 100% accuracy except for monophosphate anions (55% accuracy). However, cross-validated LDA showed 82% classification accuracy of overall prediction for 10 nucleotides which was a poor value. This rationalized that sensors of **Pydpa-Zn** and **Es-Zn** showed unsuitable binding to the monophosphate.

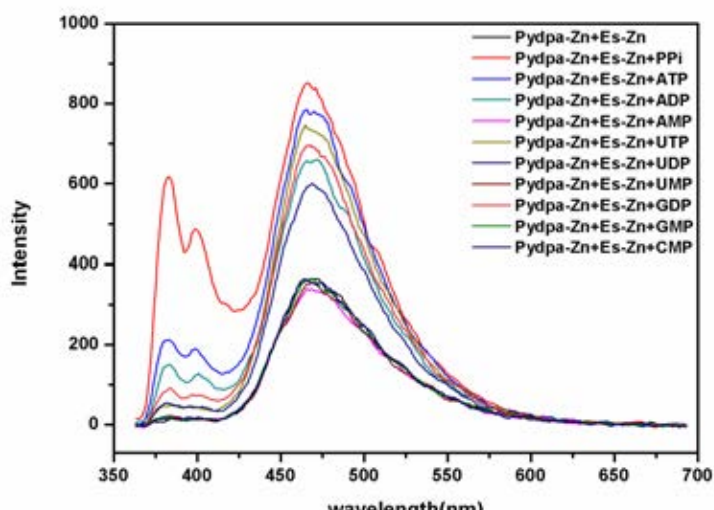


Figure 4.61. Fluorescence emission spectra of **Pydpa-Zn+Es-Zn** (1×10^{-5} M) upon the addition of various nucleotide anions (10 equiv) in aqueous solution of HEPES buffer 0.01 M, pH 7.4. ($\lambda_{\text{ex}} = 346$ nm)

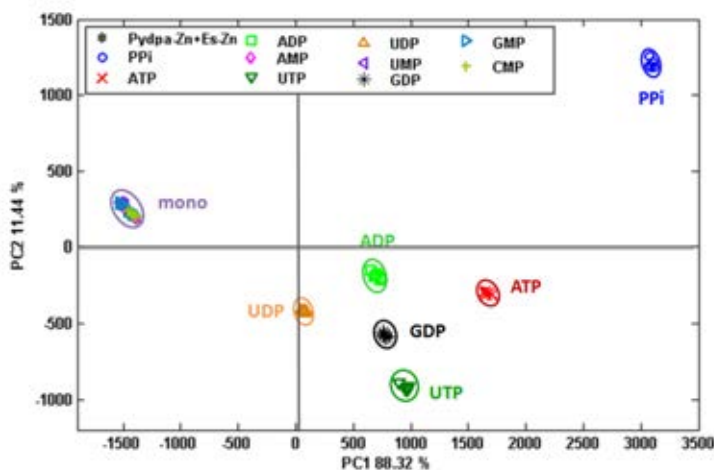


Figure 4.62. PCA score plot of **Pydpa-Zn+Es-Zn** upon the addition of various nucleotide anions (10 equiv) in aqueous solution of HEPES buffer 0.01 M, pH 7.4. The PCA score plot shows clustering for all 11 samples.

Upon the addition of nucleotides (PPI, ATP, ADP, UTP, UDP, GDP), the case of combinatorial sensor of **Pydpa-Zn+Es-Cu** demonstrated the remarkable fluorescence enhancement at 468 nm assigned to **Es-Cu**. The fluorescence band at

384 nm corresponding to **Pydpa-Zn** remained unchanged as shown in Figure 4.63. Similarly, nucleoside monophosphate groups did not induce the fluorescence spectral change. Based on the data similarity, the two dimension PCA score plot of **Pydpa-Zn+Es-Cu** suitably generated the differentiable classification of PPI, ATP, ADP, UTP, UDP and GDP clusters as shown in Figure 4.64 which displayed a two dimensional score plot of PC1 and PC2 representing 99.35 %variance. The results showed that the data of the entire spectrum gave the highest classification compared to **Pydpa-Zn+Es-Zn**. From the PCA plot of **Pydpa-Zn+Es-Zn** and **Pydpa-Zn+Es-Cu**, it is also importance to note that **Pydpa-Zn+Es-Cu** displayed a better discrimination ability than **Pydpa-Zn+Es-Zn**. To verify the classification ability, Linear Discriminant Analysis (LDA) with leave-one-out cross validation approach was used to predict the accuracy classification of the nucleotides. Cross-validated LDA shows the total accuracy of 92% while PPI, tri- and di- phosphate showed an excellent classified prediction in 100% classification accuracy and monophosphate showed 80% classification accuracy.

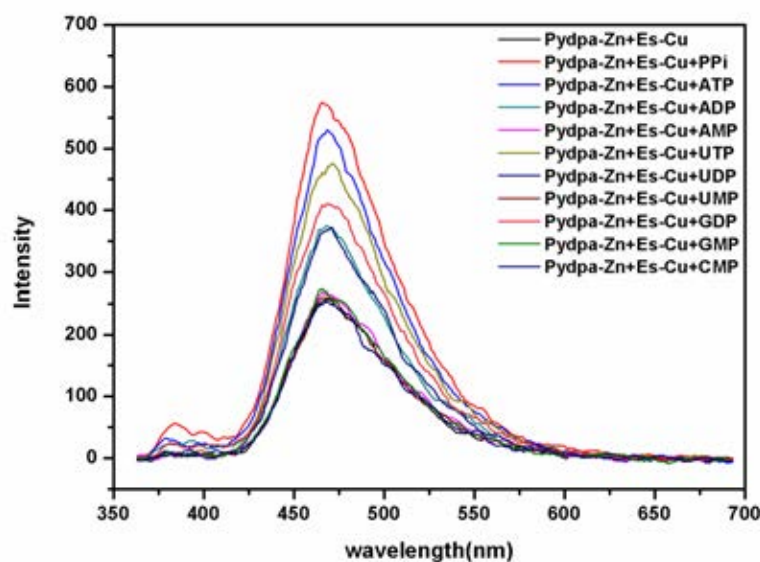


Figure 4.63. Fluorescence emission spectra of **Pydpa-Zn+Es-Cu** (1×10^{-5} M) upon the addition of various nucleotide anions (10 equiv) in aqueous solution of HEPES buffer 0.01 M, pH 7.4. ($\lambda_{\text{ex}} = 346$ nm)

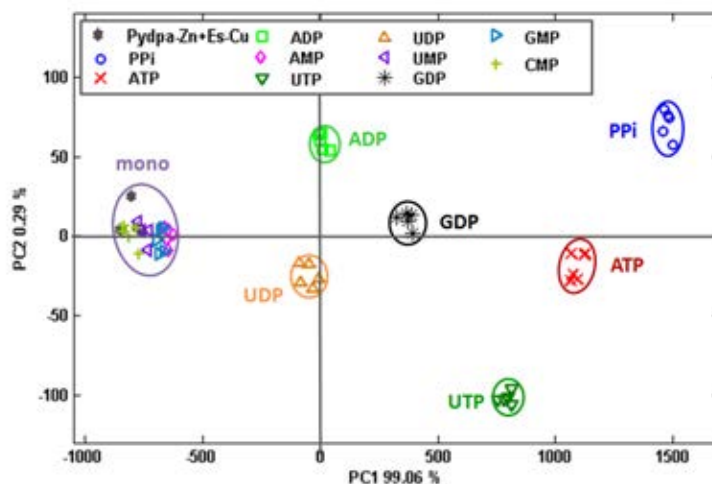


Figure 4.64. PCA score plot of **Pydpa-Zn+Es-Cu** upon the addition of various nucleotide anions (10 equiv) in aqueous solution of HEPES buffer 0.01 M, pH 7.4. PCA score plot shows clustering for all 11 samples.

For all results, fluorescence sensor array capable of discriminating 10 nucleotides with nearly 100% accuracy has been successfully constructed from the combinatorial spectra and the combinatorial sensors by using Principal Component Analysis (PCA). Interestingly, the sensor arrays excluding PPI system showed a better discrimination than the including PPI system. All of the sensor arrays excluding PPI can classify the clusters of ATP and ADP in quadrant I, while UTP cluster was separated from UDP and GDP clusters by using **Pydpa-Zn / Es-Cu** system. Moreover, the combinatorial sensor of **Pydpa-Zn+Es-Zn** and **Pydpa-Zn+Es-Cu** showed an excellent differentiation of various nucleotides (PPI, ATP, ADP, UTP, UDP, GDP). Surprisingly, the discrimination ability of the selected combinatorial sensor systems allowed an excellent promising discrimination of phosphate anion based nucleotides including PPI over the sensor arrays systems. Particularly, **Pydpa-Zn+Es-Cu** give a highly potential discrimination of phosphate anion based nucleotides with classified prediction of 92% accuracy for 10 nucleotides. Importantly, the PCA results obtained by the fluorescence changes of the mix sensing elements of **Pydpa-Zn + Es-Cu** is consistent with the fluorescence spectral changes of the individual sensing element (shown in Figure 4.37 and 4.51).

CHAPTER V

CONCLUSION

With the recognition of nucleotides as an objective, we have been designed and synthesized the molecular sensor for binding metal ion, especially Zn^{2+} . These metal complexes were applied for nucleotide detection. Firstly, we designed and synthesized molecular sensors **Monodpa** and **Didpa_1** for the modified-gold nanoparticles. From the metal sensing studies, **AuNPs-Monodpa** showed a bathochromic shift of surface plasmon band from 521 to 535 nm upon the addition of Co^{2+} ions. This result revealed that **AuNPs-Monodpa** cannot be applied to nucleotide sensing tasks. The case subject of **AuNPs-Didpa_1** displayed the red-shift of surface plasmon band from 530 to 550 nm in the presence of Zn^{2+} , Cu^{2+} and Cd^{2+} . Therefore, we designed the sensing system containing **AuNPs-Didpa_1-Zn** and **PBI-(B(OH)₂)₂** for detection of nucleotides. In our hypothesis, the nucleotides act as a bridging between Zn complex and fluorophore which can induce the energy transfer from **PBI-(B(OH)₂)₂** to AuNPs resulting in fluorescence quenching. Unfortunately, **PBI-(B(OH)₂)₂** cannot bind with nucleotides via the reaction of boronic acid and diol of ribose based nucleotides observing from no significant change in fluorescence responses upon the addition of nucleotides. Thus, we have designed a new sensing system via fluorophore displacement by nucleotides. This system used AuNPs prepared by tetraoctylammonium bromide (TOABr) as a stabilizer and **Rhodpa-Cu** as a signaling unit. The result exhibited a fluorescence quenching stemmed from the hydrophobic interaction between **Rhodpa-Cu** and TOABr based AuNPs. Upon the addition of nucleotides, we expected the competitive binding between the added nucleotides and **Rhodpa-Cu** packed on AuNPs to give a strong fluorescence of free **Rhodpa-Cu**. However, HEPES buffer containing hydrophobic chain can displace the fluorophore packed on AuNPs. Therefore, this system could not be used to detect nucleotides.

To overcome this limitation, we pay an attention to lead a new strategy to provide the best procedure for analyze the nucleotides. The Principal Component

Analysis (PCA) was used to discriminate the similar structure of nucleotides. In this study, we used pyrene and curmarin derivatives (**Pydpa** and **Es**) as a molecular sensor. The **Pydpa-Zn**, **Pydpa-Cu**, **Es-Zn** and **Es-Cu** were used as molecular sensor for binding with phosphate group based nucleotides. The stoichiometry between **Esculetin** and metal ions (Zn^{2+} and Cu^{2+}) was evaluated by Job's continuous variation method showing the stoichiometry of **Es** toward Zn^{2+} and Cu^{2+} were 2:1.

The complexation studies of these sensors (**Pydpa-Zn**, **Pydpa-Cu**, **Es-Zn** and **Es-Cu**) with various nucleotides were carried out by fluorescence spectrophotometry and applied to PCA method. It was found that most sensors showed a highly selective sensing for PPI in aqueous solution except **Pydpa-Cu**. The log *K* values of **Pydpa-Zn**, **Es-Zn**, and **Es-Cu** towards PPI were 8.83, 5.23 and 4.64, respectively. Other nucleotides cannot be discriminated by PCA method. To verify more discrimination of various nucleotides, the sensor arrays (combinatorial data) and the mixed sensors (combinatorial sensors) were constructed. Sensor arrays excluding PPI showed a better discrimination pattern of ATP, ADP, UTP, UDP and GDP cluster. Moreover, cross-validation LDA suggested that sensor array of **Pydpa-Zn / Es-Zn** showed a perfect discrimination of nucleotides in 93.33% accuracy for 9 nucleotides excluding PPI. For the combinatorial sensors, the **Pydpa-Zn+Es-Cu** showed an excellent discrimination of PPI, ATP, ADP, UTP, UDP and GDP clusters in 92% accuracy for 10 nucleotides. In comparison of both systems (sensor arrays and combinatorial sensors), we found that the discrimination ability of the combinatorial sensor systems gave a better separation than the sensor arrays systems.

REFERENCES

- [1] Steed, J. W., Atwood, J. L. *Supramolecular Chemistry*. New York: John Wiley & Sons, 1991.
- [2] Lehn, J.-M. in *Proceeding of the Centenary of the Geneva Conference Organic Chemistry: Its Language and Its State of the Art* (Kisakurek, M. V. (Ed.)). Weinheim: VCH, 1993.
- [3] Gale, P. A., Steed, J. W. *Supramolecular Chemistry: From Molecules to Nanomaterials*. New York: John Wiley & Sons, 2012.
- [4] Vogtle, F. *Supramolecular Chemistry: An introduction*. Chichesters: John Wiley & Sons, 1991.
- [5] Dietrich, B., Guilhem, J., Lehn, J.-M., Pascard, C., Sonveaux, E., Molecular recognition of anion coordination chemistry. Structure, binding constants and receptor-substrate complementarity of a series of anion cryptates of a macrobicyclic receptor molecule. *Helv. Chim. Acta.* 67(February 1984): 91–104.
- [6] Dietrich, B., Kintzinger, J.-P., Lehn, J.-M., Metz, B. Z. Stability, molecular dynamics in solution, and x-ray structure of the ammonium cryptate $[\text{NH}_4^+ \cdot \text{hexafluorophosphate}]$. *J. Phys. Chem.* 91(December 1987): 6600–6606.
- [7] Graf, E., Kintzinger, J.-P., Lehn, J.-M., LeMoigne, J. Molecular recognition. Selective ammonium cryptates of synthetic receptor molecules possessing a tetrahedral recognition site. *J. Am. Chem. Soc.* 104(March 1982): 1672–1678.
- [8] Szaciłowski, K., Macyk, W., Drzewiecka-Matuszek, A., Brindell, M., Stochel, G. Bioinorganic Photochemistry: Frontiers and Mechanisms. *Chem. Rev.* 105(August 2005): 2647-2694.
- [9] Priestley, E. B., Haug, A. Phosphorescence Spectrum of Pure Crystalline Naphthalene. *J. Chem. Phys.* 49(March 1968): 622-629.
- [10] Jaffe, H. H., Miller, Albert L. The fates of electronic excitation energy. *J. Chem. Educ.* 43(September 1966): 469.

- [11] Cao, X., Lin, W., Yu, Q., Wang, J. Ratiometric Sensing of Fluoride Anions Based on a BODIPY-Coumarin Platform. Org. Lett. 13(October 2011): 6098-6101.
- [12] Zapata, F., Caballero, A., Espinosa, A., Ta'rraga, A., Molina, P. Cation Coordination Induced Modulation of the Anion Sensing Properties of a Ferrocene– Imidazophenanthroline Dyad: Multichannel Recognition from Phosphate-Related to Chloride Anions. J. Org. Chem. 73(February 2008): 4034-4044.
- [13] Yang, M-H., Thirupathi, P. Lee, K-H. Selective and Sensitive Ratiometric Detection of Hg(II) Ions Using a Simple Amino Acid Based Sensor. Org. Lett. 13(September 2011): 5028-5031.
- [14] Xu, Z., and others. Zn²⁺-Triggered Amide Tautomerization Produces a Highly Zn²⁺-Selective, Cell-Permeable, and Ratiometric Fluorescent Sensor. J. Am. Chem. Soc. 132(December 2010): 601-610.
- [15] Ajayakumar, M. R., Mukhopadhyay, P. Single-Electron Transfer Driven Cyanide Sensing: A New Multimodal Approach. Org. Lett. 12(May 2010): 2646-2649.
- [16] Liu, Z., Wang, X., Yang, Z., He, W. Rational Design of a Dual Chemosensor for Cyanide Anion Sensing Based on Dicyanovinyl-Substituted Benzofurazan. J. Org. Chem. 76(November 2011): 10286-10290.
- [17] Kim, H. N., and others. Fluorescent Sensing of Triphosphate Nucleotides via Anthracene Derivatives. J. Org. Chem. 76(April 2011): 3805-3811.
- [18] Bazzicalupi, C., and others. Exploring the Binding Ability of Phenanthroline-Based Polyammonium Receptors for Anions: Hints for Design of Selective Chemosensors for Nucleotides. J. Org. Chem. 74(October 2009): 7349-7363.
- [19] Echevarren, A., Gala'n, A., Lehn, J.-M., de Mendoza, J. Chiral recognition of aromatic carboxylate anions by an optically active abiotic receptor containing a rigid guanidinium binding subunit. J. Am. Chem. Soc. 111(June 1989): 4994-4995.

- [20] Berger, M., Schmidtchen, F. P. Zwitterionic Guanidinium Compounds Serve as Electroneutral Anion Hosts. J. Am. Chem. Soc. 121(October 1999): 9986-9993.
- [21] Shinoda, S., Tadokoro, M., Tsukube, H., Arakawa, R. One-Step Synthesis of Quaternary Tetrapyrrolium Macrocycle as a New Specific Receptor of Tricarboxylate Anions. Chem. Commun. (December 1998): 181-182.
- [22] Bazzicalupi, C., and others. Thermodynamics of Phosphate and Pyrophosphate Anions Binding by Polyammonium Receptors. J. Am. Chem. Soc. 121(July 1999): 6807-6815.
- [23] Alfonso, I., Dietrich, B., Rebolledo, F., Gotor, V., Lehn, J.-M. Optically active hexaazamacrocycles: Protonation behavior and chiral-anion recognition. Helv.Chim. Acta. 84(February 2001): 280–295.
- [24] Petrucci, R. H. General Chemistry: Principles and Modern Applications, 5th ed., Macmillan Publishing: New York, 1989.
- [25] Brereton, R. G. Chemometrics Data Analysis for the Laboratory and Chemical Plant. England: John Wiley & Sons, 2003.
- [26] Karp, G. Cell and molecular biology concepts and experiments, 3rd ed., New York: John Wiley & Sons, 2002.
- [27] Hong, C. I., and others. Nucleoside Conjugates. 15. Synthesis and Biological Activity of Anti-HIV Nucleoside Conjugates of Ether and Thioether Phospholipids. J. Med. Chem. 39(April 1996): 1771-1777.
- [28] Jang, Y. J., and others. Highly Effective Fluorescent and Colorimetric Sensors for Pyrophosphate over H_2PO_4^- in 100% Aqueous Solution. J. Org. Chem. 70(October 2005): 9603-9606.
- [29] Plenio, H., Burth, D. Aminoferrocenes and Aminocobaltocenes as Redox-Active Chelating Ligands: Syntheses, Structures, and Coordination Chemistry1. Organometallics. 15(September 1996): 4054-4062.
- [30] Kuang, G. C., and others. Balance between Fluorescence Enhancement and Association Affinity in Fluorescent Heteroditopic Indicators for Imaging Zinc Ion in Living Cells. Inorg. Chem. 50(September 2011): 10493–10504.

- [31] Rai, S. Ravikanth, M. Synthesis of Covalently Linked Unsymmetrical Porphyrin Pentads Containing Three Different Porphyrin Subunits. J. Org. Chem. 73(October 2008): 8364–8375.
- [32] Kruppa, M. Konig, B. Reversible Coordinative Bonds in Molecular Recognition. Chem. Rev. 106(August 2006): 3520-3560.
- [33] Beck, A., Weibert, B., Burzlaff, N. Monoanionic N, N, O-scorpionate ligands and their iron(II) and zinc(II) complexes: Models for mononuclear active sites of non-heme iron oxidases and zinc enzymes. Eur. J. Inorg. Chem. 2(February 2001): 521-527.
- [34] Hegelmann, I., Beck, A., Eichhorn, C., Weibert, B., Burzlaff, N. Alkylzinc Complexes with Achiral and Chiral Monoanionic N,N,O-Heteroscorpionate Ligands. Eur. J. Inorg. Chem. (January 2003): 339-347.
- [35] Lim, N. C., and others. Coumarin-Based Chemosensors for Zinc(II): Toward the Determination of the Design Algorithm for CHEF-Type and Ratiometric Probes. Inorg. Chem. 44(February 2005): 2018-2030.
- [36] Zheng, Y., and others. Development of Fluorescent Film Sensors for the Detection of Divalent Copper. J. Am. Chem. Soc. 125(February 2003): 2680-2686.
- [37] Banthia, S. Samanta, A. Photophysical and Transition-Metal Ion Signaling Behavior of a Three-Component System Comprising a Cryptand Moiety as the Receptor. J. Phys. Chem. B. 106(April 2002): 5572-5577.
- [38] Xu, Z., Xiao, Y., Qian, X., Cui, J., Cui, D. Ratiometric and Selective Fluorescent Sensor for Cu^{II} Based on Internal Charge Transfer (ICT). Org. Lett. 7(February 2005): 889-892.
- [39] Chen, X., Jou, M. J., Yoon, J. An “Off-On” Type UTP/UDP Selective Fluorescent Probe and Its Application to Monitor Glycosylation Process. Org. Lett. 11(April 2009): 2181-2184.
- [40] Shin, A., Eiichi, K. Highly selective recognition of thymidine mono- and diphosphate nucleotides in aqueous solution by ditopic receptors zinc(II)-bis(cyclen) complexes (Cyclen) 1,4,7,10-tetraazacyclododecane. J. Am. Chem. Soc. 122(May 2000): 4542-4548.

- [41] Khatua, S., and others. Aqueous Fluorometric and Colorimetric Sensing of Phosphate Ions by a Fluorescent Dinuclear Zinc Complex. Inorg. Chem. 48(March 2009): 2993-2999.
- [42] Lee, H. N., and others. Pyrophosphate-Selective Fluorescent Chemosensor at Physiological pH: Formation of a Unique Excimer upon Addition of Pyrophosphate. J. Am. Chem. Soc. 129 (March 2007): 3828-3829.
- [43] Chen, W. H., Xing, Y., Pang, Y. A Highly Selective Pyrophosphate Sensor Based on ESIPT Turn-On in Water. Org. Lett. 13(February 2011): 1362–1365.
- [44] Lipscomb, W. N., Sträter, N. Recent Advances in Zinc Enzymology. Chem. Rev. 96(November 1996): 2375–2434.
- [45] Jose, D. A., and others. Colorimetric Sensor for ATP in Aqueous Solution. Org. Lett. 9(April 2007): 1979-1982.
- [46] Guo, Z., Zhu, W., Tian, H. Hydrophilic Copolymer Bearing Dicyanomethylene-4H-pyran Moiety As Fluorescent Film Sensor for Cu²⁺ and Pyrophosphate Anion. Macromolecules. 43(December 2010): 739–744.
- [47] Stewart, M. E., and others. Nanostructured Plasmonic Sensors. Chem. Rev. 108(January 2008): 494-521.
- [48] Sudeep, P. K., Ipe, B. I., Thomas, K. G., George, M. V. Fullerene-Functionalized Gold Nanoparticles. A Self-Assembled Photoactive Antenna-Metal Nanocore Assembly. Nano Lett. 2(December 2002): 29-35.
- [49] Manju, S., Sreenivasan, K. Detection of glucose in synthetic tear fluid using dually functionalized gold. Talanta. 85(August 2011): 2643– 2649.
- [50] Palacios, M. A., Wang, Z., Montes, V. A., Zyryanov, G. V., Jr, P. A. Rational design of a minimal size sensor array for metal ion detection. J. Am. Chem. Soc. 130(July 2008): 10307–10314.
- [51] Tan, S. S., Kim, S. J., Kool, E. T. Differentiating between fluorescence-quenching metal ions with polyfluorophore sensors built on a DNA backbone. J. Am. Chem. Soc. 133(February 2011): 2664–2671.

- [52] Hewage, H. S., Anslyn, E. V. Pattern-Based Recognition of Thiols and Metals Using a Single Squaraine Indicator. J. Am. Chem. Soc. 131(August 2009): 13099–13106.
- [53] Rochat, S., Severin, K. Pattern-based sensing with metal-dye complexes: sensor arrays versus dynamic combinatorial libraries. J. Comb. Chem. 12(July 2010): 595–599.
- [54] Niamnont, N., Mungkarndee, R., Techakriengkrai, I., Rashatasakhon, P., Sukwattanasinitt, M. Protein discrimination by fluorescent sensor array constituted of variously charged dendritic phenylene–ethynylene fluorophores. Biosensors and Bioelectronics. 26(August 2010): 863–867.
- [55] Wright, A. T., Anslyn, E. V., McDevitt, J. T. A Differential Array of Metalated Synthetic Receptors for the Analysis of Tripeptide Mixtures. J. Am. Chem. Soc. 127(November 2005): 17405-17411.
- [56] Mitra, I., and others. N-Glycan Profiling by Microchip Electrophoresis to Differentiate Disease States Related to Esophageal Adenocarcinoma. Anal. Chem. 84(March 2012): 3621-3627.
- [57] Buryak, A., Pozdnoukhov, A., Severin, K. Pattern-based sensing of nucleotides in aqueous solution with a multicomponent indicator displacement assay. Chem. Com. (May 2007): 2366–2368.
- [58] Zhao, Y., and others. Highly Sensitive and Selective Colorimetric and Off-On Fluorescent Chemosensor for Cu²⁺ in Aqueous Solution and Living Cells. Anal. Chem. 81(July 2009): 7022–7030.
- [59] Ji, X., Song, X., Li, J., Bai, Y., Yang, W., Peng, X. Size Control of Gold Nanocrystals in Citrate Reduction: The Third Role of Citrate. J. Am. Chem. Soc. 129(October 2007): 13939-13948.
- [60] Lee, K., Lee, H., Bae, K. H., Park, T. G. Heparin immobilized gold nanoparticles for targeted detection and apoptotic death of metastatic cancer cells. Biomaterials. 31 (September 2010): 6530-6536.
- [61] Wang, X., and others. A rapid and sensitive “add-mix-measure” assay for multiple proteinases based on one gold nanoparticle–peptide–fluorophore conjugate. Biosensor & Bioelectron. 26 (October 2010): 743-747.

- [62] Fink, J., Kiely, C. J., Bethell, D., Schiffrin, D. J. Self-Organization of Nanosized Gold Particles. Chem. Mater. 10(February 1998): 922-926.
- [63] Nath, N., Chilkoti, A. Label-Free Biosensing by Surface Plasmon Resonance of Nanoparticles on Glass: Optimization of Nanoparticle Size. Anal. Chem. 76(August 2004): 5370-5378.
- [64] Thomas, K. G., Zajicek, J., Kamat, P. V. Surface Binding Properties of Tetraoctylammonium Bromide-Capped Gold Nanoparticles. Langmuir. 18(April 2002): 3722-3727.
- [65] Liu, D., and others. Highly Sensitive, Colorimetric Detection of Mercury(II) in Aqueous Media by Quaternary Ammonium Group-Capped Gold Nanoparticles at Room Temperature. Anal. Chem. 82(November 2010): 9606–9610.
- [66] Dang, Y.-Q., Li, H.-W., Wang, B., Li, L., Wu, Y. Selective Detection of Trace Cr³⁺ in Aqueous Solution by Using 5,5'-Dithiobis (2-Nitrobenzoic acid)-Modified Gold Nanoparticles. Acs Appl.Mater. Interfaces. 1(July 2009): 1533–1538.
- [67] Zho, W., Lee, T. M. H., Leung, S. S. Y., Hsing, I.-M. Tunable Stabilization of Gold Nanoparticles in Aqueous Solutions by Mononucleotides. Langmuir. 23(May 2007): 7143-7147.
- [68] Sudeep, P. K., Ipe, Binil I. K., Thomas, G., George, M. V. Fullerene-Functionalized Gold Nanoparticles. A Self-Assembled Photoactive Antenna-Metal Nanocore Assembly. Nano Lett. 2(December 2002): 29-35.
- [69] Mullice, L. A., Laye, R. H., Harding, L. P., Buurm, N. J., Pope, S. J. A. Rhenium complexes of chromophore-appended dipicolylamine ligands: syntheses, spectroscopic properties, DNA binding and X-ray crystal structure. New J. Chem. 32(August 2008): 2140–2149.
- [70] Zhang, L., Dong, S., Zhu, L. Fluorescent dyes of the esculetin and alizarin families respond to zinc ions ratiometrically. Chem. Commun. (February 2007): 1891–1893.

- [71] Cho, H. K., Lee, D. H., Hong, J. -I. A fluorescent pyrophosphate sensor *via* excimer formation in water. Chem. Commun. (February 2005): 1690-1692.
- [72] Jung, H. S., and others. Cu²⁺ Ion-Induced Self-Assembly of Pyrenylquinoline with a Pyrenyl Excimer Formation. Org. Lett. 11(July 2009): 3378-3381.
- [73] Driscoll, P. F., and others. Photocurrent Generation in Noncovalently Assembled Multilayered Thin Films. Langmuir. 24(April 2008): 5140-5145.
- [74] Soto, E., MacDonald, J. C., Cooper, C. G. F., McGimpsey, W. G. A Non-Covalent Strategy for the Assembly of Supramolecular Photocurrent-Generating Systems. J. Am. Chem. Soc. 125(February 2003): 2838-2839.

APPENDIX

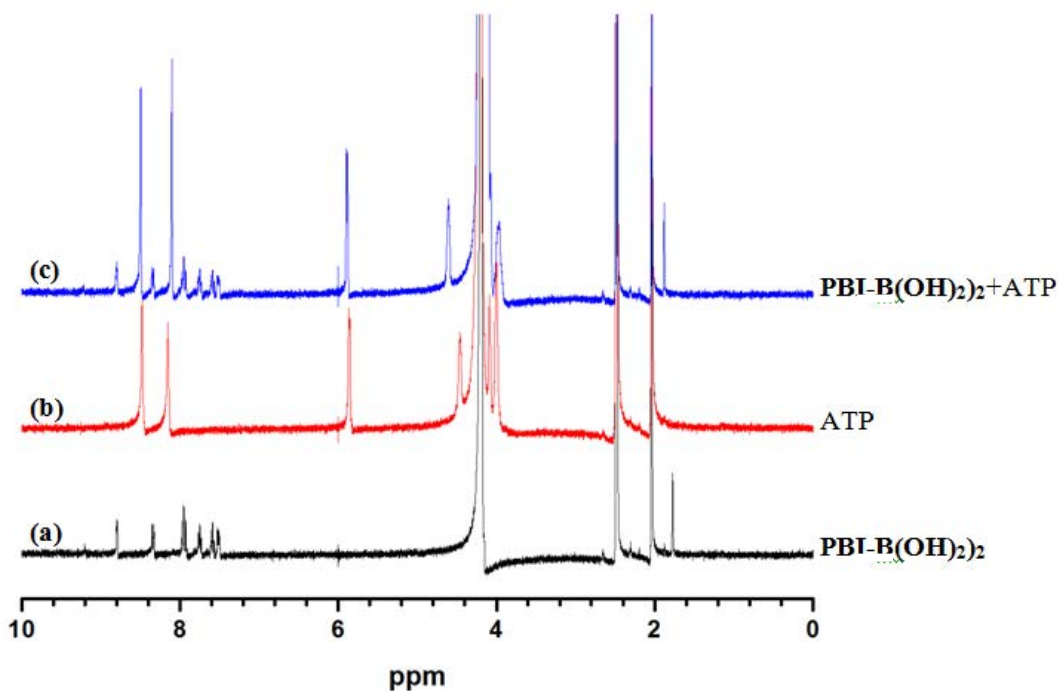


Figure A1 Compared to the NMR spectra between **PBI-(B(OH)₂)₂** (a), ATP(b) and **PBI-(B(OH)₂)₂+ATP** (c)

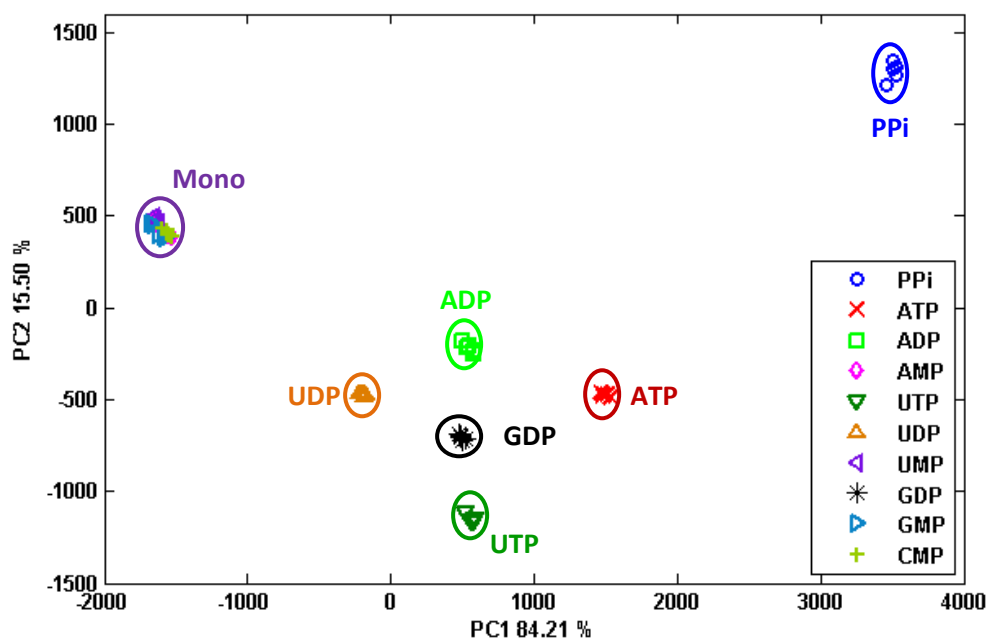


Figure A2 PCA score plot of **Pydpa-Zn / Pydpa-Zn+Es-Zn** upon addition of various nucleotide anions (10 equiv) in an aqueous solution of HEPES buffer 0.01 M, pH 7.4.

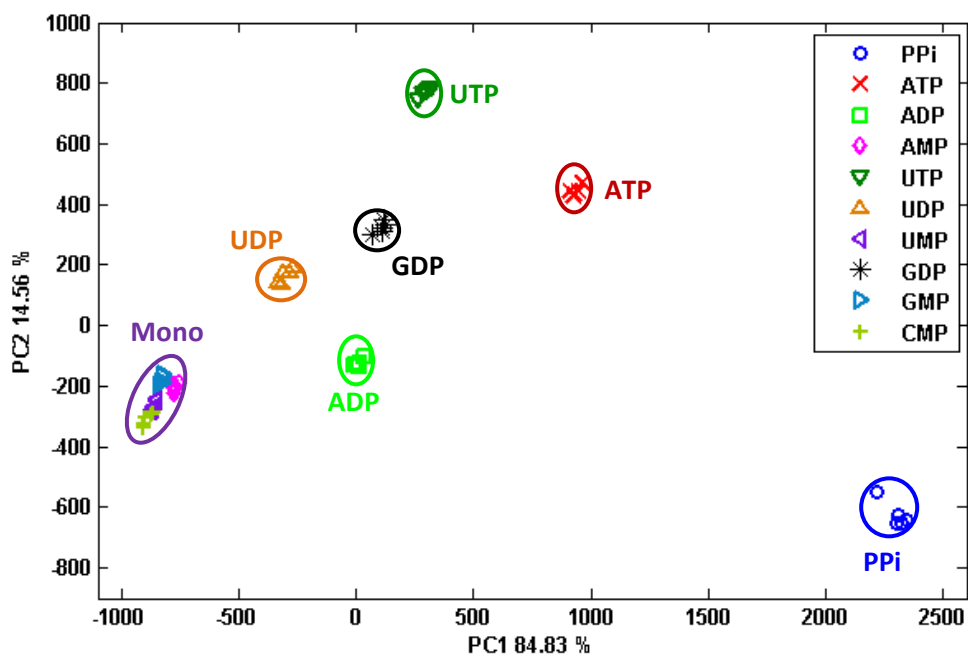


Figure A3 PCA score plot of **Pydpa-Zn / Pydpa-Zn+Es-Cu** upon addition of various nucleotide anions (10 equiv) in an aqueous solution of HEPES buffer 0.01 M, pH 7.4.

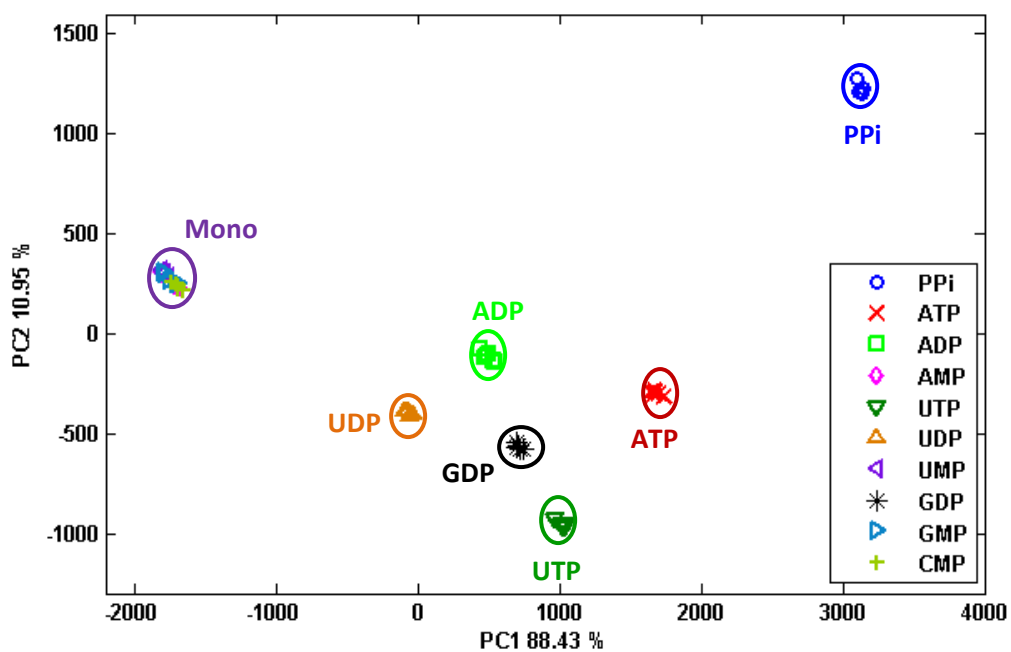


Figure A4 PCA score plot of **Es-Zn / Pydpa-Zn+Es-Zn** upon addition of various nucleotide anions (10 equiv) in an aqueous solution of HEPES buffer 0.01 M, pH 7.4.

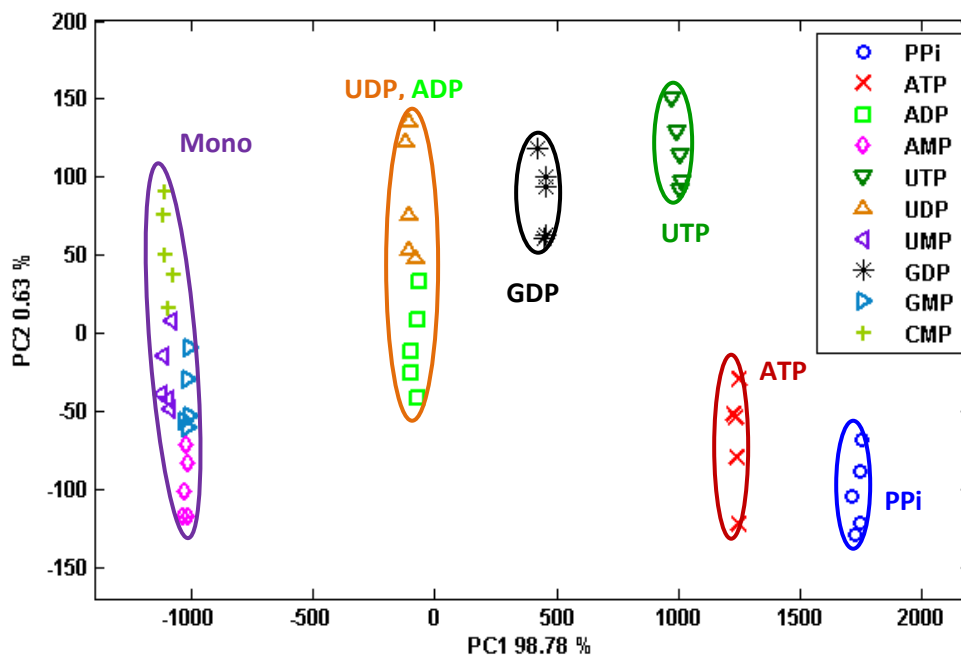


Figure A5 PCA score plot of **Es-Zn / Pydpa-Zn+Es-Cu** upon addition of various nucleotide anions (10 equiv) in an aqueous solution of HEPES buffer 0.01 M, pH 7.4.

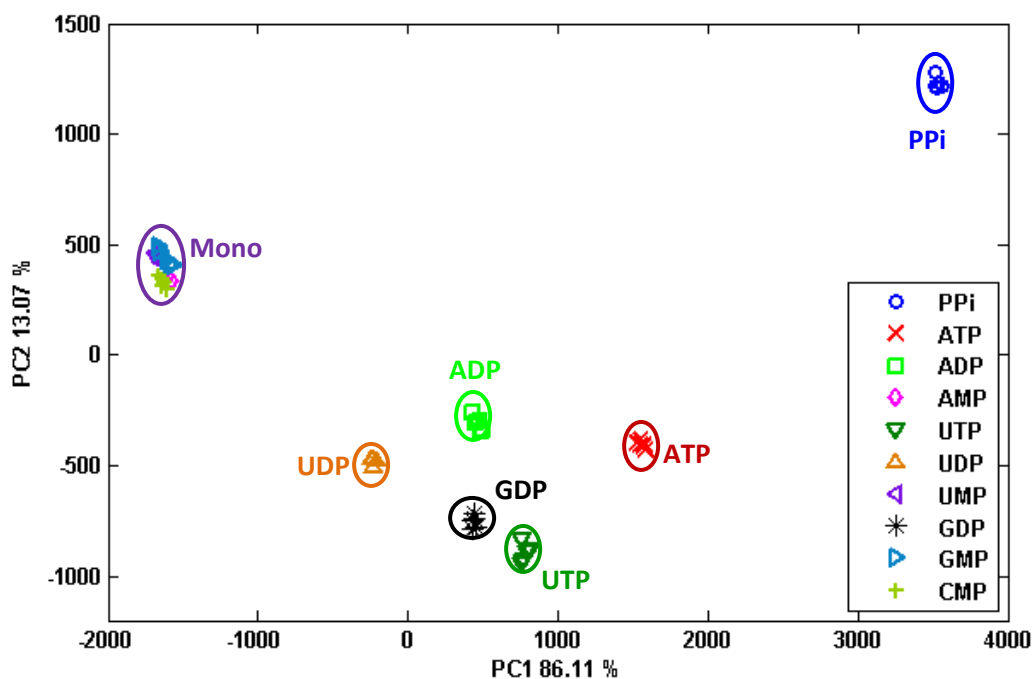


Figure A6 PCA score plot of **Es-Cu / Pydpa-Zn+Es-Zn** upon addition of various nucleotide anions (10 equiv) in an aqueous solution of HEPES buffer 0.01 M, pH 7.4.

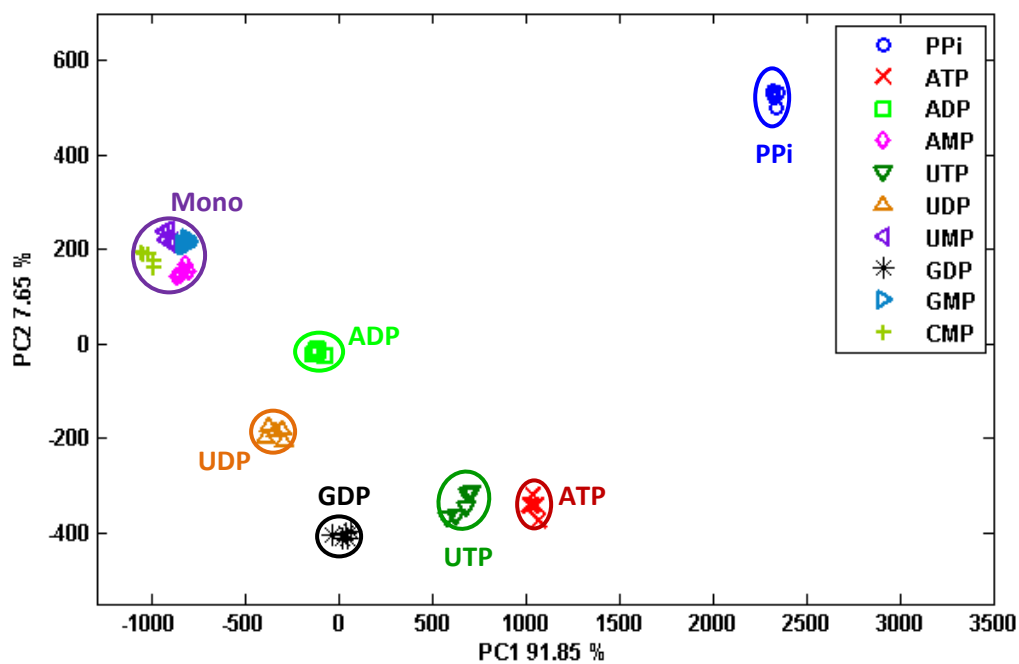


Figure A7 PCA score plot of **Es-Cu / Pydpa-Zn+Es-Cu** upon addition of various nucleotide anions (10 equiv) in an aqueous solution of HEPES buffer 0.01 M, pH 7.4.

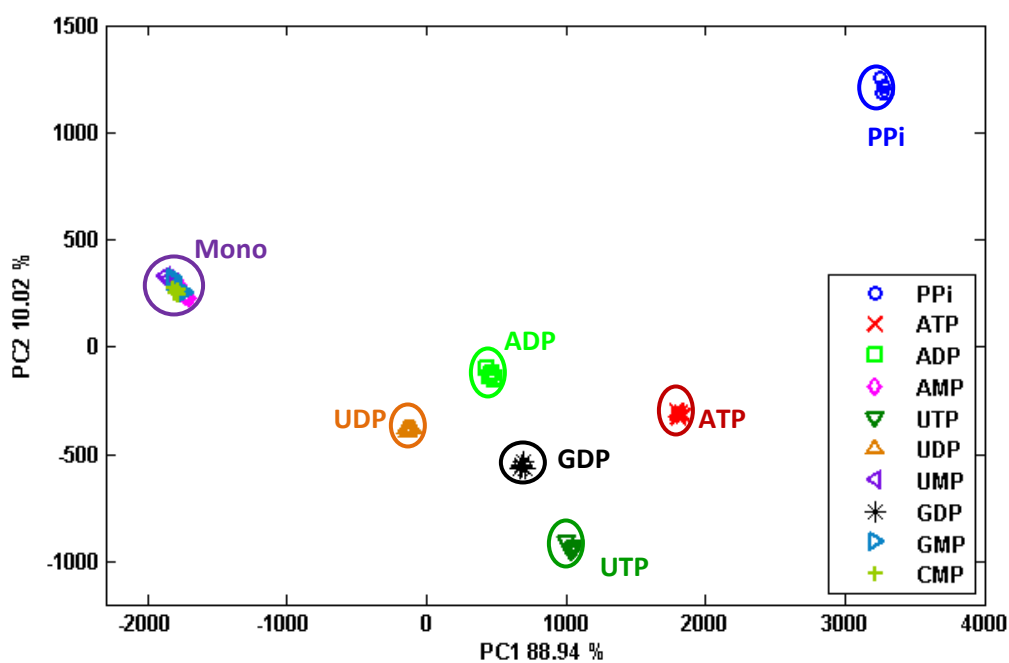


Figure A8 PCA score plot of **Pydpa-Zn+Es-Zn / Pydpa-Zn+Es-Cu** upon addition of various nucleotide anions (10 equiv) in an aqueous solution of HEPES buffer 0.01 M, pH 7.4.

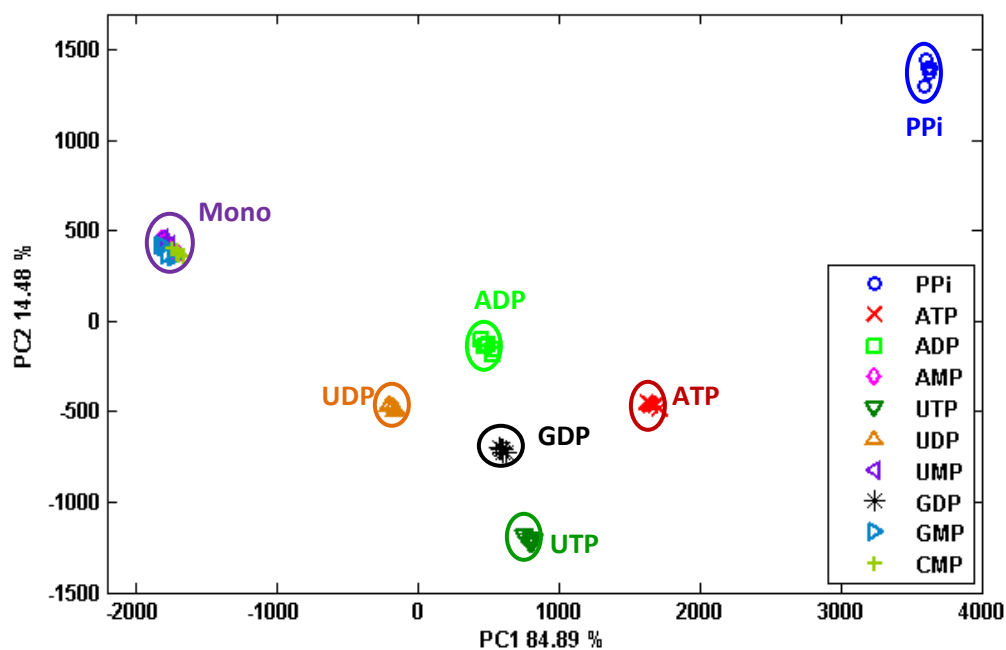


Figure A9 PCA score plot of **Pydpa-Zn / Es-Zn / Pydpa-Zn+Es-Zn** upon addition of various nucleotide anions (10 equiv) in an aqueous solution of HEPES buffer 0.01 M, pH 7.4.

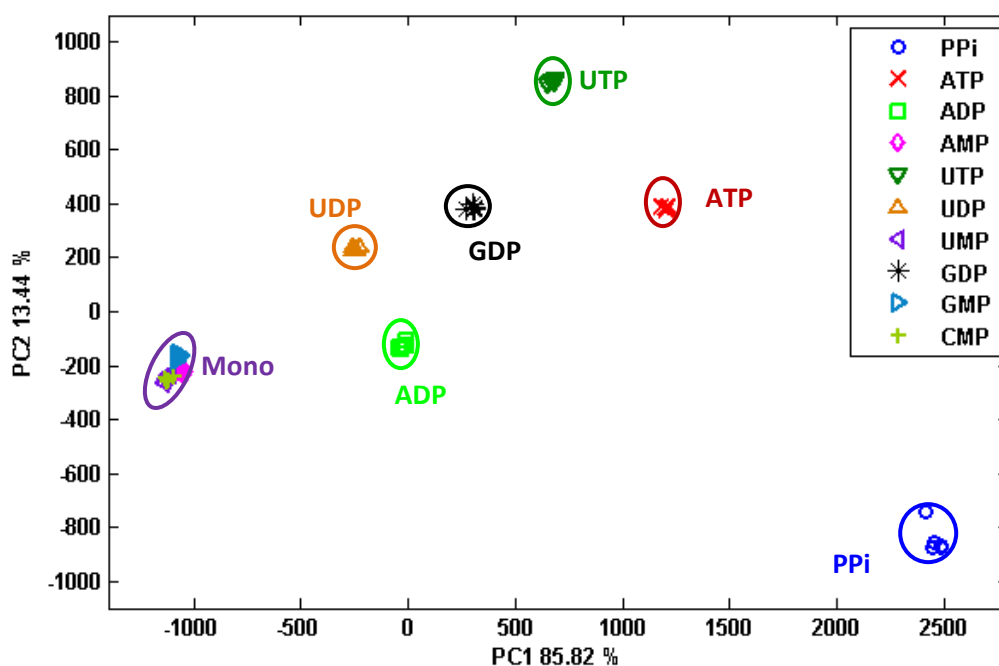


Figure A10 PCA score plot of **Pydpa-Zn / Es-Zn / Pydpa-Zn+Es-Cu** upon addition of various nucleotide anions (10 equiv) in an aqueous solution of HEPES buffer 0.01 M, pH 7.4.

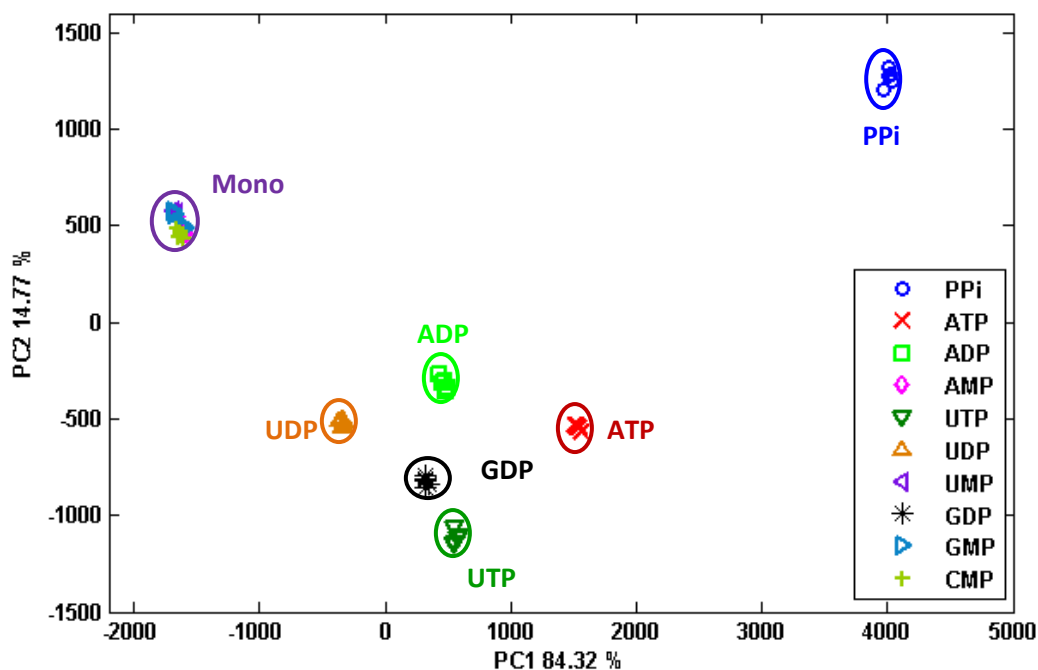


Figure A11 PCA score plot of Pydpa-Zn / Es-Cu / Pydpa-Zn+Es-Zn upon addition of various nucleotide anions (10 equiv) in an aqueous solution of HEPES buffer 0.01 M, pH 7.4.

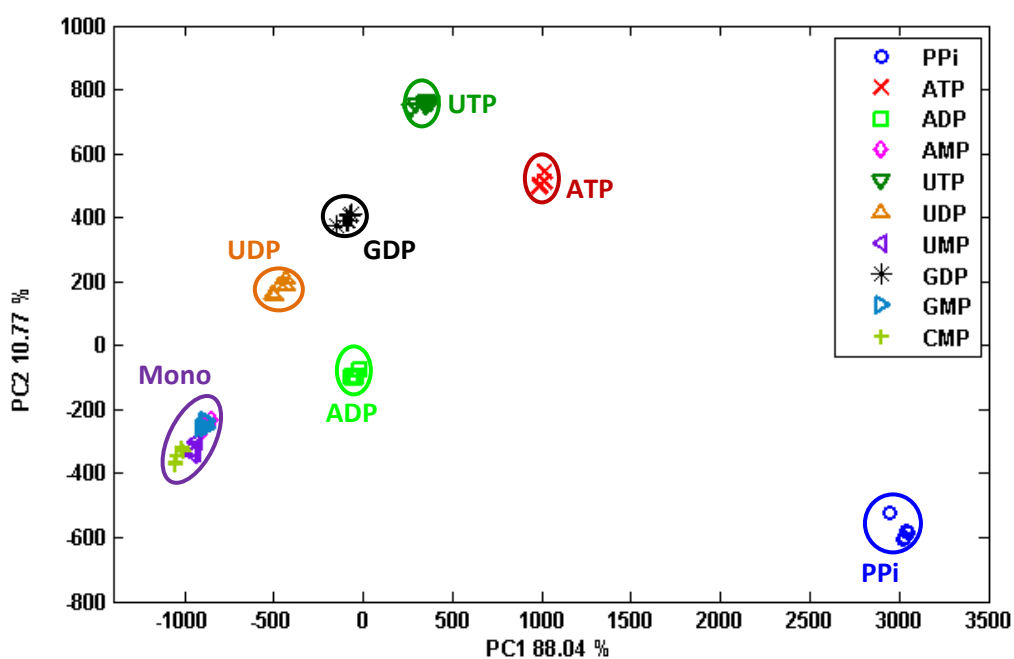


Figure A12 PCA score plot of Pydpa-Zn / Es-Cu / Pydpa-Zn+Es-Cu upon addition of various nucleotide anions (10 equiv) in an aqueous solution of HEPES buffer 0.01 M, pH 7.4.

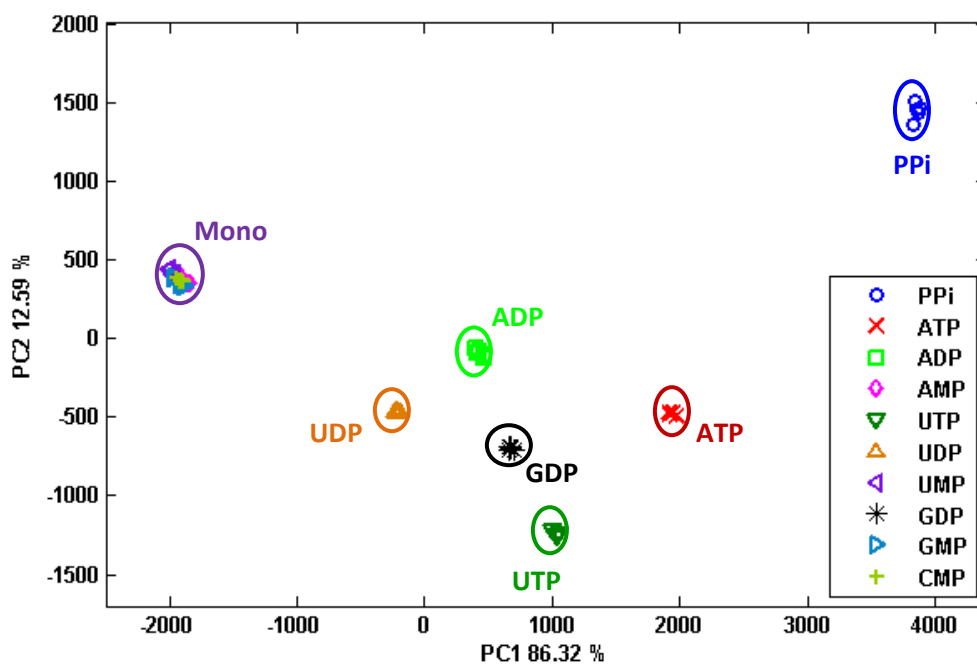


Figure A13 PCA score plot of **Pydpa-Zn / Es-Zn / Pydpa-Zn+Es-Zn / Pydpa-Zn+Es-Cu** upon addition of various nucleotide anions (10 equiv) in an aqueous solution of HEPES buffer 0.01 M, pH 7.4.

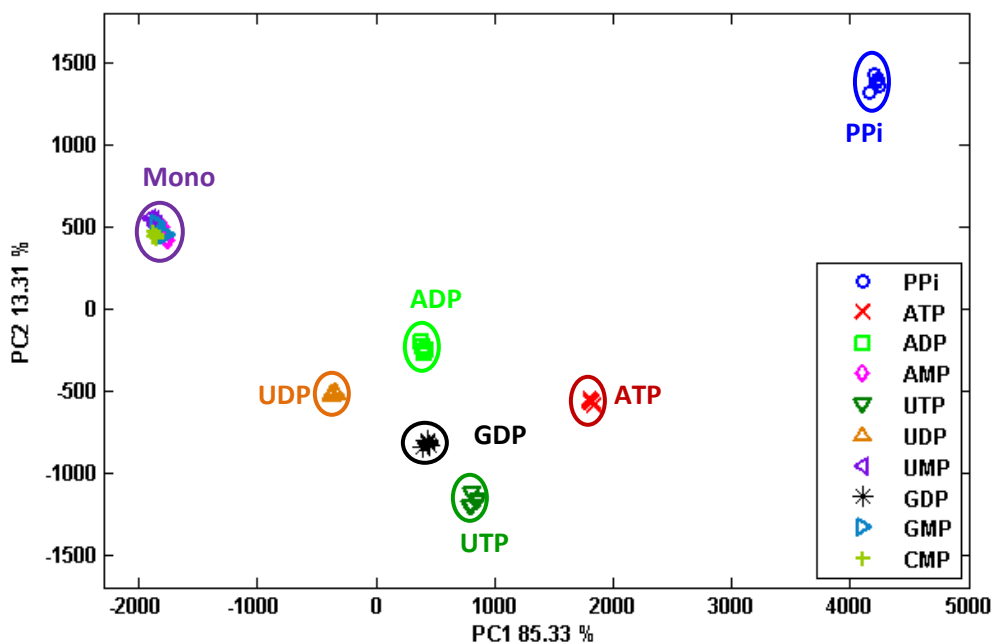


Figure A14 PCA score plot of **Pydpa-Zn / Es-Cu / Pydpa-Zn+Es-Zn / Pydpa-Zn+Es-Cu** upon addition of various nucleotide anions (10 equiv) in an aqueous solution of HEPES buffer 0.01 M, pH 7.4.

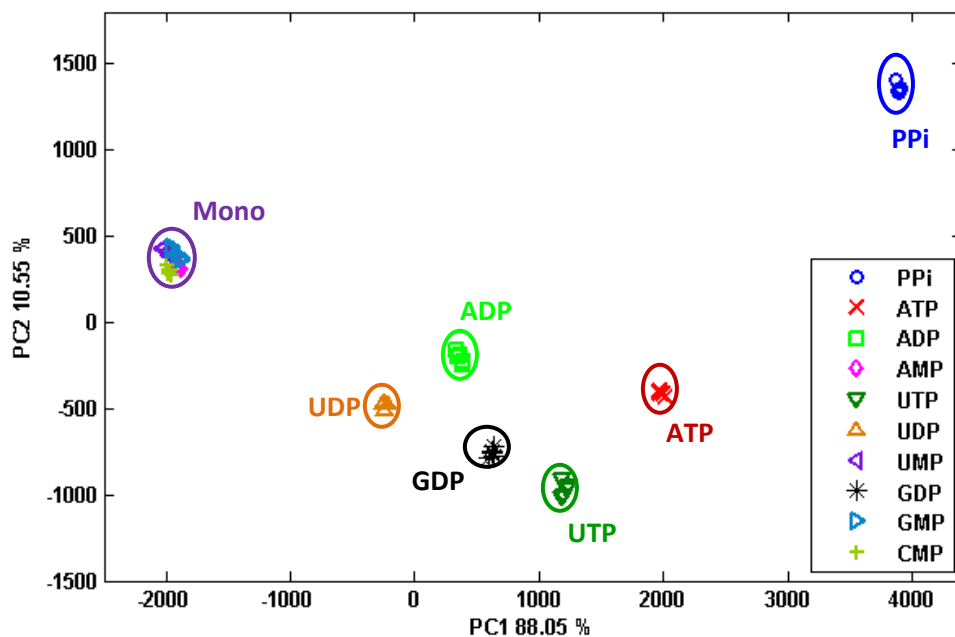


Figure A15 PCA score plot of **Es-Zn / Es-Cu / Pydpa-Zn+Es-Zn / Pydpa-Zn+Es-Cu** upon addition of various nucleotide anions (10 equiv) in an aqueous solution of HEPES buffer 0.01 M, pH 7.4.

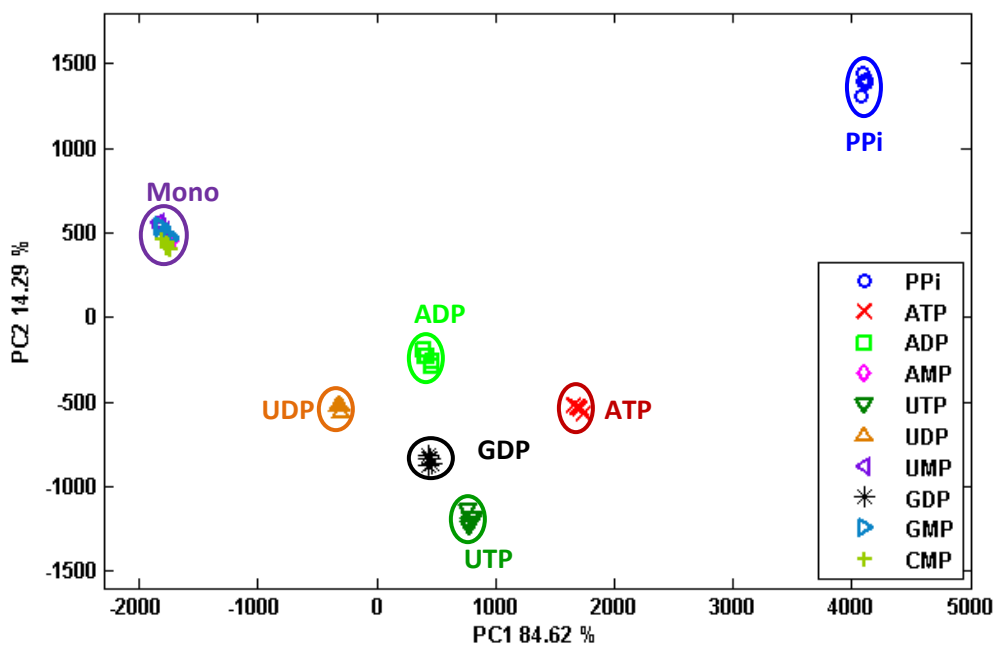


Figure A16 PCA score plot of **Pydpa-Zn / Es-Zn / Es-Cu / Pydpa-Zn+Es-Zn** upon addition of various nucleotide anions (10 equiv) in an aqueous solution of HEPES buffer 0.01 M, pH 7.4.

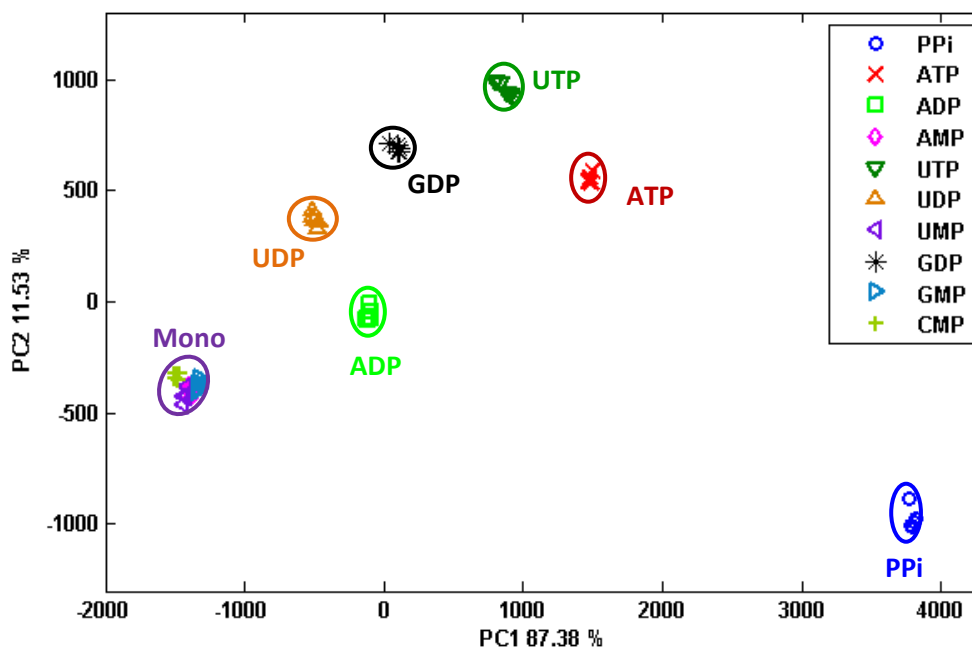


Figure A17 PCA score plot of Pydpa-Zn / Es-Zn / Es-Cu / Pydpa-Zn+Es-Cu upon addition of various nucleotide anions (10 equiv) in an aqueous solution of HEPES buffer 0.01 M, pH 7.4.

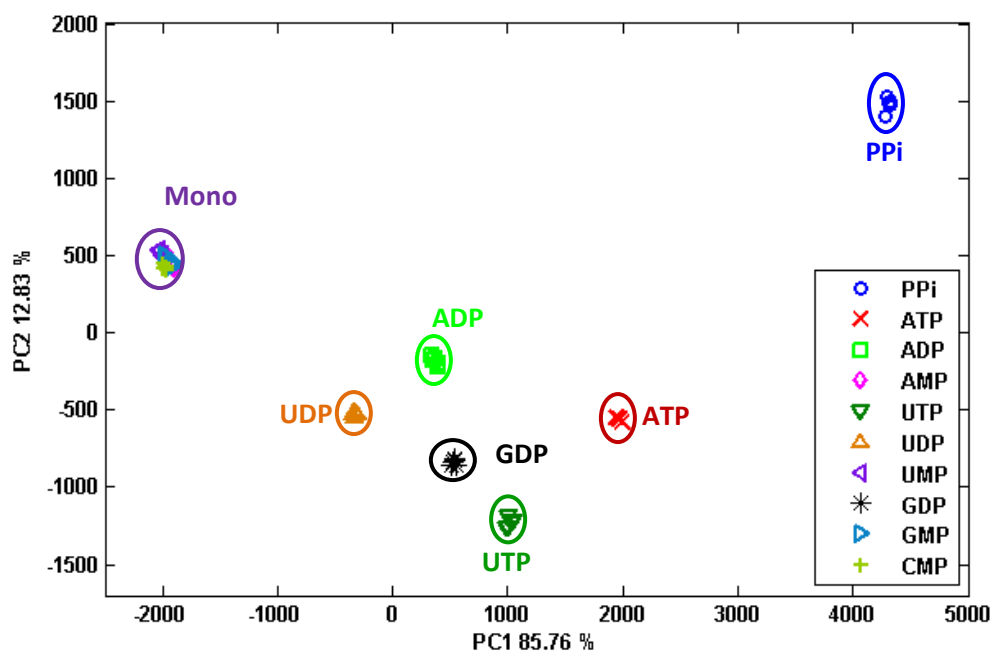


Figure A18 PCA score plot of Pydpa-Zn / Es-Zn / Es-Cu / Pydpa-Zn+Es-Zn / Pydpa-Zn+Es-Cu upon addition of various nucleotide anions (10 equiv) in an aqueous solution of HEPES buffer 0.01 M, pH 7.4.

VITA

General Information

Miss Chiraporn Chaicham was born on June 2, 1986 in Chaiyaphum, Thailand. She graduated with a high school diploma from Phukhieo School, Phukhieo Chaiyaphum in 2005. She received her Bachelor's degree of Science in Chemistry from Khonkean University in 2008. Thereafter, she has been a graduate student at the Department of Chemistry, Chulalongkorn University. Since 2006 become a member of the Supramolecular Chemistry Research Unit under supervision of Assistant Professor Dr. Boosayarat Tomapatanaget. She finished her Master's degree of Science in the academic year 2011.

Fellowships & Scholarships

- Human Resource Development in Science Project (Science Achievement Scholarship of Thailand, SAST) to support covering full tuition and stipend in academic program at Khonkean University in 2005-2008 and Chulalongkorn University in 2008-2011.